M.F. ÖZBEY

COMPARISON AND ACCURACY OF DIFFERENT METHODS TO OBTAIN MEAN RADIANT TEMPERATURE IN INDOOR ENVIRONMENT

THE GRADUATE SCHOOL OF NATURAL AND APPLIED SCIENCES
OF
ATILIM UNIVERSITY

MEHMET FURKAN ÖZBEY

A MASTER OF SCIENCE THESIS
IN
THE DEPARTMENT OF MECHANICAL ENGINEERING

JUNE 2021

ATILIM UNIVERSITY 2021

COMPARISON AND ACCURACY OF DIFFERENT METHODS TO OBTAIN MEAN RADIANT TEMPERATURE IN INDOOR ENVIRONMENT

A THESIS SUBMITTED TO
THE GRADUATE SCHOOL OF NATURAL AND APPLIED SCIENCES
OF
ATILIM UNIVERSITY

BY

MEHMET FURKAN ÖZBEY

IN PARTIAL FULFILLMENT OF THE REQUIREMENTS
FOR
THE DEGREE OF MASTER OF SCIENCE
IN
MECHANICAL ENGINEERING

JUNE 2021

Approval of the Graduate School of Natural and Applied Sciences, Atılım University.

_____

Prof. Dr. Ender KESKİNKILIÇ
Director

I certify that this thesis satisfies all the requirements as a thesis for the degree of **Master of Science in Mechanical Engineering at Atılım University**.

_____

Prof. Dr. S. Engin KILIÇ
Head of Department

This is to certify that we have read the thesis COMPARISON AND ACCURACY OF DIFFERENT METHODS TO OBTAIN MEAN RADIANT TEMPERATURE IN INDOOR ENVIRONMENT submitted by MEHMET FURKAN ÖZBEY and that in our opinion it is fully adequate, in scope and quality, as a thesis for the degree of Master of Science.

_____	_____
Asst. Prof. Dr. Bahram Lotfi SADIGH Co-Supervisor	Asst. Prof. Dr. Cihan TURHAN Supervisor

Examining Committee Members:

Asst. Prof. Dr. Ali KARAKUŞ
Mechanical Engineering Department, Middle East Technical University _____

Asst. Prof. Dr. Cihan TURHAN
Energy Systems Engineering Department Atılım University _____

Asst. Prof. Dr. Mehdi MEHRTASH
Energy Systems Engineering Department Atılım University _____

Date: *24.06.2021*

I hereby declare that all information in this document has been obtained and presented in accordance with academic rules and ethical conduct. I also declare that, as required by these rules and conduct, I have fully cited and referenced all material and results that are not original to this work.

Name, Last Name: Mehmet Furkan ÖZBEY

Signature:

ABSTRACT

COMPARISON AND ACCURACY OF DIFFERENT METHODS TO OBTAIN MEAN RADIANT TEMPERATURE IN INDOOR ENVIRONMENT

Özbey, Mehmet Furkan
MSc., Department of Mechanical Engineering
Supervisor: Asst. Prof. Dr. Cihan Turhan
Co-Supervisor: Asst. Prof. Dr. Bahram Lotfisadıgh

June 2021, 116 pages

Thermal comfort is defined as "*the state of mind which expresses satisfaction with the thermal environment"* by the American Society of Heating Refrigerating and Air Conditioning Engineers in the international standard of ASHRAE-55. Thermal comfort can be assessed with two common methods which are Predicted Mean Vote (PMV)/ Percentage of Predicted Dissatisfied (PPD) model and adaptive thermal comfort method where the occupants' behaviour is also included. These models consider thermal comfort parameters such as: two personal (clothing and metabolic rate) and four environmental (air temperature, relative humidity, air velocity and mean radiant temperature) parameters. However, the mean radiant temperature is a problematic parameter to obtain in thermal comfort calculations and/or measurements due to its complexity. Obtaining the mean radiant temperature for the indoor environment are based on different techniques such as calculation methods, measurement methods, and assumptions. However, calculation methods are very complex, while measurement methods require very expensive and difficult to obtain-instruments. On the other hand, the accuracy of the assumptions is always a question mark. To this aim, the purpose of this thesis is to compare different techniques to obtain

mean radiant temperature and find their accuracy with a reference measurement method which was conducted with a developed globe thermometer. A case building in a Csb type climate zone according to Köppen-Geiger classification, is selected as a case study. Three calculation methods and four assumptions on obtaining mean radiant temperature are compared with an in-situ measurement. The results revealed that using assumptions or calculation methods to obtain the mean radiant temperature caused a Mean Absolute Percentage Error (MAPE) up to 9.1% compared to the reference method.

Keywords: Thermal Comfort, Mean Radiant Temperature, Globe Thermometer, Indoor Environment

ÖZ

İÇ ORTAMDA ORTALAMA RADYAN SICAKLIĞINI ELDE ETMEK İÇİN FARKLI YÖNTEMLERİN DOĞRULUĞUNUN KARŞILAŞTIRILMASI

Özbey, Mehmet Furkan
Yüksek Lisans, Makine Mühendisliği Bölümü
Tez Yöneticisi: Dr. Öğr. Üy. Cihan Turhan
Ortak Tez Yöneticisi: Dr. Öğr. Üy. Bahram Lotfisadıgh

Haziran 2021, 116 sayfa

Amerikan Isıtma Soğutma ve Klima Mühendisleri Birliği (ASHRAE), ısıl konforu bir kişinin bulunduğu ortamdaki memnuniyetini ifade eden öznel ve zihinsel değerlendirme ile elde edilen zihin koşulları olarak tanımlanmıştır. Isıl konfor, geleneksel olarak Fanger'in Ortalama Tahmini Oy (PMV) / Memnuniyetsizliklerin Tahmini Yüzdesi (PPD) metodu ve kişilerin davranışlarını da içeren adaptif ısıl konfor metotları ile elde edilmektedir. Isıl konfor parametreleri kişisel parametreler (giysi değeri ve metabolizma hızı) ve çevresel parametreler (hava sıcaklığı, bağıl nem, hava hızı ve ortalama radyan sıcaklığı) olarak üzere iki farklı kategoride ele almaktadır. Bu parametreler arasında, Ortalama Radyan Sıcaklık ölçülmesinin ve hesaplanmasının karmaşık olmasından dolayı elde edilmesi zor bir faktördür. İç ortamlarda ortalama radyan sıcaklığı elde etme yaklaşımları hesaplama yöntemleri, ölçüm yöntemleri ve varsayımlar gibi farklı yöntemlere dayanmaktadır. Ancak hesaplama yöntemlerinin karmaşık olması ve ölçüm yöntemleri için kullanılacak ölçüm aletlerinin pahalı ve elde edilmesi zor araçlar olması araştırmacıları doğruluğu kesin olmayan varsayımlara yönlendirmektedir. Bu nedenle, bu çalışmanın amacı ortalama radyan sıcaklığın elde edilme yöntemlerinin ölçüm yöntemlerinden birisi olan ve bu çalışma için üretilen

küre termometresini referans alıp diğer metotlar ile karşılaştırılarak tüm yöntemlerin doğruluğunu bulmaktır. Bu çalışmada Köppen-Geiger sınıflandırmasına göre Csb tipi iklim bölgesinde bulunan bir test odası seçilmiştir ve ortalama radyatif sıcaklığı elde etmek için kullanılan 2 farklı hesaplama yöntemi ve 8 farklı varsayım yerinde ölçümle referans metodu ile karşılaştırılmıştır. Sonuçlar, ortalama radyan sıcaklığı elde etmek için varsayımların veya hesaplama yöntemlerinin kullanılmasının, referans yönteme kıyasla %9,1'e varan bir hataya neden olduğunu ortaya koydu.

Anahtar Kelimeler: Isıl konfor, Ortalama Radyatif Sıcaklık, Küre Termometresi, İç Ortam

To my Family.

ACKNOWLEDGMENTS

I would like to express my gratitude to my advisor Asst. Prof. Dr. Cihan TURHAN for the support of my study for his patience, and noticeable knowledge. His assistance always assisted me in all time of research and writing of this thesis. Besides, I would like to thank my co-advisor Bahram LOTFISADIGH for his guidance in this thesis.

Furthermore, I thank the members of thesis committee Asst. Prof. Dr. Ali KARAKUŞ, Asst. Prof. Dr. Mehdi MEHRTASH for their insightful comments.

Finally, I would like to thank my family for their all support during my full studies.

TABLE OF CONTENTS

ABSTRACT iii
ÖZ v
DEDICATION vii
ACKNOWLEDGMENTS viii
TABLE OF CONTENTS ix
LIST OF TABLES xi
LIST OF FIGURES xii
LIST OF SYMBOLS/ABBREVIATIONS xvi
CHAPTER
1. INTRODUCTION 1
2. THERMAL COMFORT AND PARAMETERS 5
2.1 Thermal Comfort 5
2.2 Thermal Comfort Parameters 9
2.2.1 Metabolic Rate (M) 10
2.2.2 Clothing Value 11
2.2.3 Relative Humidity (RH) 13
2.2.4 Air Velocity (v_a) 13
2.2.5 Air Temperature (T_a) 14
2.2.6 Mean Radiant Temperature (MRT) 15
2.3 Parameters and Their Effects on The Thermal Balance Equation 15
3. MEAN RADIANT TEMPERATURE 17
3.1 Measurement Methods 18
3.2 Calculation Methods 22
3.3 Software Programs 28
3.4 Assumptions 29
4. LITERATURE REVIEW 32
4.1 Outdoor Environment 32
4.2 Indoor Environment 36

5. METHODOLOGY 45
5.1 Case Building 47
5.2 Development of the Globe Thermometer 49
5.2.1 Construction of the Developed Globe Thermometer 51
5.2.2 Calibration of the Developed Globe Thermometer 56
5.3 Determination of the Angle Factors 59
5.4 Data Collection 62
5.5 Methods to Obtain the MRT 65
5.6 Comparison of the Results 67
6. RESULTS AND DISCUSSION 68
6.1 Calibration Results of The Developed Globe Thermometer 70
6.2 Calculation Results of the Angle Factors of the Case Building 73
6.3 Measurement Results 75
6.4 Comparison of Methods to Obtain the MRT 78
6.4.1 Comparison of the Cases: C1 and R 79
6.4.2 Comparison of the Cases: C2 and R 81
6.4.3 Comparison of the Cases: A1 and R 83
6.4.4 Comparison of the Cases: A2 and R 85
6.4.5 Comparison of the Cases: A3 and R 87
6.4.6 Comparison of the Cases: A4 and R 89
6.4.7 Comparison of the Cases: A5 and R 91
6.4.8 Comparison of the Cases: A6 and R 93
6.4.9 Comparison of the Cases: A7 and R 95
6.4.10 Comparison of the Cases: A8 and R 97
6.5 Limitations 100
7. CONCLUSIONS 102
REFERENCES 104
APPENDIX
A. AN EXAMPLE DAY FROM THE COLLECTED DATA 116

LIST OF TABLES

Table 2.1 Metabolic Rates of Some Regular Tasks.....11
Table 2.2 Some Clothing Insulation Values (Clo).....12
Table 2.3 Effect of Physiological Parameters to The Terms in Equation 1.....16
Table 3.1 Measurement Techniques to Obtain the MRT.....21
Table 3.2 Constant Table for Equations 7, 8, and 9.....24
Table 3.3 Short-wave and Long-wave Absorption Coefficients.....27
Table 3.4 List of Assumptions to Obtain the MRT.....30
Table 5.1 Utilized Equipment to Developed Globe Thermometer.....55
Table 5.2 The Technical Data of Devices Used in the Measurement Campaign for Calibration of Developed Globe Thermometer.....57
Table 5.3 The Specifications of Infrared Thermometer.....63
Table 5.4 Used Methods to Obtain MRT Values in the Thesis.....66
Table 6.1 The Calibration Results of the Developed Globe Thermometer.....71
Table 6.2 The Price of Utilized Materials in Developed Globe Thermometer.....72
Table 6.3 The Coefficients Table to Calculate the Angle Factors.....73
Table 6.4 Results of Calculation of Angle Factors.....74
Table 6.5 Statistical Criteria Results for Comparison of Cases of C1 and R.....80
Table 6.6 Statistical Criteria Results for Comparison of Cases of C2 and R.....82
Table 6.7 Statistical Criteria Results for Comparison of Cases of A1 and R.....84
Table 6.8 Statistical Criteria Results for Comparison of Cases of A2 and R.....86
Table 6.9 Statistical Criteria Results for Comparison of Cases of A3 and R.....88
Table 6.10 Statistical Criteria Results for Comparison of Cases of A4 and R.....90
Table 6.11 Statistical Criteria Results for Comparison of Cases of A5 and R.....92
Table 6.12 Statistical Criteria Results for Comparison of Cases of A6 and R.....94
Table 6.13 Statistical Criteria Results for Comparison of Cases of A7 and R.....96
Table 6.14 Statistical Criteria Results for Comparison of Cases of A8 and R.....98
Table 6.15 Statistical Criteria Results for Comparison of Calculation Methods and Assumptions with the Reference Method.....99

LIST OF FIGURES

Figure 1.1 Dispersion of Energy Consumption in the Residential Buildings in the European Union 1
Figure 1.2 The MRT as a Function of Position (Detailed information about the Calculation Method based on view factors is discussed in Chapter 3) 3
Figure 2.1 Simplified Human Heat Balance System 6
Figure 2.2 Thermal Sensation Scale 7
Figure 2.3 Changes in the PPD with respect to the PMV 8
Figure 2.4 Adaptive Thermal Comfort Chart with Acceptable Levels 9
Figure 2.5 Thermal Comfort and Parameters 10
Figure 2.6 An Example of the Calculation of Total Clothing Value 12
Figure 2.7 Relative Humidity Sensor 13
Figure 2.8 Anemometer 14
Figure 2.9 Some Types of Thermometers 15
Figure 3.1 Imaginary Enclosure in the MRT Applications 17
Figure 3.2 Methods to Obtain the MRT 18
Figure 3.3 Outlook of Industrial Globe Probe 19
Figure 3.4 Two-Sphere Radiometer 20
Figure 3.5 Advantages and Disadvantages of Measurement Methods to Obtain the MRT 22
Figure 3.6 Angle Factors for the Seated Person for Vertical Surfaces 24
Figure 3.7 Angle Factors for the Seated Person for Ceiling and Floor 25
Figure 3.8 Angle Factors for the Standing Person for Ceiling and Floor 25
Figure 3.9 Angle Factors for the Standing person for Vertical Surfaces 26
Figure 3.10 A Net Radiometer 27
Figure 4.1 The MRT distribution in different heights, widths, and orientations in an urban canyon in a study of Herrmann, J., and Matzarakis, A. 33
Figure 4.2 Measurement setup of the study of Tan, C. L. et al. 36

Figure 4.3 The occupant positions in the study of Kalmár F and Kalmár T. (where a and b represent the position 1 and 2, respectively).....38
Figure 4.4 Result of the Calculated and Measured MRT values in different positions and room length in a study of Kalmár F and Kalmár T. 38
Figure 4.5 Temperature contour plot for acrylic globe thermometers in the study of Xing, D., & Li, N. 40
Figure 4.6 The IR scanning system which estimates the MRT values in a Stadium in the study of Lee, D. S. et al. 42
Figure 4.7 Created Test Chamber and experimental setup of study of Alfano et al. 44
Figure 5.1 The Methodology of the Thesis 46
Figure 5.2 The Location of the Case Building 47
Figure 5.3 The Architectural Drawing of the Case Building 48
Figure 5.4 The Process to Obtain the Calibrated Globe Thermometer in the Study 50
Figure 5.5 Representation of the Developed Globe Thermometer with Types of Equipment. 51
Figure 5.6 Metal Spinning Process 52
Figure 5.7 Construction of the Copper Sphere for Developed Globe Thermometer 52
Figure 5.8 DS18B20 Temperature Sensor 53
Figure 5.9 Arduino Uno 53
Figure 5.10 Circuit Design of Data Collection for Calibration of Developed Globe Thermometer 54
Figure 5.11 The Technical Drawing of the Matt-Blacked Copper Sphere 55
Figure 5.12 Globe Sphere after Construction (on the left) and The Developed Globe Thermometer After Dyeing (on the right).....56
Figure 5.13 The positioning of the Developed Globe Thermometer (1) and Commercial Globe Thermometer (2) in the University Office 58
Figure 5.14 An Illustration of the Case Building 60
Figure 5.15 A Sight of Six-Walls of the Case Building 61
Figure 5.16 Infrared Thermometer (EXTECH 45230) 62
Figure 5.17 Illustration of the Data Collection.....63
Figure 5.18 The Locations of Taken Temperatures for Left and Right Walls.....64

Figure 5.19 The Locations of Taken Temperatures for Front Wall, Back Wall, Ceiling, and Floor 64
Figure 6.1 Results and Discussion Sections in the Thesis with Page Numbers. 69
Figure 6.2 Comparison of The MRT Data Stemmed from Commercial Globe Thermometer and Developed Globe Thermometer via Linear Comparative Comparison Method..... 70
Figure 6.3 Distribution of Residuals..... 72
Figure 6.4 Distribution of the MRT Data with the Reference Method in the Study 75
Figure 6.5 T_a, T_{out}, and MRT values of the data (Note: The Data Number was arrayed by dates with starting on 6th July 2020 and ending with 19th April 2021 in the Graph) 76
Figure 6.6 Distribution of the MRT Data with the Reference Method in the Study. (Note: The Data Number was arrayed by temperature values from lower to higher.) 77
Figure 6.7 The Graph for Comparison of the MRT Values of Cases with Residuals: C1 and R 79
Figure 6.8 The Graph for Comparison of the MRT Values of Cases with Residuals: C2 and R 81
Figure 6.9 The Graph for Comparison of the MRT Values of Cases with Residuals: A1 and R 83
Figure 6.10 The Graph for Comparison of the MRT Values of Cases with Residuals: A2 and R 85
Figure 6.11 The Graph for Comparison of the MRT Values of Cases with Residuals: A3 and R..... 87
Figure 6.12 The Graph for Comparison of the MRT Values of Cases with Residuals: A4 and R..... 89
Figure 6.13 The Graph for Comparison of the MRT Values of Cases with Residuals: A5 and R..... 91
Figure 6.14 The Graph for Comparison of the MRT Values of Cases with Residuals: A6 and R..... 93

Figure 6.15 The Graph for Comparison of the MRT Values of Cases with Residuals: A7 and R.....95
Figure 6.16 The Graph for Comparison of the MRT Values of Cases with Residuals: A8 and R.....97
Figure 6.17 Comparison of the Mean Squared Errors (MAPE) of 10 Compared Method. 100

LIST OF SYMBOLS/ABBREVIATIONS

a	Width of the surface (m)
A1	Resultant Temperature Method
A2	AUST (MRT) Method
A3	Equality of MRT to T_a
A4	Nagano's Assumption
A5	Inference of MRT From Globe Temperature
A6	Beshir and Ramsey's Method
A7	McIntyre's Method
A8	Equality of MRT to T_g
A_i	Actual Values, Area (m^2)
a_k	Coefficient of General Absorption for Short-Wave Radiation
a_l	Coefficient of General Absorption for Long-Wave Radiation
ASHRAE	American Society of Heating Refrigerating and Air Conditioning Engineers
ATC	Adaptive Thermal Comfort
AUST	Average Uncontrolled Surface Temperature (°C)
b	Height of the Surface (m)
BW	Back Wall
C	Convective Heat Loss (W), Comfort
c	Fenestration Constant for the Average Uncontrolled Surface Temperature, Distance of the human and surface (m)
C1	Calculation Method Based on Angle Factors Method
C2	Calculation Method Based on The Surface Areas Method
CFD	Computational Fluid Dynamics
clo	Clothing Value (m^2°C/Watt)
CTIS	Climate-Tourism/Transfer-Information-Scheme
D	Diameter (m)
E	Evaporative Heat Loss Rate (W)

e	Error
FEA	Finite Element Analysis
F_i	Angle Factor
FW	Front Wall
HVAC	Heating, Ventilating and Air Conditioning
IR	Infrared
ISO	International Standards Organization
K_i	Short-Wave Radiation (μm)
L_i	Long-Wave Radiation (μm)
LLCM	Linear Comparative Calibration Method
LW	Left Wall
M	Metabolic Rate (met)
MAPE	Mean Absolute Percentage Error
MRT	Mean Radiant Temperature (°C)
MSE	Mean Squared Error
N	Number of Data Samples
o_i	Output Value
OT, T	Operative Temperature (°C)
P	Heat Supply
p	Number of Input-Output Pairs of Data (W/m^2)
PMV	Predicted Mean Vote
PPD	Percentage of Predicted Dissatisfied
PRT	Plane Radiant Temperature (°C)
QUICK	Quadratic Upstream Interpolation for Convective Kinematics
R	Reference Method
R	Radiative Heat Loss (W)
R^2	Determination of Multiple Coefficient
RH	Relative Humidity
RMSE	Root Mean Squared Error
RW	Right Wall
S	Stress

S	Heat Storage
SIMPLE	Semi-Implicit Method for Pressure-Linked Equation
SOLWEIG	Solar and Long-Wave Environmental Irradiance Geometry
S_{str}	Radiation Heat Flux (W/m^2)
ST	Sky Type
SURM	Simple Urban Radiation Model
T	Temperature (°C)
t_i	Target Value
$Time_{cos}$	cosθ of time
$Time_{sin}$	sinθ of time
v	Velocity
W	Mechanical Work (W)
x	Independent variable
y	Dependent variable
Z_i	Forecast Values

GREEK SYMBOLS

$ß_0$	Intercept
$ß_1$	Slope
ε	Emissivity
σ	Stephan-Boltzmann Constant (5.67×108 W/m^2K^4)

SUBSCRIPTS

n	Surface Number
res	Respiratory
g	Globe
p-n	Surface Numbers for Angle Factors
b	Black Sensor
p	Polished Sensor
s	Sensor
a	Air

out	Outdoor
hs	Human Skin
o	Operative

CHAPTER 1

INTRODUCTION

Heating, Ventilating and Air Conditioning (HVAC) systems provide appropriate indoor air quality and thermal comfort for the occupants by controlling temperature while supplying and filtering the fresh air inside the buildings [1]. Buildings use any combination of the HVAC systems. For instance, while gas or oil-fired boiler and/or electric can be used for heating coils, on the other hand, chillers and air conditioners can be utilized for the cooling process [2, 3]. The buildings are responsible for 40% of the total energy consumption share in Europe [4- 6]. Moreover, the HVAC systems are responsible for 64.3% of the building's total energy consumption in the European Union (Figure 1.1) [7]. Since thermal comfort is provided by the HVAC systems, the energy consumption of the buildings is highly related with thermal comfort and thermal satisfaction of the occupants [8].

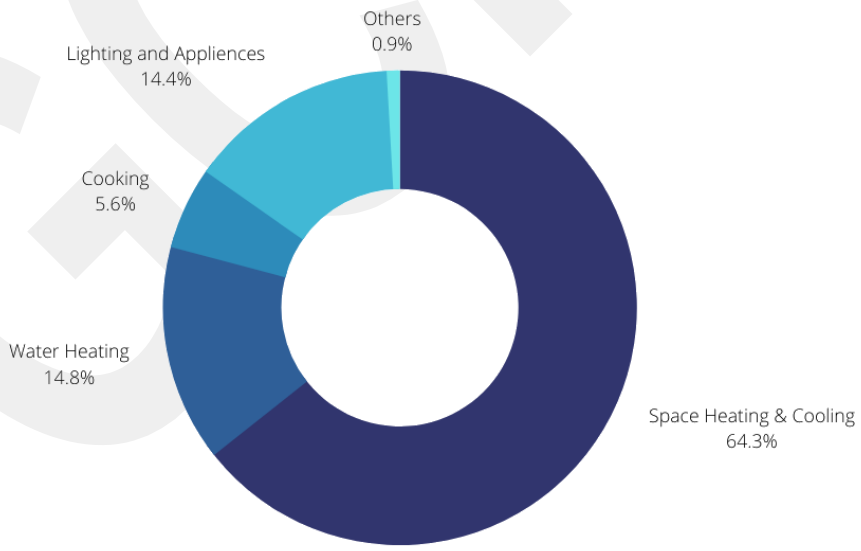

Figure 1.1. Dispersion of Energy Consumption in the Residential Buildings in the European Union [7]

Thermal comfort is defined as "*the state of mind which expresses satisfaction with the thermal environment*" by the American Society of Heating Refrigerating and Air Conditioning Engineers (ASHRAE) in an international thermal comfort standard, namely the ASHRAE Standard 55 [9]. Predicted Mean Vote (PMV)/ Percentage of Predicted Dissatisfied (PPD) model and Adaptive Thermal Comfort (ATC) model are two common methods in order to calculate the thermal comfort in a given environment.

Conventionally, six different parameters are included in the thermal comfort models, and these influencing parameters are divided into two categories; personal parameters (clothing value (clo) and metabolic rate (M)) and environmental parameters (air velocity (v_a), relative humidity (RH), air temperature (T_a) and mean radiant temperature (MRT)). While personal parameters can be obtained via tabulated tables which are identified in international standards such as ASHRAE 55 [9] and ISO 7726 [10], air velocity, relative humidity, indoor air temperature are measured with easy-to-use and cost-effective sensors. On the other hand, the attaining process of mean radiant temperature is the toughest and most problematic one within all thermal comfort parameters.

Mean Radiant Temperature (MRT) is defined as "*the temperature of a uniform, black enclosure that exchanges the same amount of heat by radiation with the occupant as the actual enclosure*" in the ASHRAE Standard 55 [9]. The MRT is a function of the occupant's position since the effect of radiation is different in different positions in a given environment [11]. Therefore, in different locations of the given environment, the MRT values can be different (Figure 1.2); thus, the MRT affects the thermal preferences of the occupants to achieve thermal comfort which can increase/decrease the energy consumption of the buildings.

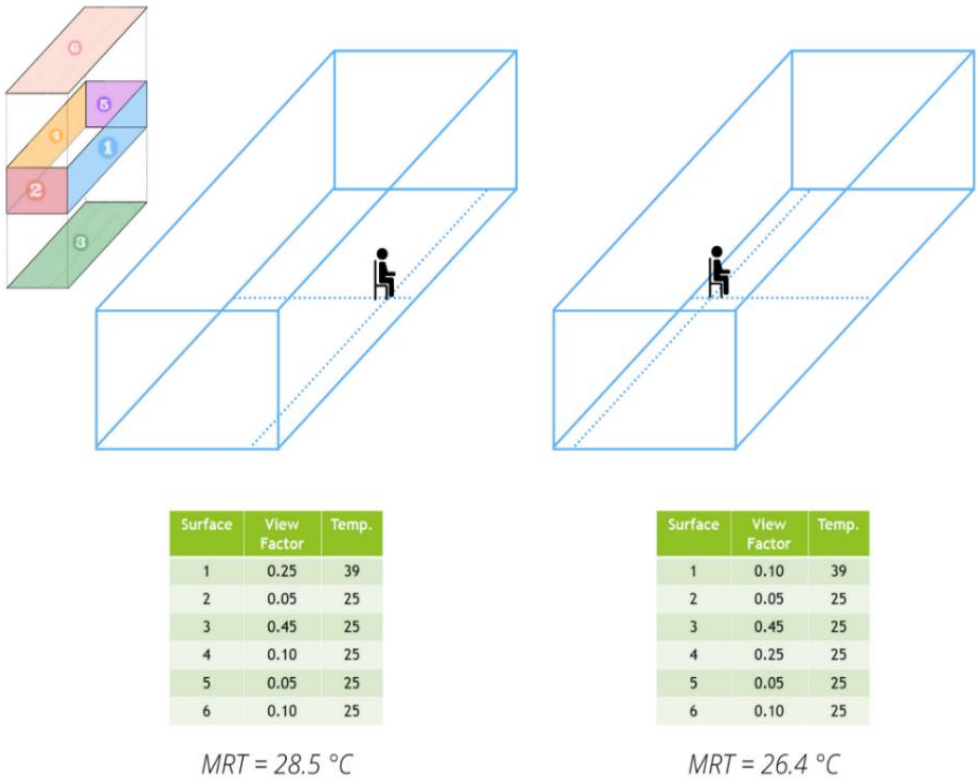

Figure 1.2. The MRT as a Function of Position (*Detailed information about the Calculation Method based on view factors is discussed in Chapter 3*)

The MRT can be obtained by calculation methods, measurement methods, software programs, and assumptions [12]. Due to the complexity of calculation methods and the difficulty of obtaining measurement techniques because of their high prices and availability problems, researchers use assumptions whose accuracies are uncertain. A detailed discussion of the methods to obtain the MRT will be given in Chapter 3.

This thesis aims to compare different techniques to attain the MRT and obtain the accuracy of the methods with a reference measurement method, measurements with a developed globe thermometer.

The thesis consists of seven chapters. The general discussions about thermal comfort and affecting parameters is discussed in Chapter 2. Besides, the detailed information about the MRT is represented in Chapter 3. Moreover, a comprehensive literature review about the MRT and its effects on indoor and outdoor applications is presented and discussed in Chapter 4. The study's methodology is expressed in Chapter 5, and

the results of this study are discussed in Chapter 6. In the final, the conclusions and future works are signified in the last chapter, which is Chapter 7.

CHAPTER 2

THERMAL COMFORT AND PARAMETERS

This chapter gives a brief overview of thermal comfort and parameters. The importance of the MRT is widely discussed in Chapter 3, separately.

2.1. Thermal Comfort

Thermal comfort is defined as "*the state of mind which expresses satisfaction with the thermal environment*" by the American Society of Heating Refrigerating and Air Conditioning Engineers (ASHRAE) in the ASHRAE 55 as given in the Introduction part of the thesis [9].

In human anatomy, the heating and cooling mechanism is operated to arrange the body temperature normally at 37°C [13, 14]. When the body temperature is higher than 37°C, the body's cooling mechanism (i.e., increasing skin blood flow and sweating) is operated to increase heat loss. In the case of the body temperature is lower than 34°C, the heating mechanism of the body (i.e., decreasing skin blood flow and shivering) is operated to generate heat (Figure 2.1) [3, 4]. In both cases, the human body transmits signals to the brain consistently. The difference between signals, which determine the heating or cooling system's operation, causes the feeling of either cold or hot while achieving thermal comfort/sensation as well [13]. In other words, thermal comfort/sensation is achieved by reaching the thermal equilibrium of the human body [13- 18].

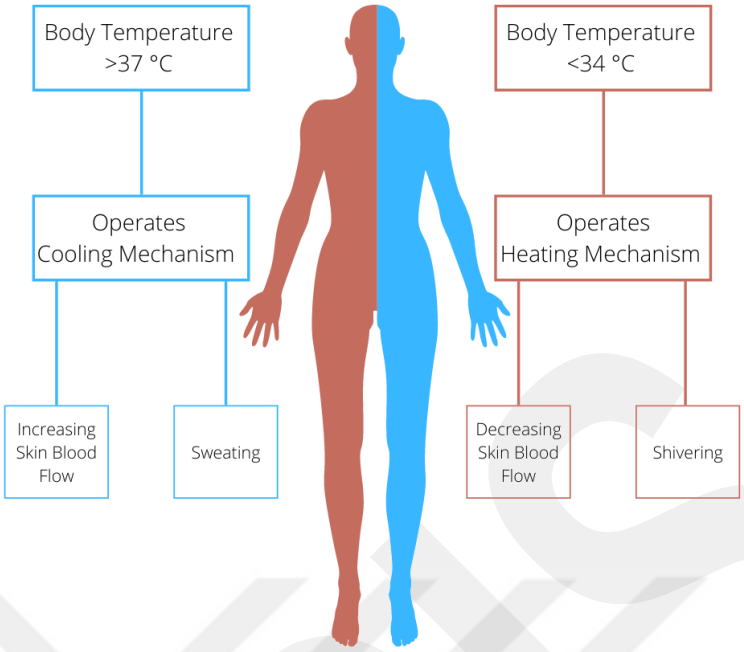

Figure 2.1 Simplified Human Heat Balance System [16]

Thermal comfort is intensely connected to the thermal equilibrium of the human body with the environment. The First Law of Thermodynamics explains the energy equilibrium in order to determine heat transfer between the human body and the environment. [19- 21]. To achieve thermal comfort, different characteristics such as metabolic rate, mechanical work, evaporative heat loss rate, and convective and evaporative heat loss, are considered in the heat balance equation. Applying the First Law of Thermodynamics makes it possible to access the human body's thermal balance with equation 2.1 [10].

$$S = (M - W) - (C_{res} + E_{res} + C + R + E) \quad (2.1)$$

Here, S signifies the heat storage, which is zero while heat loss and generation are in equilibrium. M states the metabolic rate, which is defined as the heat generation, related to the muscular activity in the human body. W represents the mechanical work, while E signifies the evaporative heat loss rate, which is released heat energy from the human body through evaporation processes such as vapour that comes with breathing and sweating. C_{res} defines the respiratory convective heat loss, and E_{res} represents the

respiratory evaporative heat loss. Finally, *R* and *C* describe radiative and convective heat loss, respectively. It is worth bearing in mind that radiation is a straight heat loss from the human body, while convection is the heat loss from the human body owing to air movement [22].

To calculate the thermal comfort and the level of dissatisfaction by using environmental and personal parameters of the thermal comfort, as foreshadowed, the Predicted Mean Vote (PMV) / Predicted Percentage of Dissatisfied (PPD) model was introduced by Fanger [19].

The PMV index predicts a large group of occupants' thermal comfort by taking the average thermal sensation votes of a large group using a seven-point thermal sensation scale [9, 23]. The seven levels of thermal scale include the terms representing how occupants feel in the current environment and terms characterized by numbers between -3 and +3. If the PMV value is between -0.5 and +0.5 values, the thermal environment is considered as acceptable, according to the ASHRAE Standard 55 [9]. The ASHRAE scale with seven levels is used to calculate the thermal sensation shown in Figure 2.2 [9, 19].

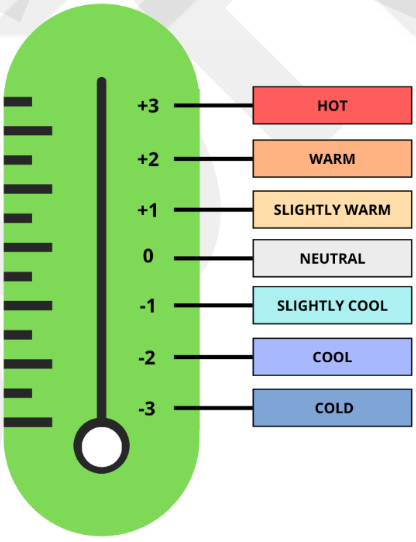

Figure 2.2. Thermal Sensation Scale [9, 19]

PPD is used to determine the percentage of dissatisfied people in an environment. By knowing the PMV value, the PPD value can be easily found by the following equation [9].

$$PPD = 100 - 95 \times \exp\left[-(0.03353 \times PMV^4 + 0.2179 \times PMV^2)\right] \quad (2.2)$$

Since there are individual differences between occupants, it is impossible to make an environment that satisfies everyone. If the PMV is calculated as zero, 5% of occupants are still dissatisfied. Moreover, the PPD should be lower than 10% for a comfortable environment [8]. Figure 2.3 shows the relationship between the PMV and PPD. When the PMV is equal to 0, which means that neutral thermal comfort is achieved, the PPD is 5%, meaning that 5% of people are dissatisfied with the given environment [19].

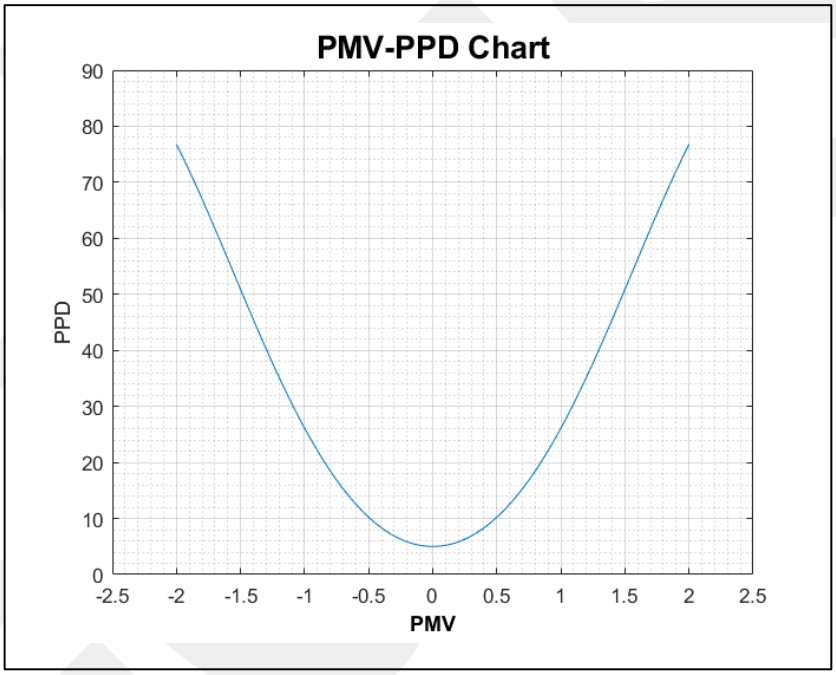

Figure 2.3. Changes in the PPD with respect to the PMV [24]

In naturally ventilated buildings, where the mechanical ventilation was not existed, the operative temperature may differ; thus, the thermal comfort models hard to obtain [25]. Therefore, in naturally ventilated buildings, ATC models are applied. The ATC models consider not only physiological parameters but also psychological and behavioural factors. In the principles of ATC, occupants can change the behaviours and factors which affect their thermal comfort. For instance, opening or closing windows, changing their clothes, or changing their activity levels [9].

ATC models mainly deal with outdoor temperature (T_{out}) and operative temperature (OT) [26]. The ASHRAE-55 [9] indicates two different acceptable levels, which are 90% and 80% in order to reach thermal comfort in different mean outdoor temperature and operative temperature values. Equations 2.3 and 2.4 signify the upper and lower limits of the acceptable range of 80% while Equations 2.5 and 2.6 represent the upper and lower limits of the acceptable range of 90%, as shown in figure 2.4.

$$Upper\ Limit_{80\%} = 0.31T_{out} + 21.3 \quad (2.3)$$

$$Lower\ Limit_{80\%} = 0.31T_{out} + 14.3 \quad (2.4)$$

$$Upper\ Limit_{90\%} = 0.31T_{out} + 20.3 \quad (2.5)$$

$$Upper\ Limit_{90\%} = 0.31T_{out} + 15.3 \quad (2.6)$$

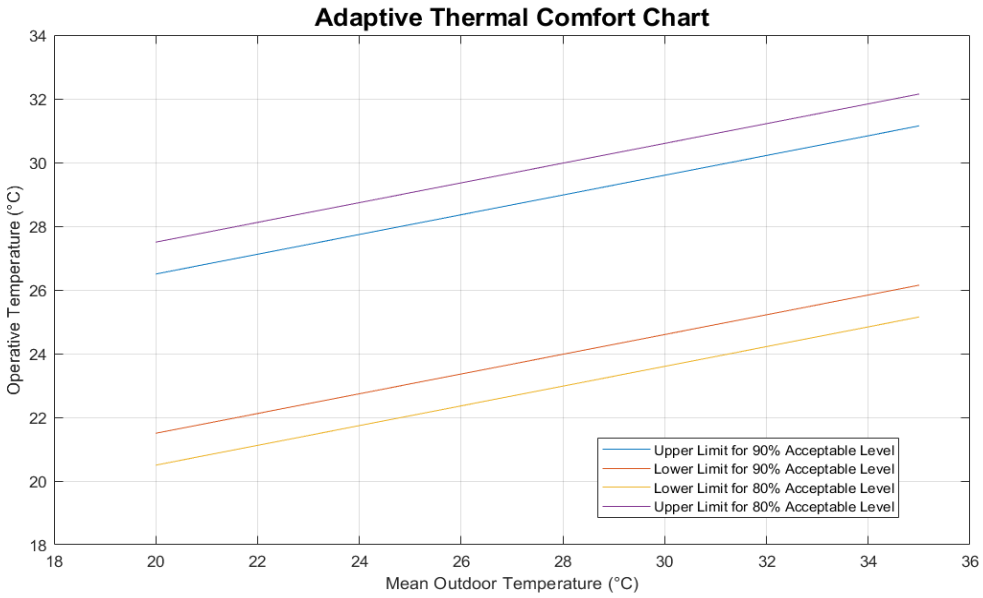

Figure 2.4 Adaptive Thermal Comfort Chart with Acceptable Levels [9]

2.2. Thermal Comfort Parameters

Thermal comfort is influenced by six factors including two personal and four environmental parameters. The personal parameters are metabolic rate (M), and clothing value (clo) while environmental parameters are namely relative humidity (RH), air velocity (v_a), air temperature (T_a), and the MRT (Figure 2.5) [9, 19].

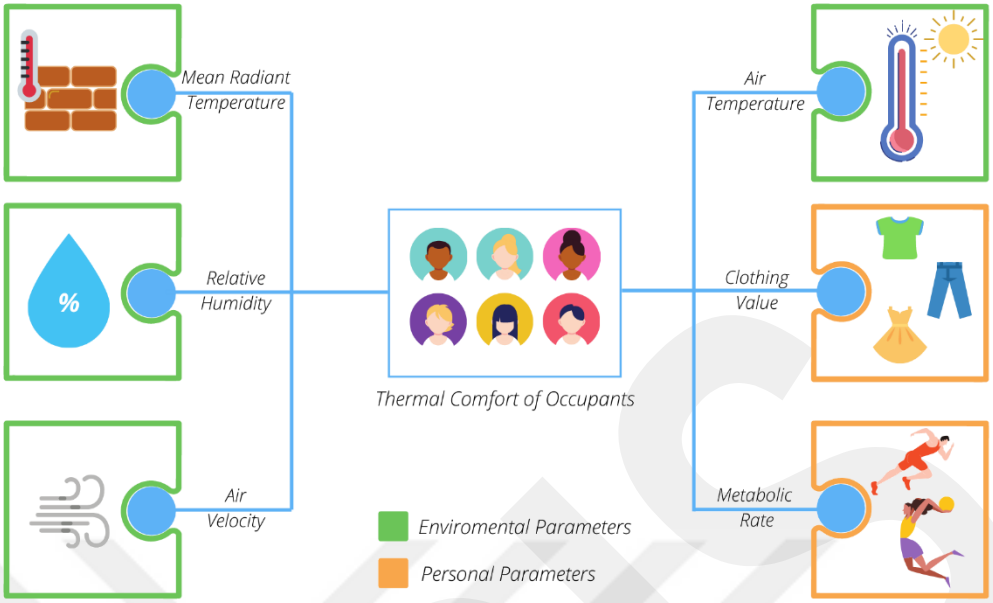

Figure 2.5 Thermal Comfort and Parameters [9]

The sensitivities of personal and environmental parameters are different. The personal parameters are more sensitive than environmental parameters [27]. Specifically, the metabolic rate is the most sensitive parameter which affects thermal comfort [27].

2.2.1. Metabolic Rate (M)

The metabolic rate (M) represents a chemical reaction process in the body in order to produce energy [22]. The amount of produced energy depends on the muscular activities where chemical reactions are converted into heat and released from the body [28]. The metabolic rate is shown in "Met", where 1 Met is equal to 58.15 Watt/m^2 on the body surface [9]. Approximately, a normal adult has a body surface area of 1.7 m^2 [28], and a person with an activity level of 1 Met has a heat loss of 100 Watts. The metabolic rate is the lowest while sleeping activity, which is equal to 0.7 Met, and the highest at sport activities since the muscular activities are increased. When the occupants are more active, the metabolic rate is higher by generating more heat [9]. The average activity level for the last one hour is used to evaluate the metabolic rate, owing to the body's heat capacity [19, 29, 30]. Metabolic rates in typical tasks are depicted in table 2.1.

Table 2.1. Metabolic Rates of Some Regular Tasks [9]

Resting			**Driving/ Flying**		
	Met Units	**W/m2**		**Met Units**	**W/m2**
Sleeping	0.7	40	Automobile	1-2	60-115
Seated, Quiet	1	60	Aircraft, routine	1.2	70
Standing, Relaxed	1.2	70	Aircraft, combat	2.4	140
Miscellaneous Occupational Activities			Heavy Machine	3.2	185
	Met Units	**W/m2**	**Walking (on a level surface)**		
Cooking	1.6-2	95-115		**Met Units**	**W/m2**
House Cleaning	2-3.4	115-200	0.9 m/s	2	115
Pick and Shovel Work	4-4.8	235-280	1.2 m/s	2.6	150
Miscellaneous Leisure Activities			**Office Activities**		
	Met Units	**W/m2**		**Met Units**	**W/m2**
Dancing	2.4-4.4	140-255	Writing	1	55
Tennis	3.6-4	210-270	Typing	1.1	65
Basketball	5-7.6	290-440	Lifting/packing	2.1	120

2.2.2. Clothing Value

The second personal parameter which affects the thermal comfort is clothing, which reduces body heat losses due to the insulation effect [31]. Clothing is classified with the insulation value. The unit of clothing insulation is clo, where 1 clo is equal to 0.155 m^2°C/Watt [9, 31]. For instance, some of the clothing insulation values are given in table 2.2 [9, 31].

Table 2.2. Some Clothing Insulation Values (Clo) [9, 31]

Shoes		**Underwear**		**Shirt & Blouses**	
Sandals	0.02	T-shirt	0.08	Short sleeve, dress shirt	0.12
Leather Shoes	0.08	Full Slip	0.16	Long sleeve, dress shirt	0.25
Sport Shoes	0.12	Long Underwear Top	0.02	Long sleeve, sweatshirt	0.34
Snow Boot	0.2	Long Underwear Bottom	0.15	**Socks**	
Coat		**Sweaters**		Ankles-high athletic socks	0.02
Leather Jacket	0.46	Sleeveless, thin-thick	0.13-0.22	Calf-Length Socks	0.03
Down Jacket	0.69	Long Sleeve, thin-thick	0.25-0.36	Panty Hose	0.02

The entire clothing insulation is the summation of all garments on the human body [9]. For instance, Figure 2.6 depicts a basketball player. A basketball player's clothing value is calculated as the sum of the clothing values of a shirt, shorts, socks, shoes, and underwear.

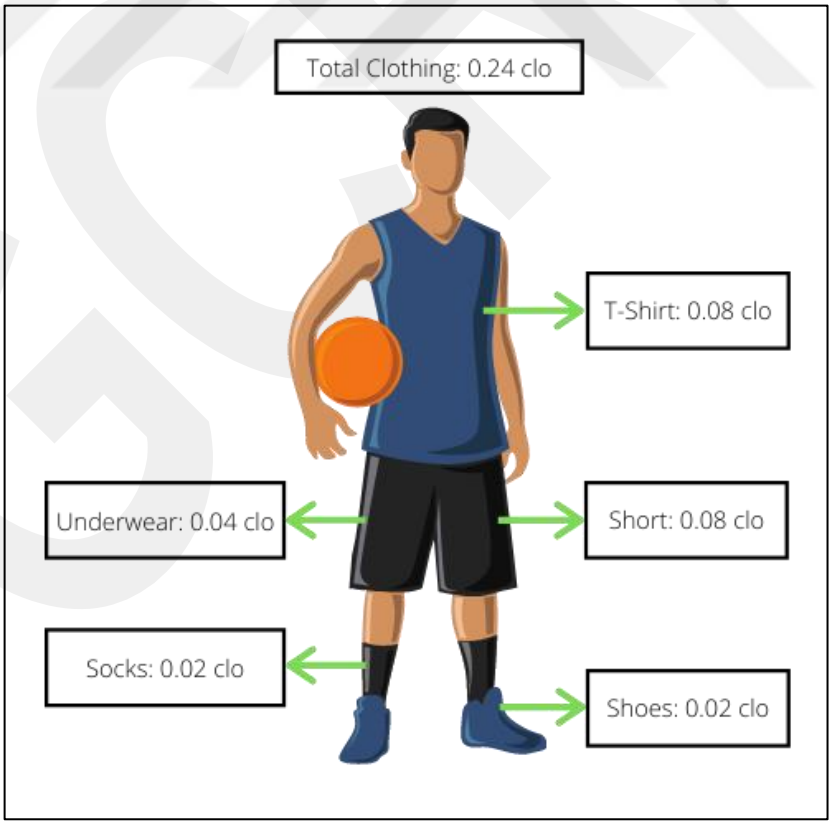

Figure 2.6. An Example of the Calculation of Total Clothing Value

2.2.3. Relative Humidity (RH)

The relative humidity (RH) is the ratio of the amount of water vapour in the air to the maximum amount of water vapour that the air can hold at the specific temperature and the pressure. [9, 19, 32]. Relative humidity can be measured with a relative humidity sensor (Figure 2.7). The standards recommend that the relative humidity should be controlled in a range between 30% and 70% in an indoor environment [33]. High relative humidity values cause lower evaporation and increased skin temperature, which affects the convective heat loss and radiation heat loss from the human body, thus creates an uncomfortable environment for the occupant [34]. On the other hand, occupants do not feel comfortable when the air is exceptionally dry [35].

Figure 2.7. Relative Humidity Sensor [36]

2.2.4. Air Velocity (v_a)

Air velocity (v_a) is described as the air change rate and measured by an anemometer (Figure 2.8). Air velocity impacts the heat loss by convection while air movement in cold environments carries draught on the human body [37]. The accessible limits are described for a person with a Met value of less than 1.2, air-speed should not be greater than 0.25 meters per second according to the ASHRAE Standard 55 [9]. The air velocity accessible limits can be increased by increasing the operative temperature, however, the air velocity should be in between a range of 0.4 m/s to 0.9 m/s between

26°C and 30°C of operative temperatures [38]. Moreover, the adverse effects of increasing indoor temperature on the thermal sensation can be prevented by increasing air speed inside the room by using fans [39].

Fig 2.8. Anemometer [40]

2.2.5. Air Temperature (T_a)

Air temperature (T_a) is the essential parameter since it is the surrounding temperature of the human body and can be measured with various thermometers – such as glass and mercury thermometers, digital thermometers, thermocouples, and infrared thermometers – (Figure 2.9) [37]. The air temperature is directly affected occupant productivity, thermal comfort, and motivation [41- 43]. The optimum temperature range to achieve neutral thermal comfort is between 22°C and 26°C [43].

Figure 2.9. Some Types of Thermometers

2.2.6. Mean Radiant Temperature (MRT)

The mean radiant temperature (MRT) represents another source of heat perception radiation. MRT is defined as "*the temperature of a uniform, black enclosure that exchanges the same amount of heat by radiation with the occupant as the actual enclosure*" in the ASHRAE Standard 55 [9]. Although the MRT is not taken into account as a vital parameter in the thermal comfort studies in the past years, owing to an inadequate number of developments [44- 46], the importance of the MRT to the thermal comfort is studied in some research [47- 50]. Mean radiant temperature is discussed in detail in Chapter 3.

2.3. Parameters and Their Effects on The Thermal Balance Equation

The physiological parameters which affect the thermal comfort are included in the thermal balance equation (Equation 2.1) [22]. Table 2.3 describes the relations between physiological parameters and the thermal balance equation.

Table 2.3. Effect of Physiological Parameters to The Terms in Equation 2.1 [22]

The Terms in Thermal Balance Equation	**Physiological Parameters**					
	M	**Clothing Value**	**T_a**	**v_a**	**MRT**	**RH**
W	X					
C_{res}	X		X			
E_{res}	X					X
C		X	X	X		
R		X			X	

Since the metabolic rate influences breathing and sweating levels, the respiratory convective and evaporative heat loss are also affected. Radiation and convective heat loss can be changed due to the insulation effect of garments [9, 22]. Air temperature plays a significant role in convection heat transfer, directly affecting any convective heat loss. Relative humidity level causes a lower or high evaporation rate; thus, directly influences the evaporative heat loss [22].

CHAPTER 3

MEAN RADIANT TEMPERATURE

Mean Radiant Temperature (MRT) is defined as "*the temperature of a uniform, black enclosure that exchanges the same amount of heat by radiation with the occupant as the actual enclosure*" (Figure 3.1) [9]. Another definition of the MRT is "*the weighted average temperature of the floor, ceiling, and walls*" [1].

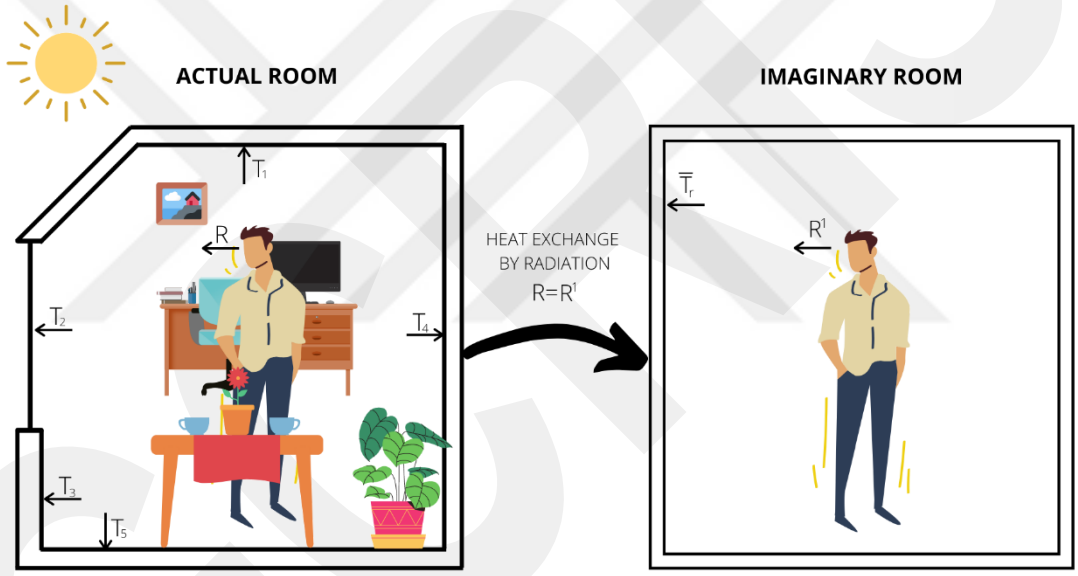

Figure 3.1. Imaginary Enclosure in the MRT Applications

The MRT is the most problematic parameter among the environmental parameters to obtain thermal comfort [51]. While other environmental parameters can easily be measured via low-cost and simple-to-use sensors, determining the MRT requires more high-cost devices and software programs or complex calculation methods or inaccurate assumptions.

The MRT can be obtained by using measurement methods, calculation methods, software programs, and/or assumptions (Figure 3.2).

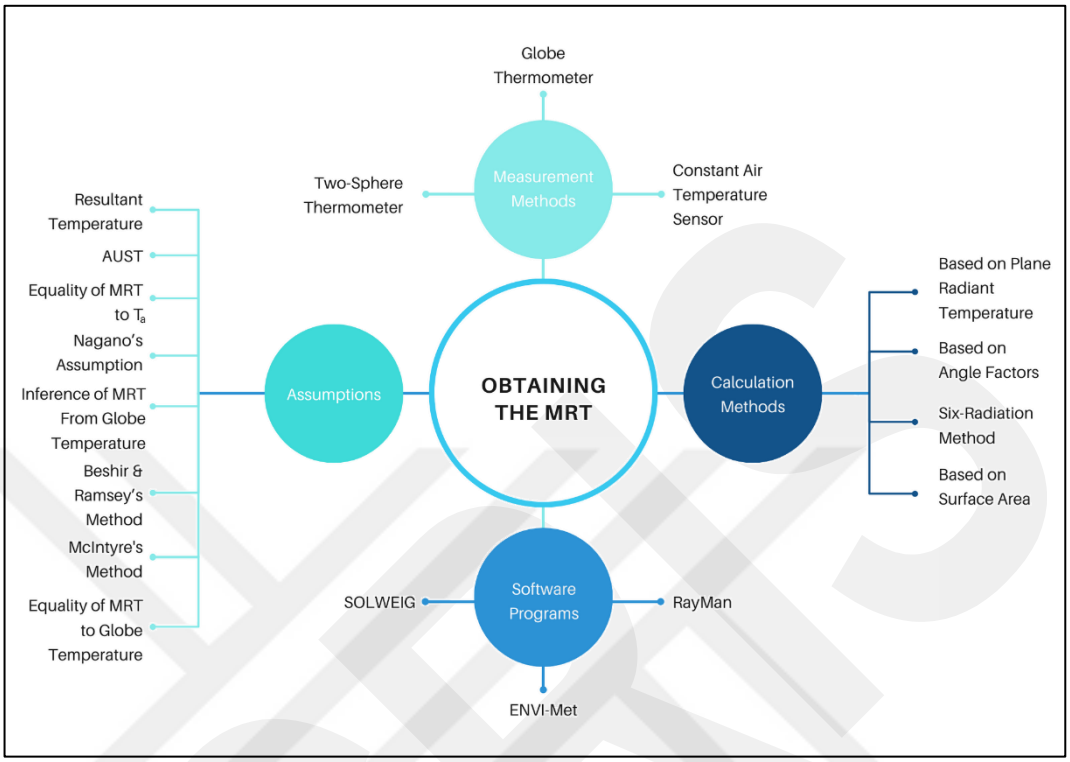

Figure 3.2. Methods to Obtain the MRT

3.1. Measurement Methods

Measurement methods are the most accurate ones to obtain the MRT [51, 52]. ISO 7726 [10] indicates the measurement techniques of whole environmental parameters as well as the MRT. A matt-black globe thermometer, a two-sphere radiometer, and constant air temperature sensors are used as measurement devices for determining the MRT [10].

Globe thermometer (Figure 3.3) is one of the most common measurement methods to obtain the MRT since the device is accessible and easy-to-use [53- 56]. Vernon developed the globe thermometer in 1932 by intending to obtain the MRT for the indoor environment [53]. The standard globe thermometer has a 150 mm diameter, and 0.4 mm thick hollow copper matt-black sphere with a temperature sensor – such as a thermocouple, mercury bulb, etc. – which is located in the centre of the globe.

Despite the fact that the first globe thermometer was developed in 1932, the first applications of globe thermometers for indoor and outdoor environments were in 1970s [57, 58].

Figure 3.3. Outlook of Industrial Globe Probe [59]

Vernon [53] indicated that the response time where the equilibrium is reached between the air inside the globe thermometer and environment should be between 20 to 30 minutes, approximately. The high response time can be decreased by decreasing the globe's diameter since the copper sphere's air volume is smaller. When the globe's diameter reduces, the response time decreases and the accuracy of the globe thermometer decreases since the external surface of the globe, which absorbs the radiation, is smaller [60, 61].

Two-sphere radiometer (Figure 3.4) consists of two spheres with different emissivity, and these devices are generally polished and black in the market. Since the ellipsoid shape is closely matched with the human body, the standards recommend to use ellipsoid shape ones [10, 61]. Both spheres are heated and are subjected to the same loss of convective heat. The heat supply to the black and polished sensor is different

since the black and polished sensor's emissivity values are different, and this difference leads to measuring radiation [61].

Figure 3.4. Two-Sphere Radiometer [62]

Constant air temperature is also revealed as a measurement method to obtain the MRT in the ISO 7726 [10]. The MRT is measured with a sphere or ellipsoid sensor, which is controlled at the same temperature as the surrounding air temperature [61]. Different emissivity values and diameters cause accuracy problems on the measurements [12].

The equations in order to obtain the MRT with measurement methods – globe thermometer, Radiometer, and Constant Air Temperature Sensor – can be found in Table 3.1. Furthermore, the advantages and disadvantages of measurement methods are discussed in Figure 3.5.

Table 3.1. Measurement Techniques to Obtain the MRT [10, 63]

Measurement Devices	**Equations**	**Equation Nu.**	**Abbreviations in Equations**
Globe Thermometer	$MRT = \left[(T_g + 273.15)^4 + \frac{1.1\times10^8\times v_a^{0,6}}{\varepsilon_g {D_g}^{0.4}} \times (T_g - T_a)\right]^{0.25} - 273.15$ (°C)	(3.1)	T_g: Globe Temperature (°C) v_a: Air Velocity (m/s) ε_g: Emissivity of Globe D_g: Diameter of Globe (m) T_a: Air Temperature (°C)
Two-Sphere Radiometer	$MRT = \sqrt[4]{T_s^4 + \frac{P_p - P_b}{\sigma(\varepsilon_b - \varepsilon_p)}}$ (°K)	(3.2)	T_s: Sensor Temperature (°K) P_p: Heat Supply to Polished Sensor (W/m^2) P_b: Heat Supply to the Black Sensor (W/m^2) ε_b: Black Sensor Emissivity ε_p: Polished Sensor Emissivity σ: Stephan-Boltzmann Constant (5.67 × 10^8 W/m^{2}K^4)
Constant Air Temperature Sensor	$MRT = \sqrt[4]{T_s^4 - \frac{P_s}{\sigma\varepsilon_s}}$ (°K)	(3.3)	T_s: Sensor Temperature (°K) P_s: Heat Supply to the Sensor (W/m^2) ε_s: Emissivity of Sensor σ: Stephan-Boltzmann Constant (5.67 × 10^8 W/m^{2}K^4)

	Advantages	Disadvantages
Globe Thermometer	• Easy to Calculate • Direct Measurement of the Thermal Radiation Charge on the Occupant • High Traceability • Easy to find in Market	• High Response Time (20-30 min) • Approximation applied to the Convective and Radiative Heat Transfer coefficients. • Discrete Measurements • Black Globe's emissivity value is different from the represented clothing. (especially in the situation of direct exposition to the solar radiation)
Two Sphere Radiometer (Spherical or Ellipsoidal)	• Compensation of the Convective Thermal Load • Direct Assessment of the Radiative Thermal Load on the Person	• Black Paint and Reflective Sphere Emissivity Values • The Complexity of the Thermostating Loop of the Spheres • Not Enough Widespread • Discrete Measurements
Constant Air Temperature Sensor	• Compensation of the Convective Thermal Load • Direct Estimation of the Radiative Thermal Load on the Occupant	• Uncertain and Variant Emissivity Values of Sensors • The Complexity of the Thermostat Loop of the Spheres (Especially if MRT > T_a) • Not Enough Widespread • Discrete Measurements

Figure 3.5. Advantages and Disadvantages of Measurement Methods to Obtain the MRT [12]

The ISO 7726 [10] indicates that all measurement methods to obtain the MRT should provide the characteristics of instruments. These characteristics are divided into two categories, depending on the thermal environment type, for moderate environments– Class C (comfort) – and for severe (extreme cold/or hot) environments – Class S (stress). The required and desirable accuracies for measurement devices are specified for the MRT measurements between 10°C and 40°C as ± 2°C and ± 0.2°C respectively in moderate environments (Class C) [10].

3.2. Calculation Methods

The another most used technique to obtain the MRT is calculation methods. Four different calculation methods are existed in the literature, namely calculation method with plane radiant temperatures, the calculation method based on angle factors, which is the most frequently utilized calculation method in researchers, six-radiation method,

which considers long-wave and short-wave radiation in same priority, and calculation based on surface areas [51, 52, 64- 73].

The Plane Radiant Temperature (PRT), which is used in the calculation of the radiant asymmetry, is described as "*the uniform surface temperature of an enclosure in which the incident radiant flux on one side of a small plane element is the same as in the actual environment*" [10, 64]. This method admits a standing or seated person without acknowledging the location of the occupant. The MRT can be calculated for a standing or a seated person by using PRTs with equation 3.4 and 3.5, respectively.

$$MRT_{standing} = 0.08\left[PRT_{up} + PRT_{down}\right] + 0.23\left[PRT_{left} + PRT_{right}\right] + 0.35\left[PRT_{front} + PRT_{back}\right]/[2 \times (0.08 + 0.23 + 0.35)]\ (°C) \quad (3.4)$$

$$MRT_{seated} = 0.18\left[PRT_{up} + PRT_{down}\right] + 0.22\left[PRT_{left} + PRT_{right}\right] + 0.30\left[PRT_{front} + PRT_{back}\right]/[2 \times (0.18 + 0.22 + 0.30)]\ (°C) \quad (3.5)$$

The PRT is not included in the thesis, thus, more information can be found about the PRT in the [12, 65- 67].

One of the alternative calculation methods to acquire the MRT is a calculation method based on angle factors. Angle factors represent the radiation heat fluxes between both the human body and the environment [10]. This method considers both location (seated and standing) and position of a person and assumes the shape, size, and relative positions of surfaces in relation to the person. The approach is difficult and time-consuming as it needs at least 24 calculations describing four faces per side for the six surfaces surrounding the occupant [68- 70]. The angle factors can be calculated by equations 3.6, 3.7, and 3.8, with constant values which are depicted in table 3.2 [10, 11]. Moreover, the ISO 7726 [10] gives some graphs to effortlessly estimate angle factors (Figures 3.6 to 3.9).

$$F_{max}(1 - e^{-(a/c)/\tau})(1 - e^{-(b/c)/\gamma}) \quad (3.6)$$

$$\tau = A + B(a/c) \quad (3.7)$$

$$\gamma = C + D(b/c) + E(a/c) \tag{3.8}$$

Table 3.2. Constant Table for Equations 3.6, 3.7 and 3,8 [10, 11]

	F_{max}	A	B	C	D	E
Seated Person (Wall & Window)	0.118	1.216	0.169	0.717	0.087	0.052
Seated Person (Floor & Ceiling)	0.116	1.396	0.130	0.951	0.080	0.055
Standing Person (Wall & Window)	0.120	1.242	0.167	0.616	0.082	0.051
Standing Person (Floor & Ceiling)	0.116	1.595	0.128	1.226	0.046	0.044

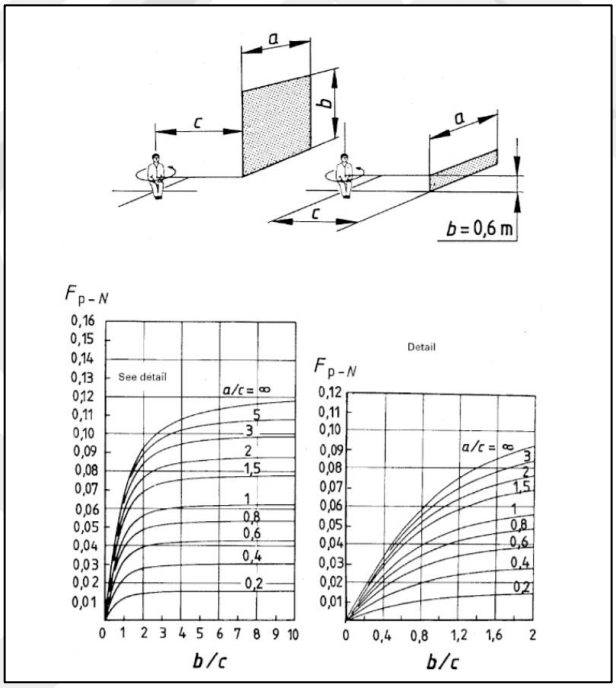

Figure 3.6 Angle Factors for the Seated Person for Vertical Surfaces [10, 11]

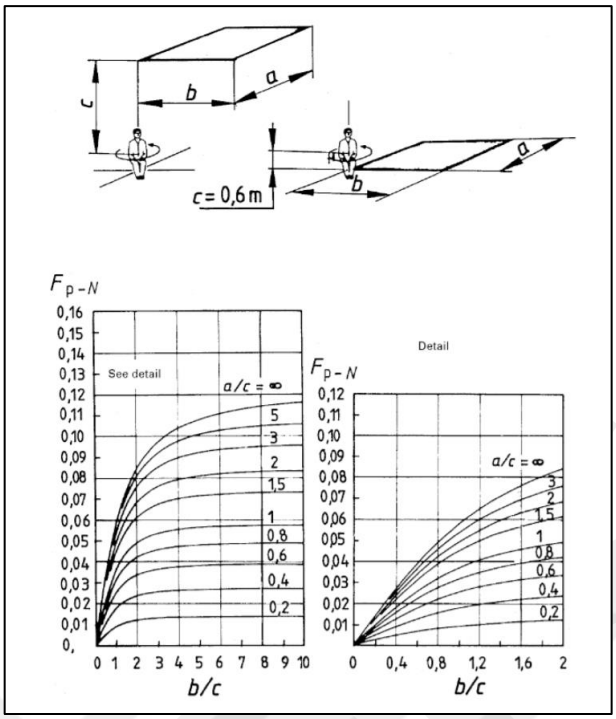

Figure 3.7. Angle Factors for the Seated Person for Ceiling and Floor [10, 11]

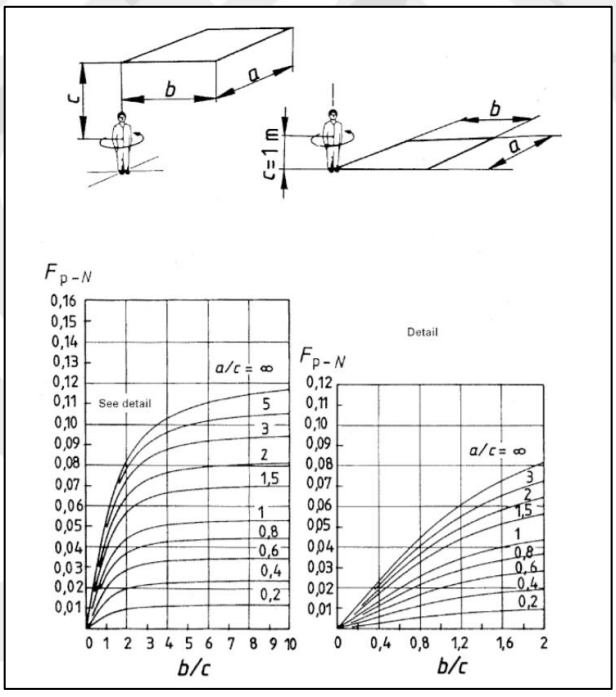

Figure 3.8. Angle Factors for the Standing Person for Ceiling and Floor [10, 11]

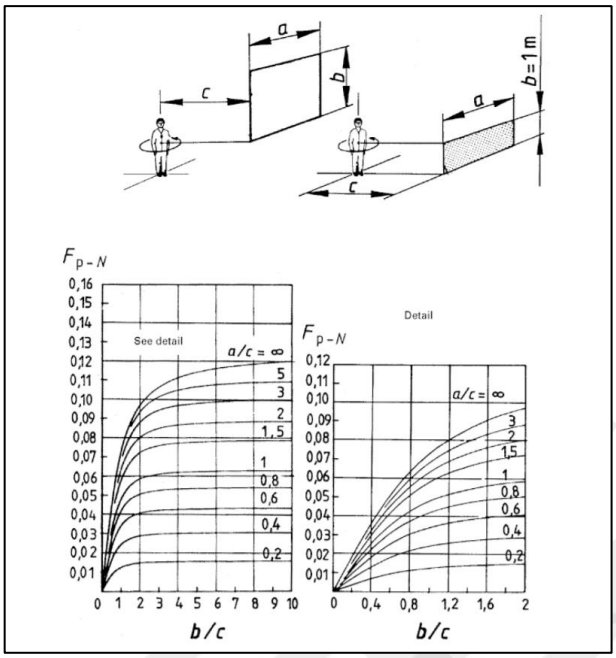

Figure 3.9. Angle Factors for the Standing person for Vertical Surfaces [10, 11]

After finding the angle factors, the MRT can be obtained with equation 3.9 [12].

$$MRT = \left[\sum_{i}^{n} F_{p-i} T_i\right] = T_1 F_{p-1} + T_2 F_{p-2} + \cdots + T_n F_{p-n} \qquad (3.9)$$

Here, T_n is the nth surface temperature (°C) and F_{p-n} represents the angle factor between nth surface and occupant [12].

Another calculation method is the six-radiation method, which is generally used in outdoor applications and where both the short-wave and long-wave radiations are essential. The six-radiation method assumes the occupant body as a uniform cylinder. The method considers the absorbed radiation flux through the occupant body that can be found by using Equation 3.10 with the aid of a net radiometer (Figure 3.10), which is used to measure radiation fluxes from six perpendicular directions at the same time [71, 72]. It is worth to note that the net radiometers for the direct measurement of the MRT are very expensive and require the usage of more sensors or measurements in the directions for the calculation of the plane radiant temperature values.

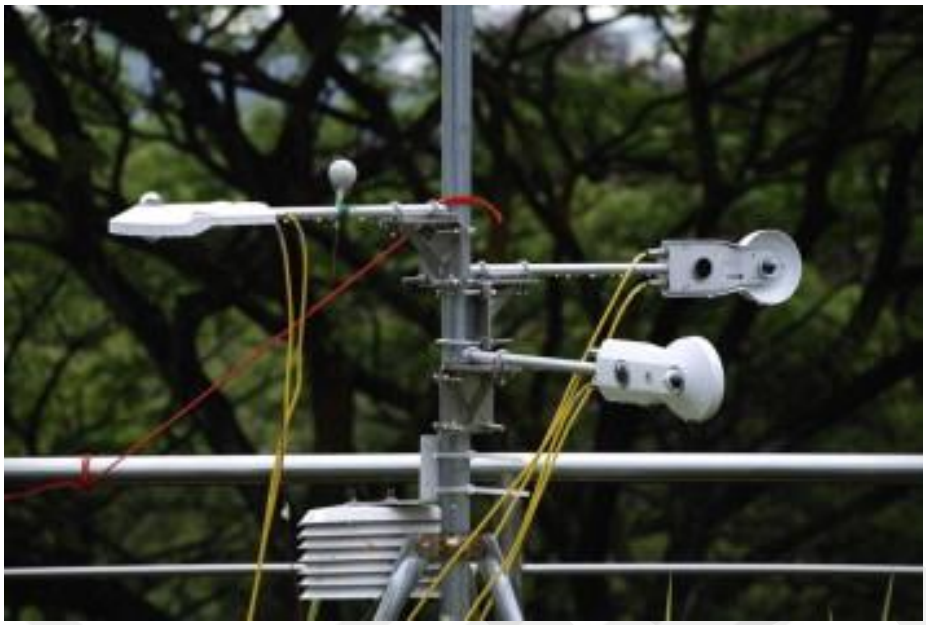

Figure 3.10. A Net Radiometer [55]

$$S_{str} = \sum_{i=1}^{6} F_i \times (a_k K_i + a_l L_i) \quad (3.10)$$

where S_{str} represents radiation flux (W/m^2), which is absorbed by the human body, F_i defines angle factors, a_k and a_l signifies the coefficient of general absorption for short-wave and long-wave radiation, respectively, K_i and L_i defines the short-wave (λ=0.3 – 3μm) and long-wave (λ= 3 – 100μm) radiation at six directions, respectively. Absorption coefficients a_k and a_l is shown in table 3.3 [51, 52].

Table 3.3. Short-wave and Long-wave Absorption Coefficients [51, 52]

Absorption Coefficients	**Skin**	**Clothing**	**Standard Value**
$\boldsymbol{a_l}$	0.99	0.95	0.97
$\boldsymbol{a_k}$	0.55-0.85	0.4-0.9	0.7

Once found the S_{str}, the MRT can be obtained with Equation 3.11.

$$MRT = \left({S_{str}}/{\varepsilon_{hs}\sigma}\right)^{0.25} - 273.2\ (°C) \quad (3.11)$$

where ε_{hs} defines the emissivity coefficient of human skin (0.95) [71], and σ is Stephan-Boltzmann constant (5.67×10^8 W/m^{2}K^4) [71].

The last calculation method to obtain the MRT is the calculation method based on the surface areas method. The technique utilizes surrounding surfaces instead of angle factors and based on the weighted average of surface temperatures. Thus, the position (seated or standing) and the occupant's location is not considered in this method. The MRT can be found using this method via Equation 3.12 [1, 54, 73].

$$MRT = \frac{T_1 A_1 + T_2 A_2 + \cdots + T_n A_n}{A_1 + A_2 + \cdots + A_n} \tag{3.12}$$

Here, T_n is the nth surface average temperature (°C), and A_n signifies the area of the nth surface (m^2).

3.3. Software Programs

MRT can be obtained through modelling and simulating the environment with software programs which are frequently used for outdoor applications. RayMan, ENVI-Met and SOLWEIG (Solar and Long-Wave Environmental Irradiance Geometry) are commonly used programmes to obtain the MRT [74- 80].

Since its user-friendly interface and availability for free usage, the RayMan is widely used to obtain the MRT among researchers who work in urban planning and thermal comfort fields [74- 76]. The RayMan simulates and computes the MRT based upon the temporal specification, geographical location, meteorological and morphological input, and topographical data [75, 76]. Furthermore, the RayMan calculates the MRT at street level with a point approach.

The ENVI-Met is another software program which is used for outdoor environment of different urban design options [77, 78]. The ENVI-Met simulates the interaction of surface, plants, and air-based on a detailed 3D computational fluid dynamic and energy

balance model in the outdoor environment. On the contrary of the RayMan, the ENVI-met calculates a surface approach to obtain the MRT at the street level.

Both the RayMan and the ENVI-Met calculate the MRT at a street level according to Fanger's [19, 51] concept. The surroundings are divided into several divisions (free atmosphere, various building surfaces and the ground surface) for which the direct, diffuse, and diffusely reflected short-wave and the emitted long-wave radiation components are taken into account. At street level, the long-wave radiation fluxes are assumed one-half from sky and buildings and one-half from the ground [79]. Nevertheless, in complex urban conditions, the long-wave radiation absorbed by the standing body starts largely from the surrounding walls; thus, it is crucial to consider the side directions for more reliable estimation of the MRT.

The SOLWEIG model simulates the MRT based on surface morphology, geographical information (altitude and coordinates) and meteorological parameters (air temperature, relative humidity, global short-wave radiation) [79, 80]. The high-resolution digital elevation models (DEMs) are represented to model complex outdoor surface morphology in the SOLWEIG, and the SOLWEIG can manage extensive domains. [79, 80]. The most important benefit of the SOLWEIG is to overcome with low sun elevation angles that produce problems during using the RayMan [79, 80].

3.4. Assumptions

The difficulties and disadvantages of the measurement and calculation methods to obtain the MRT have forced researchers to prefer uncomplicated assumptions. These assumptions are generally derived from statistical studies or equalities [81- 84]. The most popular assumption is the equality of MRT to T_a [81, 82]. The assumptions which are used in the studies are depicted in Table 3.4.

Table 3.4. List of Assumptions to Obtain the MRT

Assumption Name	**Formula**	**Eq. Number**	**References**
Resultant Temperature	$MRT = 2T_o - T_a$ where T_o=T_g [48, 85] and v_a<0.2 m/s	(3.13)	[17, 54]
AUST (Average Uncontrolled Surface Temperature) (MRT)	$MRT = T_{air} - \frac{7c}{T_{out} - 45}$ *c=0.5 in without outdoor exposure* *c=1 in one side exposed fenestration <5%* *c=2 in one side exposed fenestration >5%* $T_{out} < 45°C$	(3.14)	[83, 86]
Equality of MRT to T_a	$MRT = T_a$	(3.15)	[9, 87- 90]
Nagano's Assumption	$MRT = 0.99T_a - 0.01$	(3.16)	[84, 91]
Inference of MRT From Globe Temperature	$T_g = \frac{MRT + 2{,}35 * T_{air} {v_a}^{0.5}}{1 + 2{,}35 * {v_a}^{0.5}}$ $MRT = T_g + 2{,}35 * {v_a}^{0.5}(T_g - T_a)$ $MRT = 1.75T_g - 0.75T_a$ $(if\ v_a = 0.1\ m/s)$	(3.17)	[92, 93]
Beshir and Ramsey's Method	$MRT = T_g + 1.8{v_a}^{0.5}(T_g - T_a)$	(3.18)	[95, 96]
McIntyre's Method	$MRT = T_g + 2.44{v_a}^{0.5}(T_g - T_a)$	(3.19)	[67, 96- 99]
Equality of MRT to T_g	$MRT = T_g$	(3.20)	[100, 101]

Even though the assumptions are used because of their simplicity, these assumptions' accuracy is still doubtful. A comprehensive comparison of these assumptions with in-situ measurements is needed.

CHAPTER 4

LITERATURE REVIEW

This chapter includes a detailed literature review about the MRT by considering the indoor and outdoor environment studies, respectively. Since the thesis topic is related with the indoor environments, the studies on outdoor environments are given in the first instance.

4.1. Outdoor Environment

Herrmann and Matzarakis, [102] utilized the effect of urban configuration on the MRT by using the RayMan software and represented with Climate-Tourism/Transfer-Information-Scheme (CTIS). The MRT data was collected based on data from the urban climate station for the period from 1 September 1999 to 31 December 2009. The study clarified that the MRT was affected by urban configuration because of the changes in the radiative fluxes. The width, height, and orientation of an urban canyon were found as vital for the assessment of specific thermal bioclimatic conditions (Figure 4.1) [102].

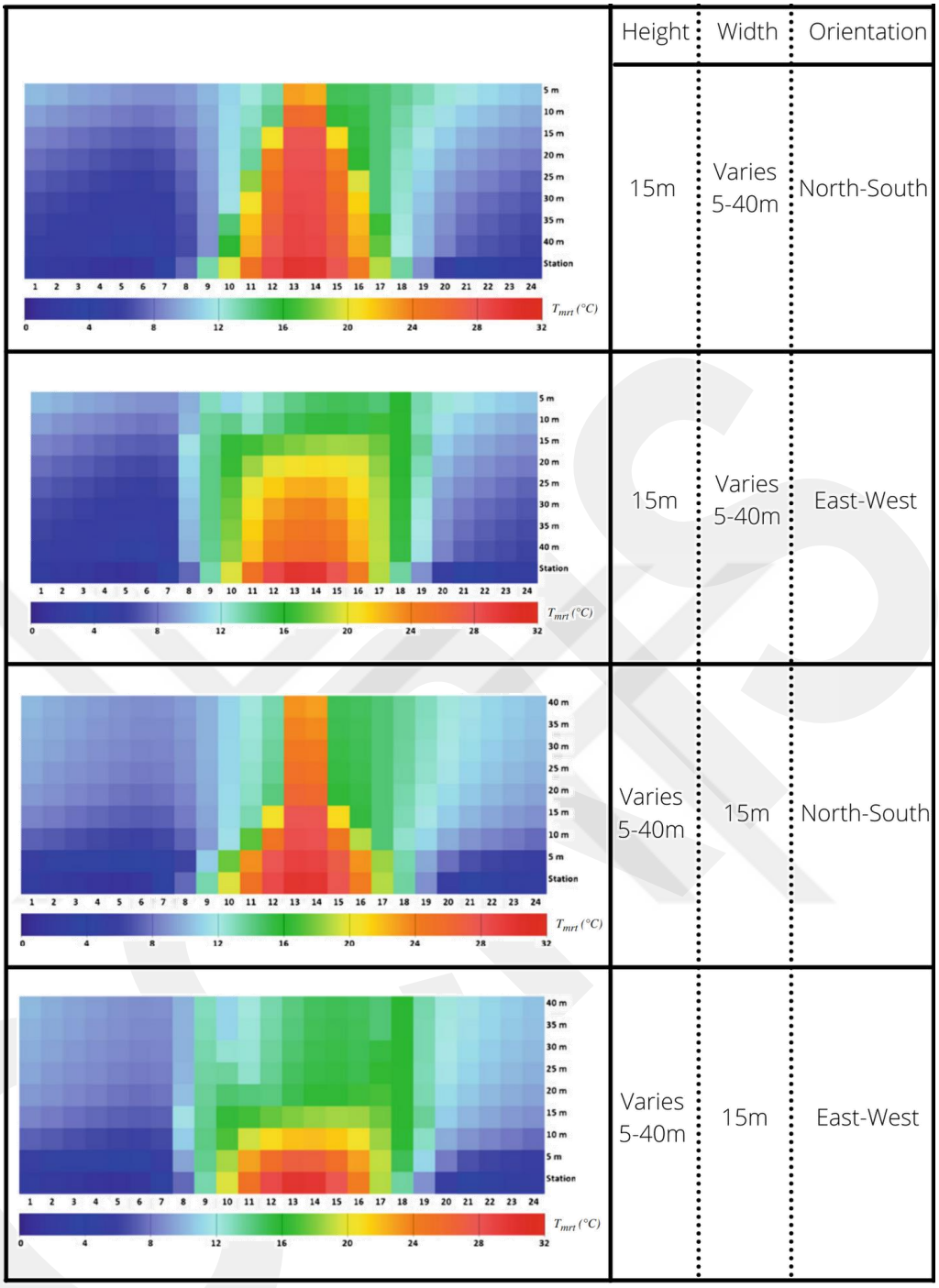

Figure 4.1. The MRT distribution in different heights, widths, and orientations in an urban canyon in a study of Herrmann and Matzarakis [102]

Thorsson et al. [76] compared the MRT values by utilizing different aspects to get the MRT, which were 38 mm Globe Thermometer, the Rayman Software v1.2, and the six-radiation method. It should be noted that, in this study, the angle factors were taken from the study of Höppe [52] instead of calculating them. The results revealed that

even though the difference between the three methods was small in clear summer conditions (26 July 2006), the difference between the three methods was increasing in the autumn season (11 October 2005). The difference between the 38mm grey globe thermometer, with applied mean convection coefficient to get more accurate results, and the six-radiation method was relatively small. However, the RayMan application underestimates the MRT values in the morning, afternoon, and at low sun elevations in general.

Chen et al. [71] compared the MRT values with different computer programs, which are the Rayman, the SOLVEIG, and the ENVI-met in the outdoor environment via using the six-radiation method and black globe thermometer. After the experiment was conducted, the authors compared the MRT values stemmed from the globe thermometer and the six-radiation method for the outdoor environment. After applying a regression analysis between them, the authors found R values for clear and cloudy sky conditions as 0.55 and 0.71, respectively. On the side of software programs, for one-dimensional calculations, the RayMan and for two-dimensional calculations, the SOLVEIG was giving the best accurate results, among others. R values were found as 0.90 for RayMan, 0.25 for ENVI-Met and 0.57 for SOLWEIG by comparing the simulated MRTs with calculated ones [71].

Marino et al. [103] compared the MRT values using a black globe thermometer and applying the six-radiation method in the outdoor environment for 15 days to determine the globe thermometer was an option or not for the outdoor environment. In this experiment, the average MRT values that stemmed in the globe thermometer in 10 minutes were considered instead of individual data. The results indicate that there is a minor difference between the MRT values stemmed from the black globe thermometer and the six-radiation method (R^2= 0.9867).

Al-Hafith et al. [92] investigated the effect of courtyard geometry on the MRT and the globe temperature with different areas, width-length ratios, heights, and courtyard orientation forms in Baghdad using ENVI-met and IES-VE simulation tools. The results have illustrated that the difference in conditions of courtyards may lead to the difference between the globe temperature and the MRT up to 15°C.

Tan et al. [55] compared the six-radiation method and 40mm grey globe thermometer in the urban environment to identify the effect of nature on the MRT in a tropical outdoor climate. The results extrapolate that in both calculation and measurement methods, greeneries, such as trees and shrubs, and large water bodies, like lakes, significantly affect the MRT during the all-day instead of after nightfall. The authors indicated that urban design is used to regulate the MRT in outdoor environments.

Fischereit [104] introduced an open-source and modular Simple Urban Radiation Model (SURM) to obtain the MRT in the outdoor environment. The SURM was validated using the six-radiation method and the calculation based on the angle factor in sunny conditions, which has the highest heat stress, for simple urban system models. The results revealed that the SURM might be an option for simple urban systems by introducing accurate results. The Complex urban systems and cloudy weather conditions can be adjusted since the SURM can be easily altered since the SURM is a modular and open source. For example, both the algorithm, which Reindl et al. [105] developed and the clearness index that Staiger [106] advised might be used to simulate cloudy weather conditions.

Tan et al. [107] investigated the effects of installation of vertical greenery on to the MRT for the outdoor environment. The measurements were conducted in 2 different walls, which have two different systems – Suntory Midorie System and Shimizu Parabienta System –, different values of Leaf Area Index (one of urban greenery classification), different dimensions and various types of plants used (Figure 4.2). The detailed explanations of systems can be found in [107]. The results indicated that greenery implementation to the wall has affected and reduced fluctuations of surface temperature and the MRT significantly during the day, both in the morning and at night. The highest MRT difference between the wall, where the implementation of greenery is available or not, was found at 12.9°C [107].

Figure 4.2. Measurement setup of the study of Tan et al. [107]

4.2. Indoor Environment

Dave et al. [82] conducted an experiment to clarify the difference between the MRT and T_a in different places, climate zones and building types. The authors found the median absolute difference as 0.4°C between the MRT and T_a. On the basis of their findings, the authors suggested that for cooling systems, the operative temperature sensor was not needed owing to the MRT is nearly equal to the indoor air temperature [82].

Walikewitz et al. [108] used three different globe thermometers, with different surface colours, which caused the different emissivity values and diameters, and six-radiation method for sitting & standing person were compared to reach the relationship between air and mean radiant temperature in a university building. The authors indicated that the difference between the MRT and T_a exceeds up to 1.3°C according to air temperature. Moreover, the authors identified that if the T_a and MRT are taken equal, this equality gives wrong results for considering human health in summer conditions due to the possibility of underestimating heat stress [108].

Yoo [109] developed the MRT calculation method into rectangular and non-rectangular geometries. Rooms which have different wall temperatures, shapes, and window sizes were used to see the effectiveness. As a result, the author developed a new method and computer program, namely "COMFORT" for the MRT calculation in a non-rectangular space. The distribution of the MRT is implemented as a boundary condition function of a model room and its shape.

Kalmár and Kalmár [110] conducted a comprehensive experiment about the relation between room geometry with the MRT in several heights between 2.5 m and 4 m and two different occupant positions (Figure 4.3) in the room. In this study, the MRT values found using the calculation method based on angle factors, used to compare the room geometry. In the final of the study, the globe thermometer was used to obtain the MRT values to analogize with the MRT, which was obtained via calculation method. The results indicated that the MRT has a parabolic variation with dimensions of the room, and the MRT affected by the occupant's position, and external temperature. For instance, in a room with 3 m width and 6 m length, while the MRT found nearly 20°C in 2.5 m height, it was approximately 22°C in a height level of 4 m in 5°C constant external temperature. Moreover, the different position gave different MRT values in the same condition since the angle factors changed. Consequently, the authors compared the measured and calculated MRT results for rooms which have 3.2 m height and 6 m width and different room lengths. When the calculated MRT values were generally higher than the measured MRT values for position 1, it was the opposite for position 2 (Figure 4.4) [110].

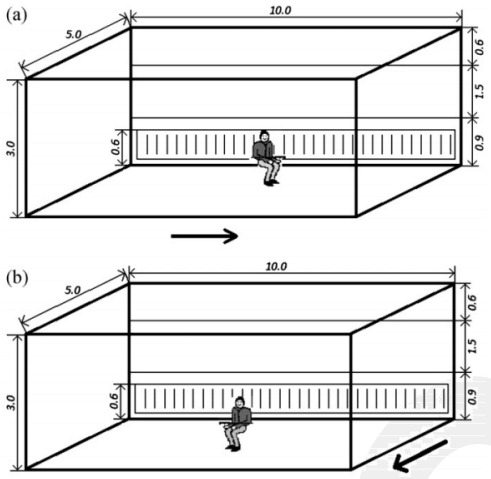

Figure 4.3. The occupant positions in the study of Kalmár and Kalmár (where a and b represent the position 1 and 2, respectively) [110]

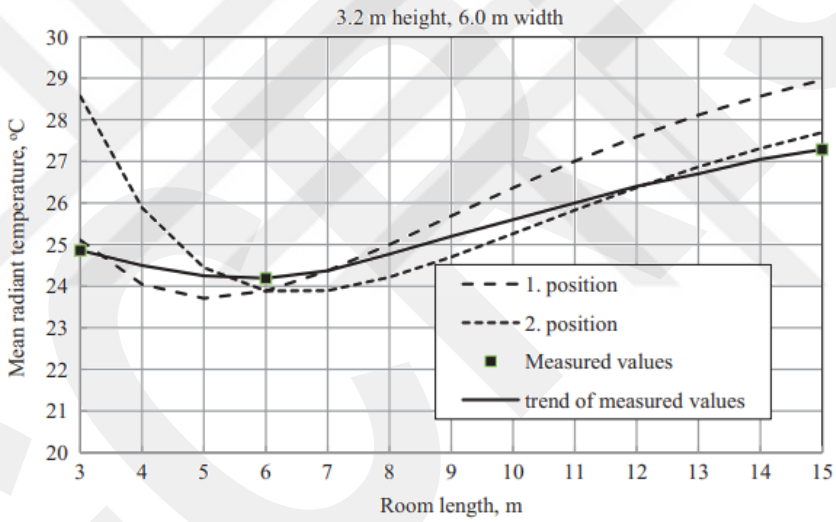

Figure 4.4 Result of the Calculated and Measured MRT values in different positions and room length in a study of Kalmár and Kalmár [110]

Aviv et al. [111] explained that the MRT distribution might be dissimilar in places due to the differences in room geometry and properties of the wall materials. To regulate uniform MRT distribution and achieve different conditions for each occupant, locating different room locations, the authors created a piping system in a room and created a 3D simulation to examine the consequences of configuration for the MRT. In this research, the MRT values were compared and verified with the black globe thermometer. The experiment results showed that it is possible to create different

conditions in different locations in the room to achieve thermal comfort of occupants. The finding of the research helped to minimize energy consumption in the buildings. The MRT difference between coldest and hottest points in the room was found 6°C in 3D simulation and 3°C in black globe thermometer, respectively. Moreover, the authors also indicated that the heat source location significantly affected the MRT and occupant thermal comfort and the problem might be solved by climatizing the room locations separately by the well-design piping system in the room [111].

Xing and Li [112] created a three-dimensional heat transfer model for globe thermometers by using Computational Fluid Dynamics (CFD) coupled with Finite Element Analysis (FEA). After validating the theoretical model with literature, the model was used to compare several globe thermometers with different shell material and diameters to compare their thermal behaviour in radiant cooling indoor environments. The study revealed that the diameter of the globe thermometer might affect the globe temperature related to shell material. While comprising of metal globe thermometers, with 50 mm and 150 mm diameters, respectively, the temperature difference between globe temperatures was found 0.01°C; the difference was found 1.2°C for acrylic globe thermometers (Figure 4.5), which had the same diameter as metal ones since the acrylic has low thermal conductivity value. Moreover, while the air temperature at the centre of the 150 mm acrylic globe thermometer was 26.26°C, it was 25.9ºC for metal globe thermometers. [112].

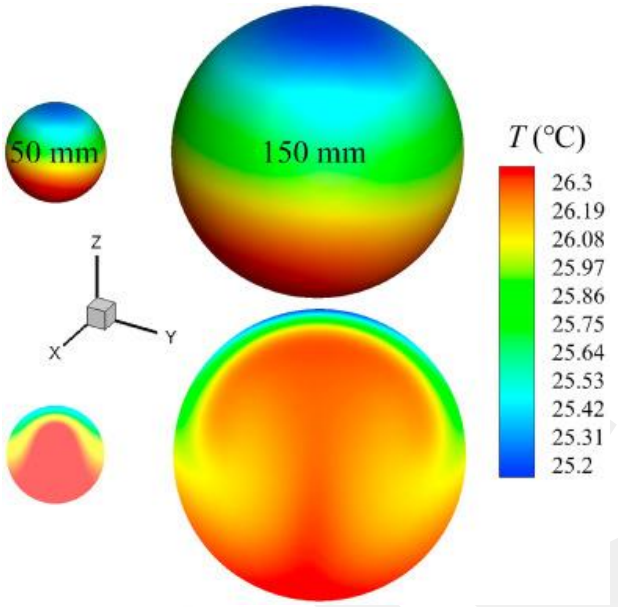

Figure 4.5. Temperature contour plot for acrylic globe thermometers in the study of Xing and Li [112]

Turhan [113] performed an experiment in order to compare the energy consumption and thermal comfort values of two HVAC systems, which were driven based on operative temperature and T_a in a university office building by collecting the thermal sensation vote from occupants via a developed mobile application. The results showed that operative temperature driven controlled HVAC device satisfied more comfortable environment while the energy consumption was slightly higher. In other words, the study demonstrated the importance of the MRT to achieve thermal comfort [113].

Guo et al. [68] evaluated the T_a and the MRT values at a high spatial resolution by using measurement - by using calculation method based on angle factors – and simulation technique – via ANSYS Fluent – for a radiant heated workshop. The study showed that the T_i and the MRT were considerably affected by outdoor temperature. The MRT in the workshop varies more than T_a since the difference between T_a and surrounding walls. While the T_a variation was between ±2°C, the MRT changed up to 8°C inside the given environment [68].

Simone and Olesen [114] conducted an experimental study to find out the effect of thermal exchange between the human body and its environment by creating three different experimental chambers, which considered T_a>MRT, T_a<MRT, T_a=MRT. The

study proved that using the equality of the MRT and T_a in thermal comfort studies caused up to a 1-point error in the thermal sensation scale [114].

Gan [50] analyzed the effect of glazing on the MRT and thermal comfort. In this study, the MRT values were calculated by using the calculation method with plane radiant temperatures. The study indicated that the unbalanced and/or various MRT distribution (radiant asymmetry) causes a decrease in thermal comfort. Moreover, the rectangular windows providing better thermal comfort instead of square windows. Furthermore, using a double-glazing window reduce the radiant asymmetry and thermal discomfort [50].

Gan [73] developed a computer program to determine the thermal comfort in mechanically ventilated environments by using Computational Fluid Dynamics (CFD). Airflow was modelled by using Semi-Implicit Method for Pressure-Linked Equation (SIMPLE) [115] algorithm with the staggered grid; momentum equations were solved with Quadratic Upstream Interpolation for Convective Kinematics (QUICK) [116] scheme and the MRT found by using calculation of plane radiant temperature, calculation method based on angle factors, and calculation method based on the surface areas method. The results revealed that taking MRT distribution as a uniform causes an error in PPD up to 7.5% and the prediction became worse when T_a=MRT. Moreover, the difference between calculation method based on angle factors and calculation method based on the surface areas method found smaller than 0.1°C due to small difference (< 10°C) between room surface temperature [73].

Han et al. [117] constructed a MRT regression model to determine the ideal cooling set-point temperature of HVAC systems for office buildings in summer conditions. This model was created by considering T_a, T_{out}, weather conditions, and time, resulting in a R^2 value of 0.936, which satisfied ASHRAE Guideline 14 [118]. Moreover, the implementation of the MRT for the set-point temperature of the HVAC system improved thermal comfort by 38.5%. Furthermore, the found regression equation was shown as Equation 4.1.

$$MRT = 6.382 + 0.914T_a + 0.086T_{out} - 1.060ST - 0.712Time_{sin} - 0.459Time_{cos} \quad (4.1)$$

Here, the ST defines the sky type, $Time_{sin}$ and $Time_{cos}$ are represented sin θ of time and cos θ of time, respectively. More details can be found in [117].

Lee et al. [119] proposed a new measurement method to obtain the MRT in large spaces via an infrared thermal imaging camera (IR camera). A large dome stadium with a closed space in Seoul, Korea, was selected as a case study. The developed measurement method included calculated angle factors by using a simplified model of stadium and mean indoor surface temperatures and confirmed with the globe thermometer measurement method. The methodology of the study is depicted in Figure 4.6. The results showed that the MRT difference between the new method and the globe temperature was less than 1°C. Moreover, the IR camera showed that the surface temperatures could differ with location and orientation [119].

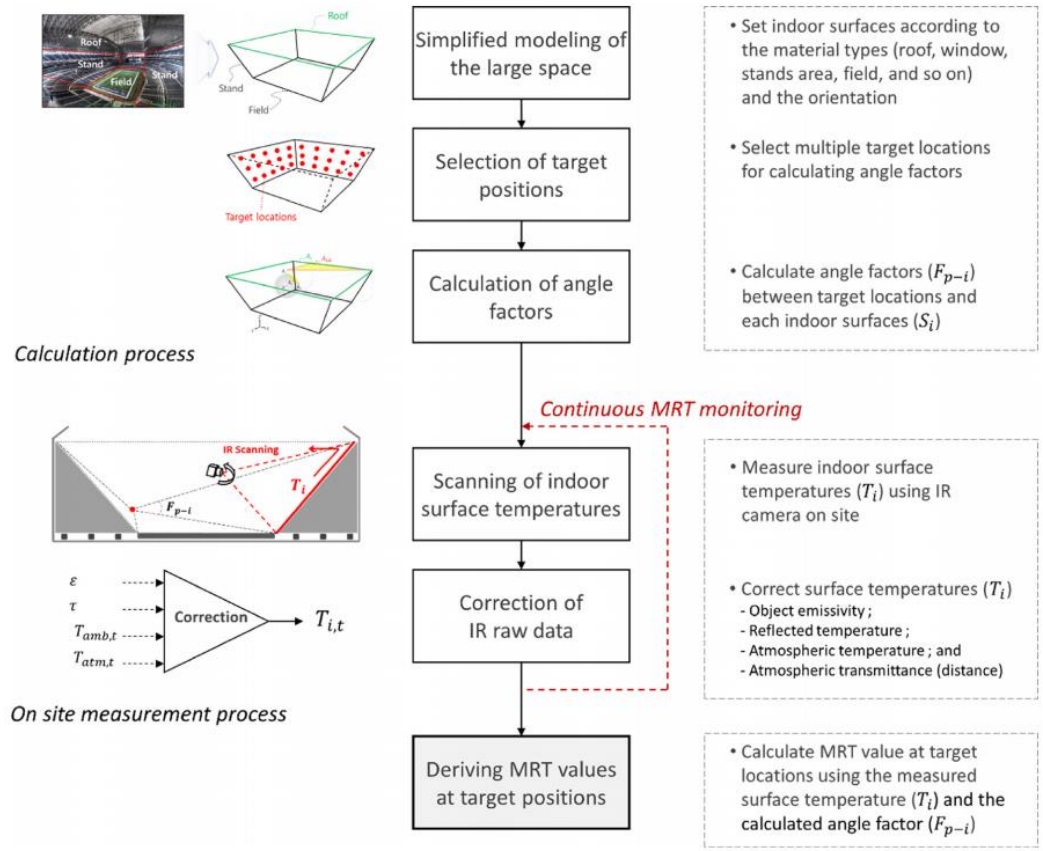

Figure 4.6. The IR scanning system which estimates the MRT values in a Stadium in the study of Lee et al. [119]

Alfano et al. [12] investigated different measurement and calculation methods to obtain the MRT by encountering the international standard requirements (ISO 7726[10]). The comparison was made with obtained MRT values from;

- Globe thermometer (Taken as a reference)
- Calculation method based on view factors (by using different instruments to determine the wall temperatures, which are thermocouples, thermal-camera, infrared thermometer)
- Calculation method based on plane radiant temperatures by using Net Radiometer

In order to compare these methods, the authors created a special test chamber, which represented in Figure 4.7 with the experimental setup. The authors examined the MRT differences by applying the plate temperature as 10°C and 40°C. The results revealed that while the biggest differences occurred between reference with obtained MRT by using net radiometers (up to 4°C), the calculation method based on view factors was the closest one (<1°C). Since the thermal camera has a better spatial resolution and the possibility to adjust the emissivity of the measurement surface [120], the thermal camera was given the closest results with the reference values in an aspect of determining wall temperatures. Moreover, the error between the MRT values by obtaining with different methods was increasing by increasing the MRT temperature. Lastly, the authors remarked that the consequences of thermal environment assessment often appear ambiguous since the variation between the MRT values [12].

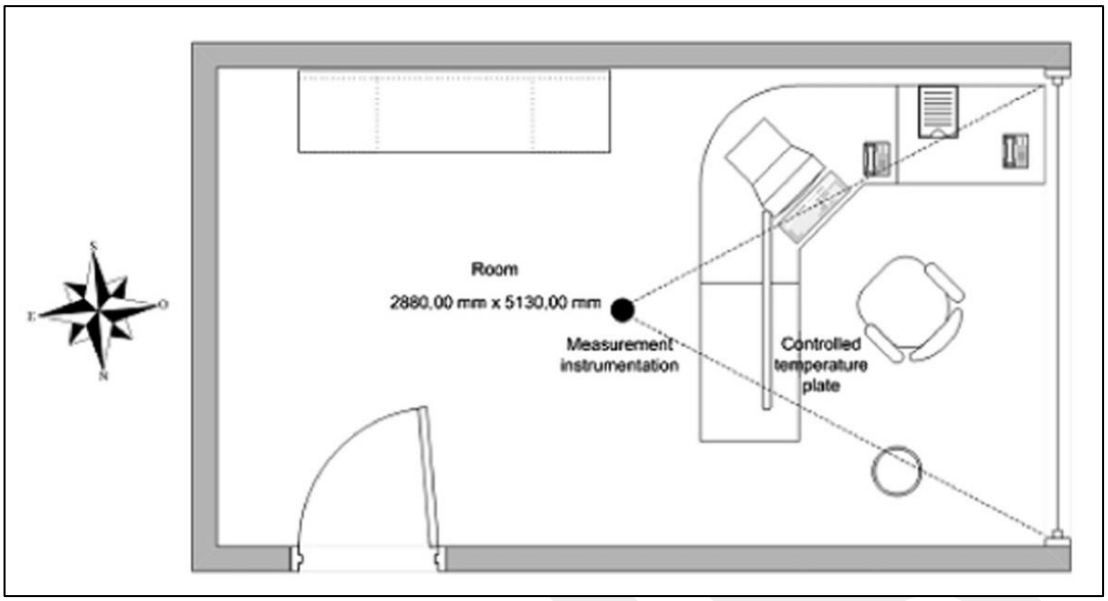

Figure 4.7. Created Test Chamber and experimental setup of study of Alfano et al. [12]

The aim of the thesis is to find and compare the accuracy of assumptions to obtain the MRT – which not existed in the literature – by comparing the measurement method – which is described as the most accurate method [51, 52] – of globe thermometer.

CHAPTER 5

METHODOLOGY

The methodology of the thesis includes six different sub-sections: definition of the case building, development of a new globe thermometer, calculation of angle factors for the case building, measurement campaign, methods to obtain the MRT, and comparison of the results. Figure 5.1 illustrates the methodology of the thesis.

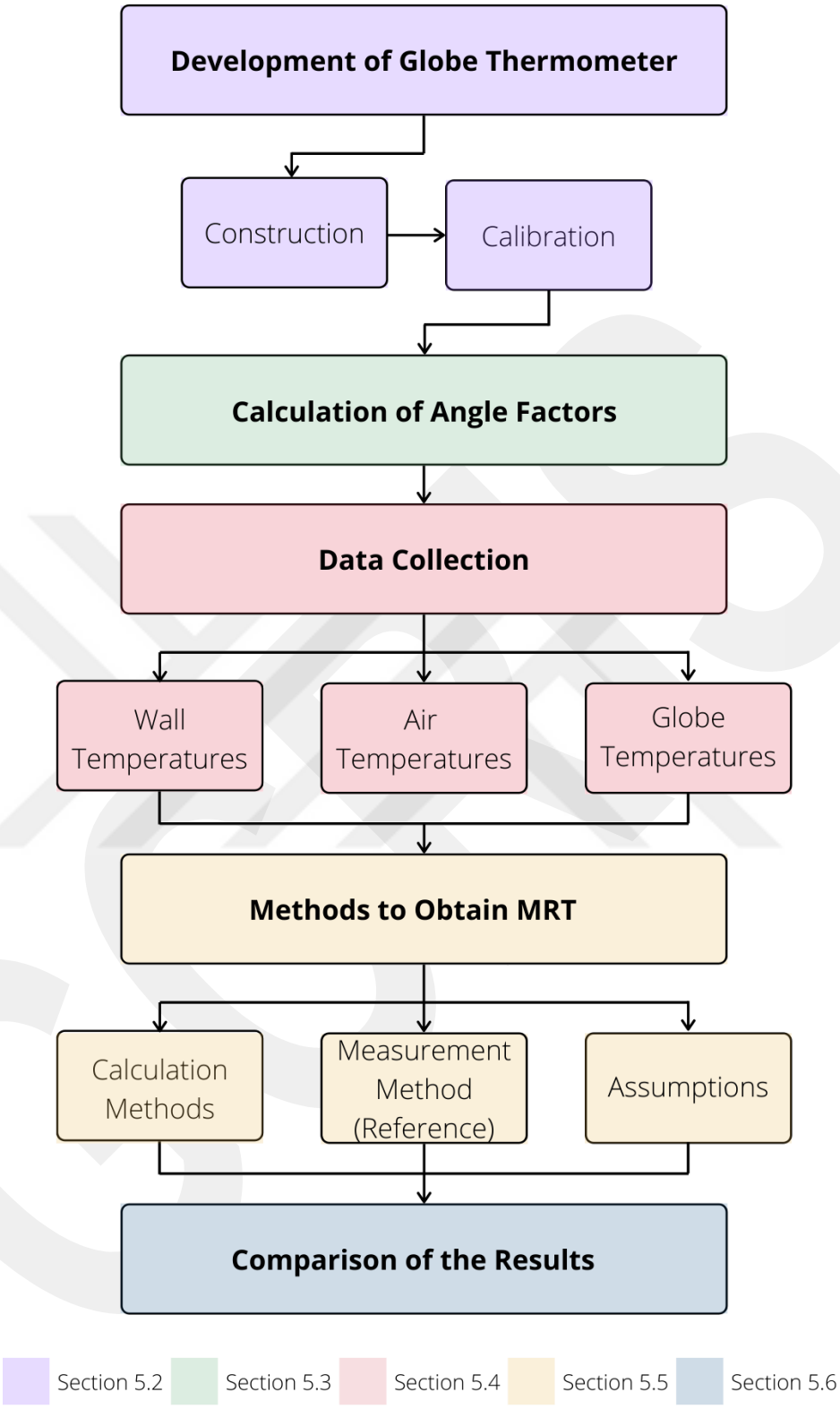

Figure 5.1. The Methodology of the Thesis

5.1. Case Building

An office building at Atılım University, Ankara/Turkey (39.81°N 32.72°E), which is classified as Csb type climate zone according to Köppen-Geiger Climate Classification [121] was selected as a case building. The location of the case building was depicted in Figure 5.2. The average temperature of the winter season (January, February, and December) and summer season (June, July, and August) varies between 0.7°C to 2.6°C and 20.3°C to 23.7°C, respectively in Ankara [122].

Figure 5.2. The Location of the Case Building

The case building dimensions are 4.7m in depth, 3.25m in width, and 2.8m in height. Furthermore, the case building contains one large window (window to wall ratio is 3.6) in the south direction. The detailed architectural drawing of the case building was depicted in Figure 5.3.

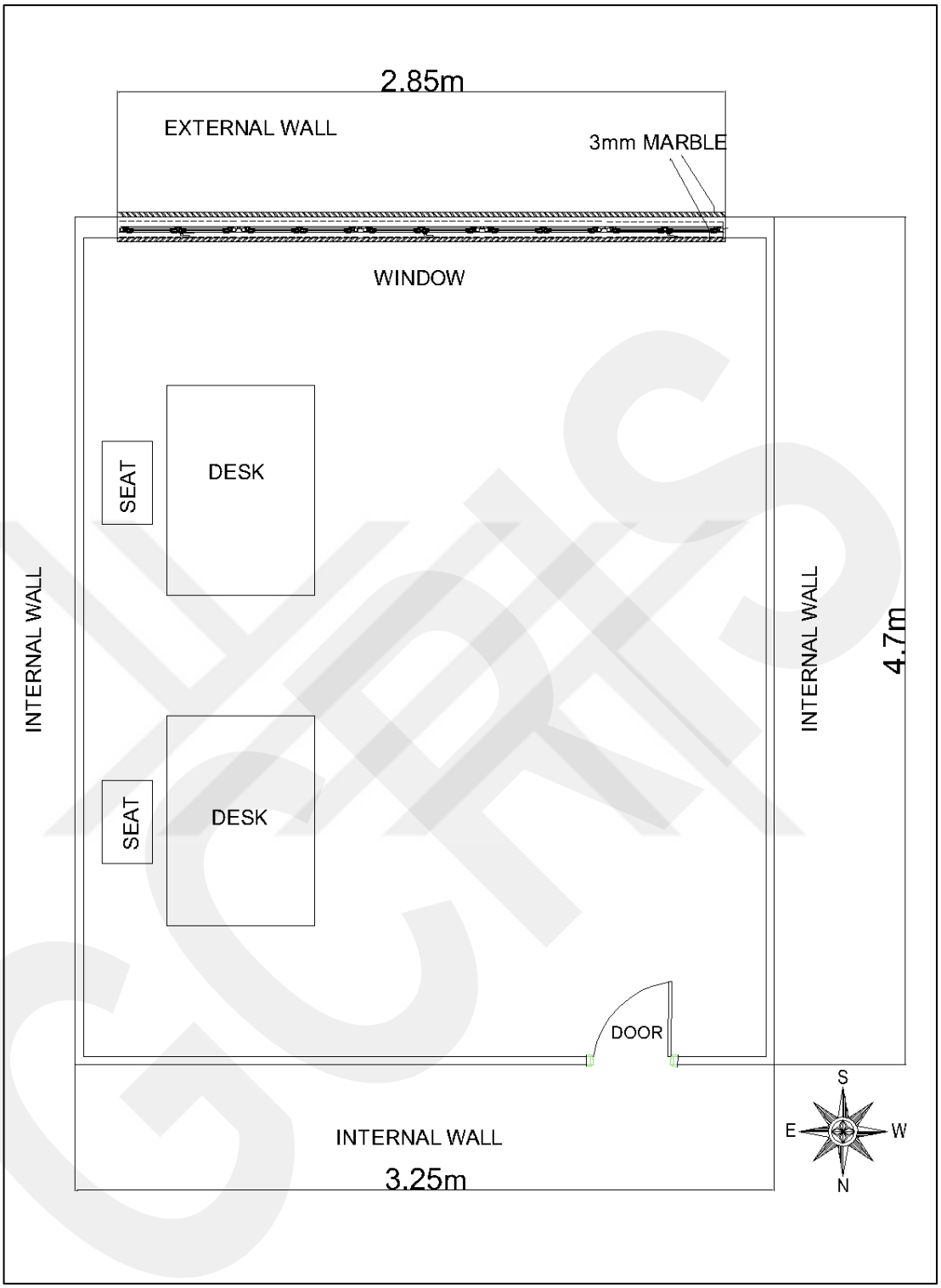

Figure 5.3. The Architectural Drawing of the Case Building

5.2. Development of the Globe Thermometer

In the study, the MRT values were obtained by using one of the measurements methods, the globe thermometer. It is worth to remind that the detailed explanations about the measurement methods are discussed in Section 3.1.

Instead of using a commercial globe thermometer, the globe thermometer was developed by the author of the thesis because of the high price of the industrial one. Development of the globe thermometer includes the design, manufacturing of the copper sphere, construction of globe thermometer, measurements, and calibration processes. The method to obtain the developed globe thermometer is represented in Figure 5.4.

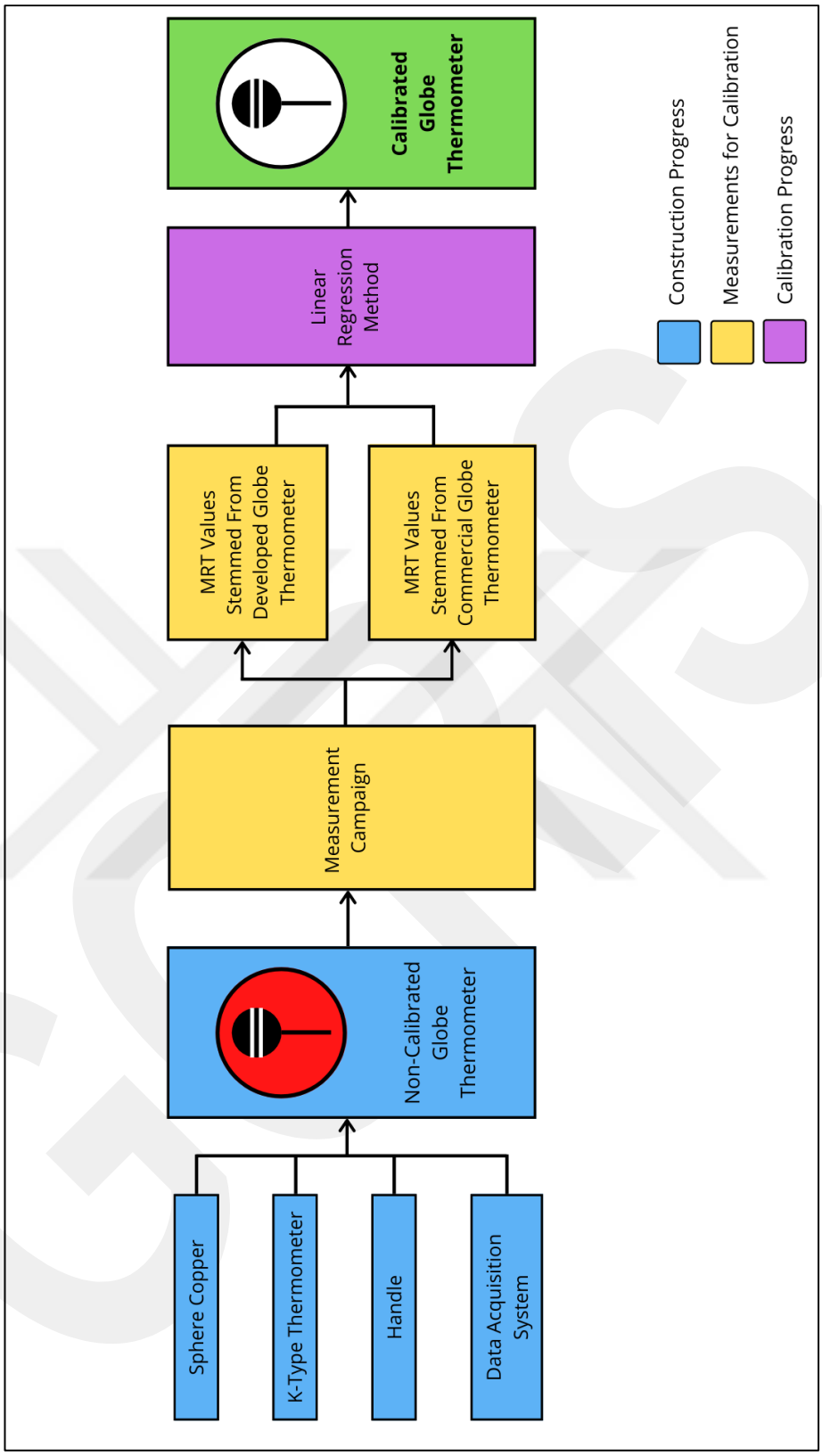

Figure 5.4. The Process to Obtain the Calibrated Globe Thermometer in the Study

5.2.1. Construction of the Developed Globe Thermometer

A matt-black painted copper sphere, a K-type temperature sensor, a non-conductive handle, and a data acquisition system were used in the development process of the globe thermometer (Figure 5.5).

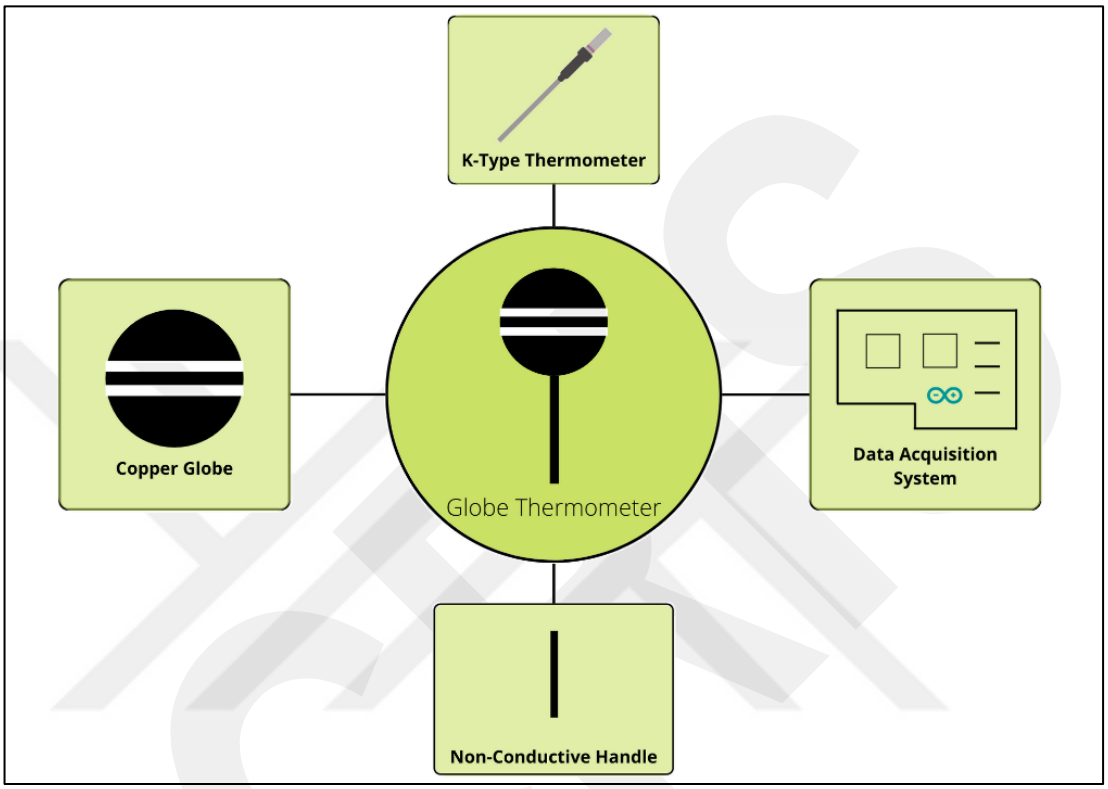

Figure 5.5. Representation of the Developed Globe Thermometer with Types of Equipment

The material of the sphere was selected as copper since not only the high heat conductivity (398 W/mºC [123]) value of the copper but also the same material was used in the original globe thermometer by Vernon [53]. The copper sphere was shaped out of a copper plate with a thickness of 0.6 mm, using spinning process [124]. Metal spinning is a forming process which provides to manufacture of hollow, axially symmetric metal components [124, 125]. Generally, in the spinning process, the flat workpiece (sheet metal) is held between a mandrel and tailstock, and then the force is delivered by roller. The applied force causes the sheet metal work to be wrapped over the mandrel, thus taking its final shape. The components which are named and used in metal forming are represented in Figure 5.6.

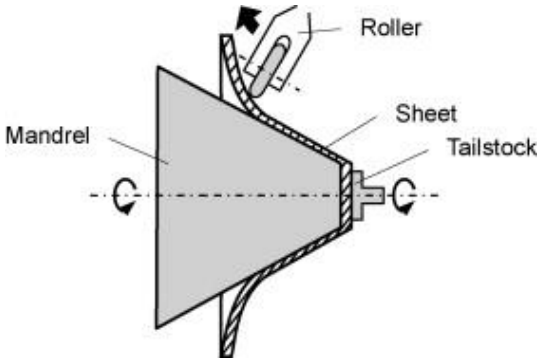

Figure 5.6. Metal Spinning Process [125]

The copper sphere of the developed globe thermometer was manufactured with a conventional spinning process. Moreover, the spinning process has different classifications, and more details about classifications can be seen in [125, 126]. The progress of the construction of the copper sphere is depicted in Figure 5.7. After the forming process, the copper sphere was sleekly painted to matt black colour to reach maximum emissivity value (ε= 0.96 [10, 124, 126]). Moreover, the handle and stand of the developed globe thermometer were also painted matt-black to prevent reflection.

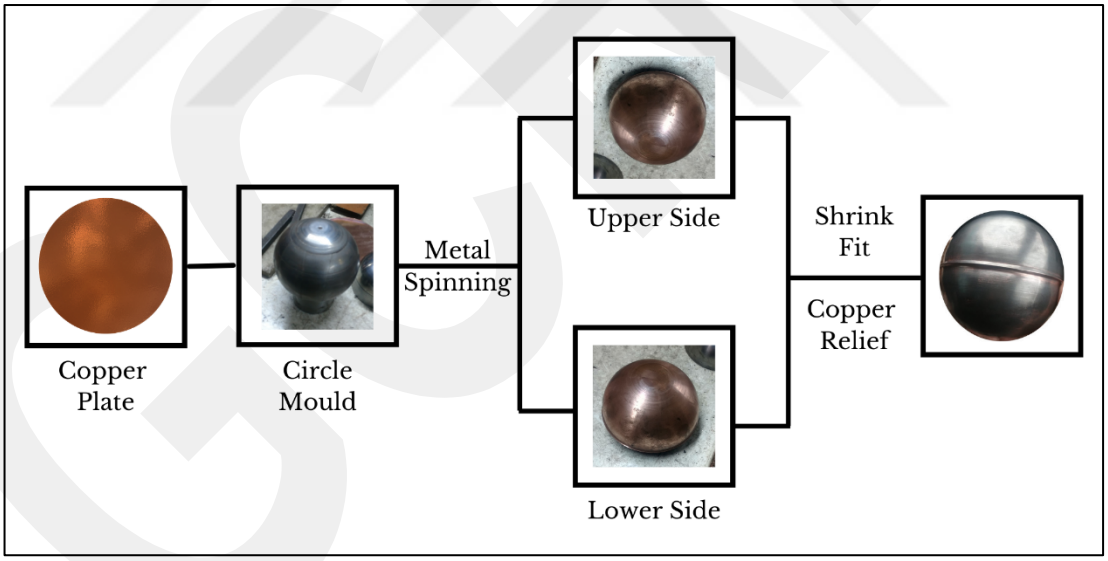

Figure 5.7 Construction of the Copper Sphere for Developed Globe Thermometer

ISO 7243 [127] identifies the tolerance values of temperature sensors to utilize for a globe thermometer. The maximum tolerance value is specified ±0.5 °C for the range between 20°C to 50°C and ±1°C for the range between 50°C to 120°C. A K-Type thermometer – DS18B20 Sensor [128] (Figure 5.8) – was selected to encounter the

requirements of the ISO 7243. The accuracy of the selected K-type temperature is ± 0.5 °C between -10°C to 85°C temperature range [128].

Figure 5.8. DS18B20 Temperature Sensor [129]

On the other hand, the data acquisition system was provided via a microcontroller; Arduino Uno [129] (Figure 5.9). Furthermore, the final circuit design is depicted in Figure 5.10. It should be noted that the temperature sensor was placed inside the copper sphere and the data was stored in an SD-card.

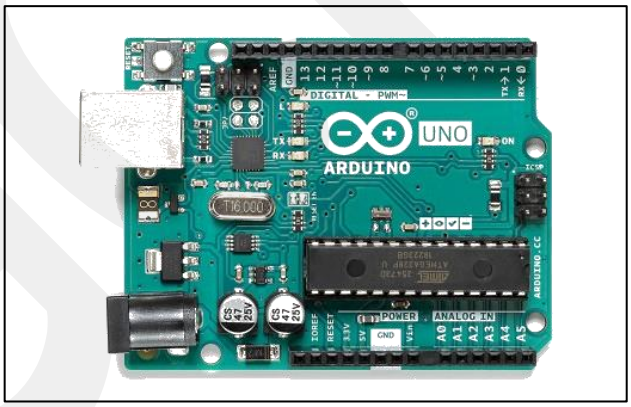

Figure 5.9. Arduino Uno [129]

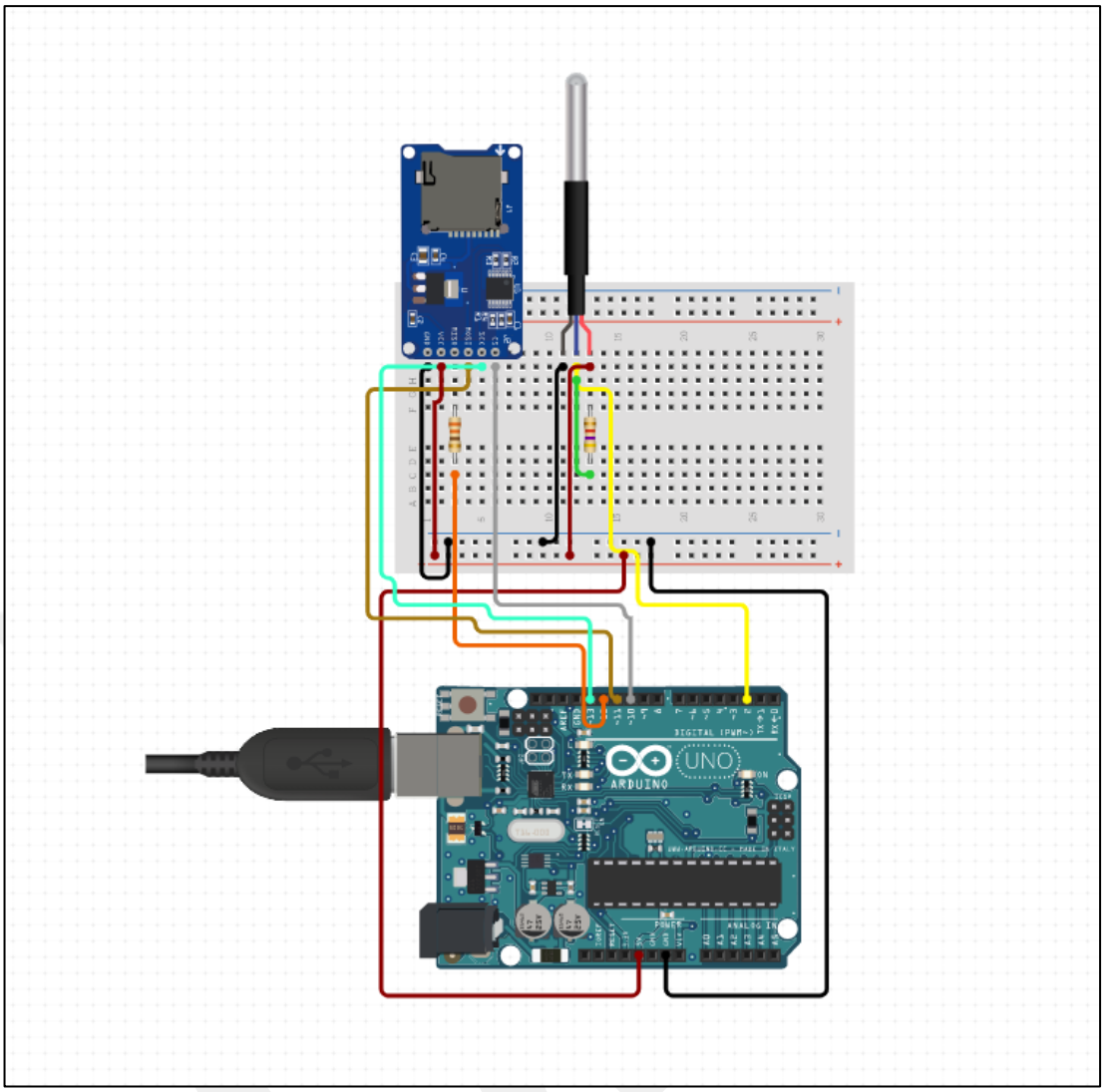

Figure 5.10. Circuit Design of Data Collection for Calibration of Developed Globe Thermometer

In conclusion, the non-conductive handle (cylindric wood) was mounted in the centre of the copper sphere to measure the MRT values at 1.1 m height according to the ASHRAE 55 [9]. The specifications of used equipment are depicted in Table 5.1. The technical drawing of the matt-blacked copper sphere is depicted in Figure 5.11, while the final picture of the developed globe thermometer is represented in Figure 5.12.

Table 5.1. Utilized Equipment to Developed Globe Thermometer

Equipment	Model	Specifications		
Copper Sphere	-	Diameter	135 mm	
		Thickness	0.6 mm	
Microcontroller / Data Acquisition System	Arduino Uno [129]	Digital I/O Pins	14	
		Input Voltage (Recommended)	7-12V	
		Clock Speed	16 MHz	
		Length	68.6 mm	
		Width	53.4 mm	
		Weight	25	
K type Temperature Sensor	DS18B20 [128]	Temperature Range	-55°C to 125°C	
		Temperature Error	-10°C to 85°C	±0.5°C
			-30°C to 100°C	± 1°C
			-55°C to 125°C	± 2°C
		Resolution	0.0625°C (12 bits)	
Non-Conductive Handle	-	Material	Wood	
		Height	Outside of the Copper Sphere	1.0325m
			Inside of the Copper Sphere	0.0525m
		Cylinder Diameter	Outside of the Copper Sphere	Ø20 mm
			Inside of the Copper Sphere	Ø11 mm

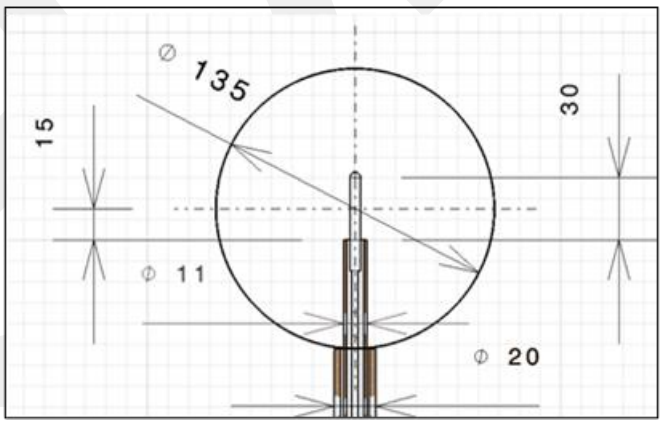

Figure 5.11. The Technical Drawing of the Matt-Blacked Copper Sphere.

Figure 5.12. Globe Sphere after Construction (on the left) and The Developed Globe Thermometer After Dyeing (on the right).

5.2.2. Calibration of the Developed Globe Thermometer

The measurement campaign for calibration of the developed globe thermometer was conducted between 23rd January 2020 to 1st February 2020 during the winter season. The temperature data collected by arranging set temperatures from 16 to 22°C via mechanical ventilation. The v_a is calculated as 0.1 m/s in the office [9] and to prevent any disturbances in the v_a, the window and door were kept closed for the duration of the measurement. It should be indicated that the calibration was processed in the absence of occupants during the measurements.

The large window of the case building (window to wall ratio is 3.6) causes a difference in the MRT with respect to the T_a. Values of the T_a were procured via a temperature sensor of the DHT22 [130], which was in-built on the developed globe thermometer handle. Concurrently, a well-known calibrated commercial globe thermometer – TESTO Globe Thermometer 0602 0743 [59] – operated to compare the data with a developed one. The specifications of the temperature sensor and the commercial globe thermometer are depicted in table 5.2. The MRT data were collected with 5-minute

intervals between 09:00 to 17:00 and stored in the SD card every day. The positions of the developed and commercial globe thermometers are illustrated in Figure 5.13.

Finally, since the copper sphere contains air and k-type temperature inside, the system must reach the equilibrium when the heat gain by radiation is equal to heat loss by convection and radiation. Thus, the calibration process started after reaching equilibrium for both globe thermometers after 20 minutes [53, 131].

Table 5.2. The Technical Data of Devices Used in the Measurement Campaign for Calibration of Developed Globe Thermometer

Device	**Model**	**Specifications**		
Temperature and Relative Humidity Sensor	DHT22 [130]	Temperature	Measuring Range	40 to 80°C
			Accuracy	<±0.5°C
			Resolution	0.1°C
		RH	Measuring Range	0-100%
			Accuracy	±2% (Max ±5%)
			Resolution	0.1%RH
Commercial Globe Thermometer	TESTO Globe Thermometer 0602 0743 [59]	Temperature	Measuring Range	0C-120°C
			Accuracy	Class 1 According to EN 60584-2 [132, 133]
				Accuracy at 22 °C is ±1 digit
				40 to +1000°C (±1.5°C) or ±t x 0.004
		Weight		385g
		Dimensions		250 x 250 x 150 mm
		Emissivity		0.95
		Probe Head Diameter		150 mm
		Product Colour		Black
Micro SD Card Adapter Reader Module	CATALEX SD Card Module [134]	Power Voltage		5V
		Current		80mA
		Interface Electrical Potential		5V
		Support Card Type		Micro SD Card (<2GB)
		Size		42x24x12mm
		Weight		5g

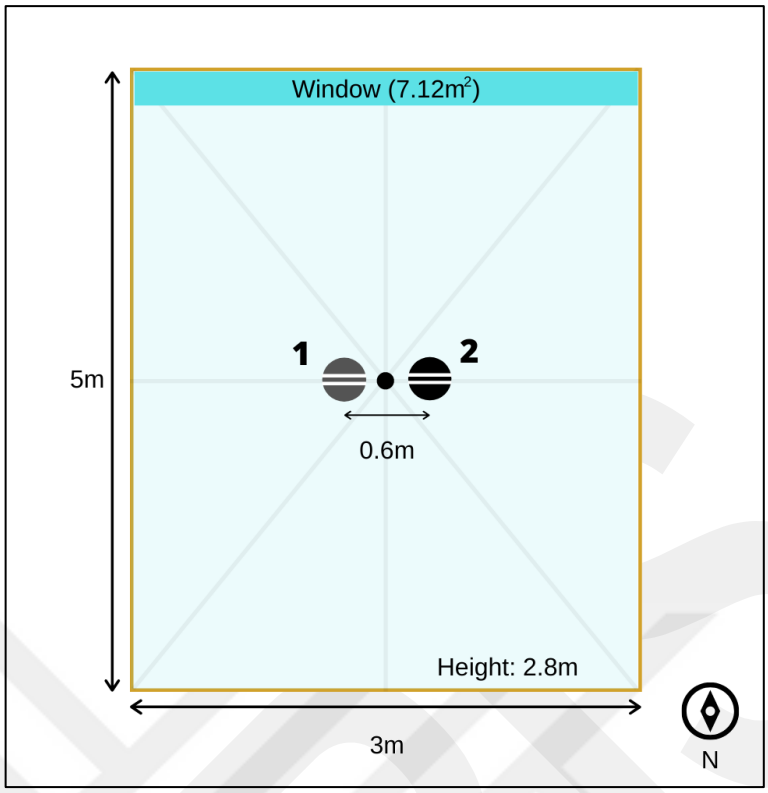

Figure 5.13. The positioning of the Developed Globe Thermometer (1) and Commercial Globe Thermometer (2) in the University Office

After obtaining the MRT data from developed and commercial globe thermometers, the calibration of the developed globe thermometer was completed via Linear Comparative Calibration Method (LLCM). The LCCM tries to predict the interaction between two different variables by transforming the measurement data into a linear equation [135, 136]. The linear regression model is expressed in equation 5.1.

$$y = \beta_0 + \beta_1 x + e \tag{5.1}$$

Here, β_0 represents the intercept, β_1 enacts the slope, x and y are independent and dependent variables respectively, finally e signifies the error, which is the difference between the observed value of the y and the straight line. ($\beta_0 + \beta_1 x$) [135, 136].

An X-Y chart was plotted to execute a regression analysis with the MRT data from both developed and commercial globe thermometers using the MATLAB [137] in order to determine the relationship between a dependent (the MRT values stemmed from developed globe thermometer) and independent (the MRT values stemmed from commercial globe thermometer) variables. The regression model fit line was obtained

through the middle of all points in the chart by using a computer program, MATLAB [137]. Note that the more considerable error value (e) represents the line's less definite [135, 136]. Moreover, Mean Squared Error (MSE) and Determination of Multiple Coefficient (R^2) were used to figure out the accuracy of the developed globe thermometer. The calculations of the MSE and R^2 are shown in equations 5.2 and 5.3, respectively [138].

$$MSE = \frac{1}{p}\sum (t_i - o_i)^2$$

$$R^2 = 1 - \frac{\sum_i |t_i - o_i|^2}{\sum_i (o_i)^2} \tag{5.2}$$

Here, t_i defines the target, o_i expresses the output, and p is the number of input-output pairs of i^{th} data [138]. (5.3)

5.3. Determination of the Angle Factors

The angle factors were calculated for the case building, which was defined in section 5.1 by using equations 3.6, 3.7, and 3.8 and Table 3.2. It is vital to underline that the angle factor calculations were calculated for a seated occupant (looking direction: west), and the developed globe thermometer represented the occupant with its position (Figure 5.14). It is worth bearing in mind that the calculation method based on angle factors was discussed in section 3.2. The outlook of the six-walls of the case building is depicted in Figure 5.15 while the coefficients of a, b, c, a/c and b/c (used in equations 3.6, 3.7, and 3.8) for six walls are given in table 5.3. The calculations were done considering the head level of the seated occupant [139], which was indicated in the ASHRAE 55 [9] as 1.1 m.

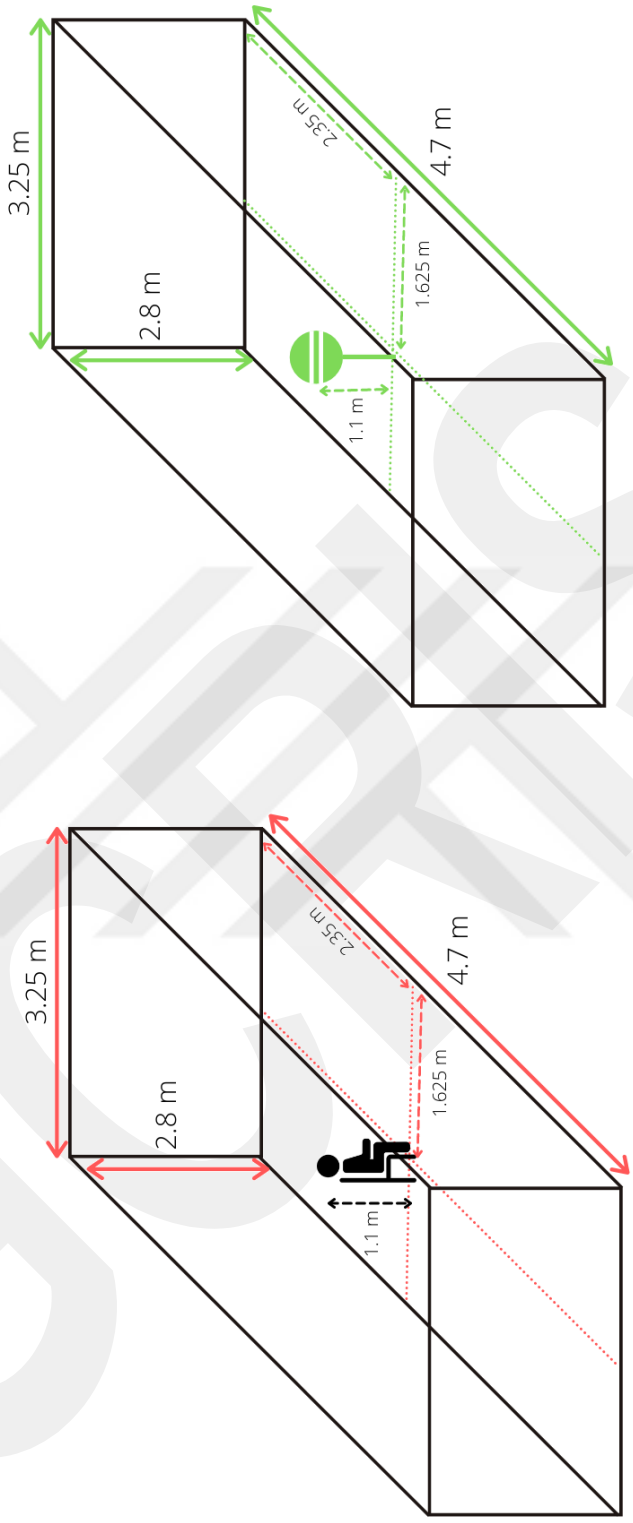

Figure 5.14. An Illustration of the Case Building

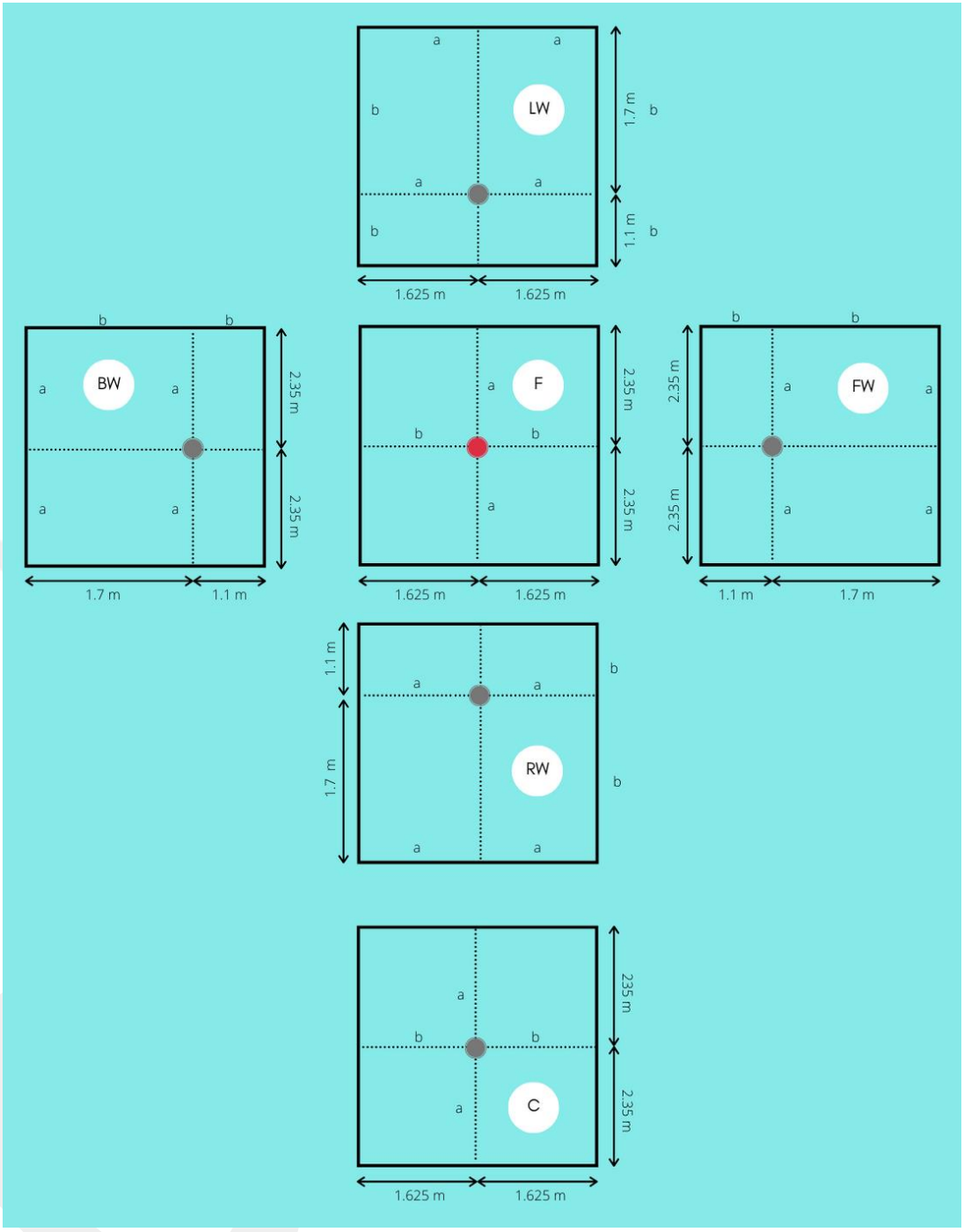

Figure 5.15. A Sight of Six-Walls of the Case Building

5.4. Data Collection

The wall temperatures and air temperatures were measured with an infrared thermometer – EXTECH 42530 [140] (Figure 5.16) – by an occupant inside the case building. The temperature data were collected between 6th July 2020 and 19th April 2021 with 10 minutes intervals between 09:00-17:00. The infrared thermometer specifications are given in table 5.3, while an illustration of data collection is depicted in Figure 5.17. The globe temperature values were measured with the same developed globe thermometer. The wall temperatures were measured from 5 different locations of six walls, as depicted in Figures 5.18 and 5.19. It should be noted that the curtains were closed while taking the wall temperatures in order to prevent the short-wave radiations. Furthermore, the radiator inside the room was not operated to prevent any disturbances in the MRT. In addition, the temperature of the radiator was collected via an infrared thermometer simultaneously with wall temperatures since it is a different material than the wall.

Figure 5.16. Infrared Thermometer (EXTECH 45230) [140]

Table 5.3. The Specifications of Infrared Thermometer [140]

Specifications	**Range / Details**
Range	-50°C to 538°C
Accuracy	±2%
Resolution	0.1°C
Emissivity (ε)	0.95
Dimensions	211x89x38mm
Weight	200g

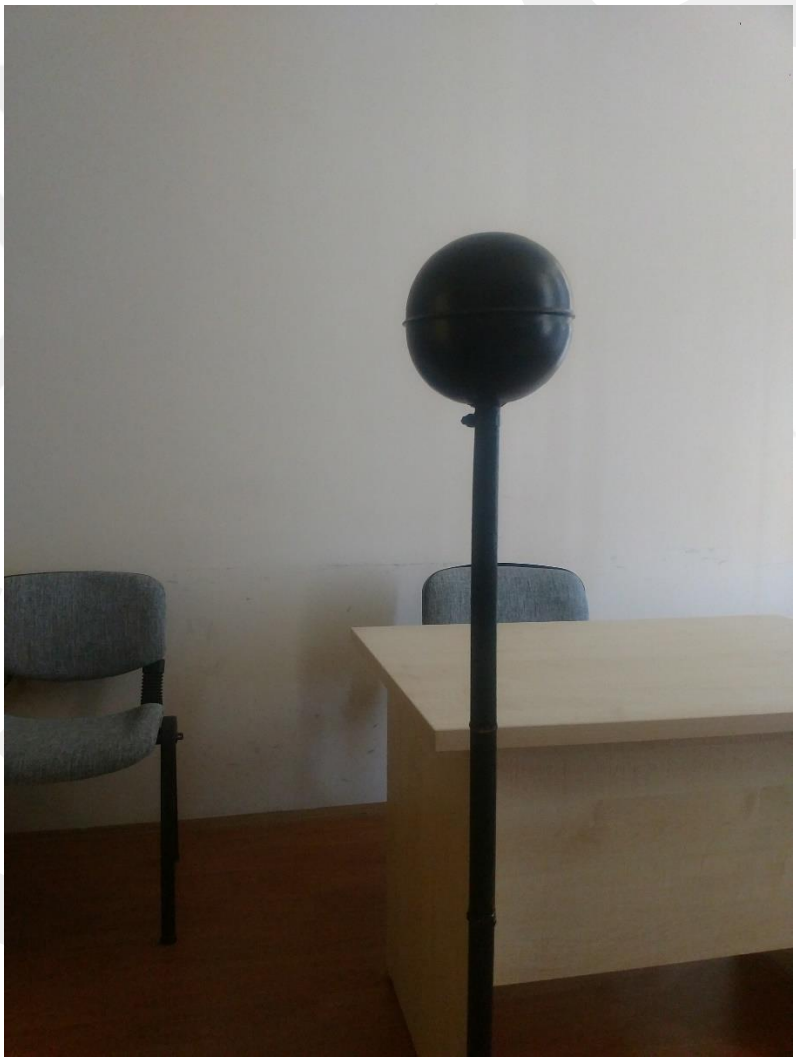

Figure 5.17. Illustration of the Data Collection

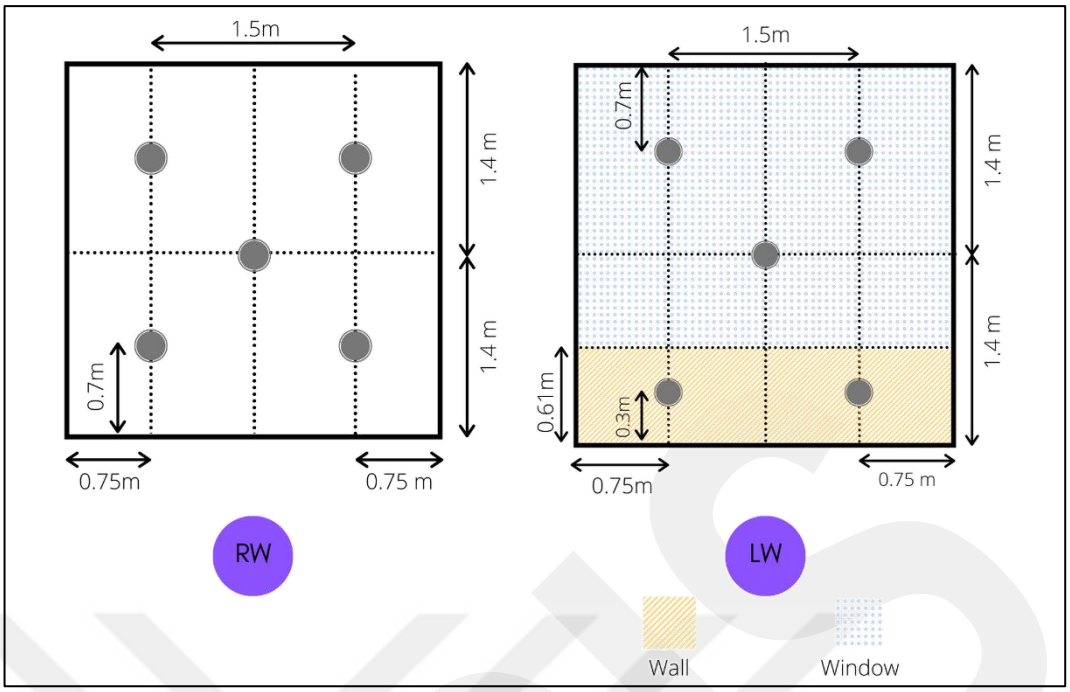

Figure 5.18. The Locations of Taken Temperatures for Left and Right Walls

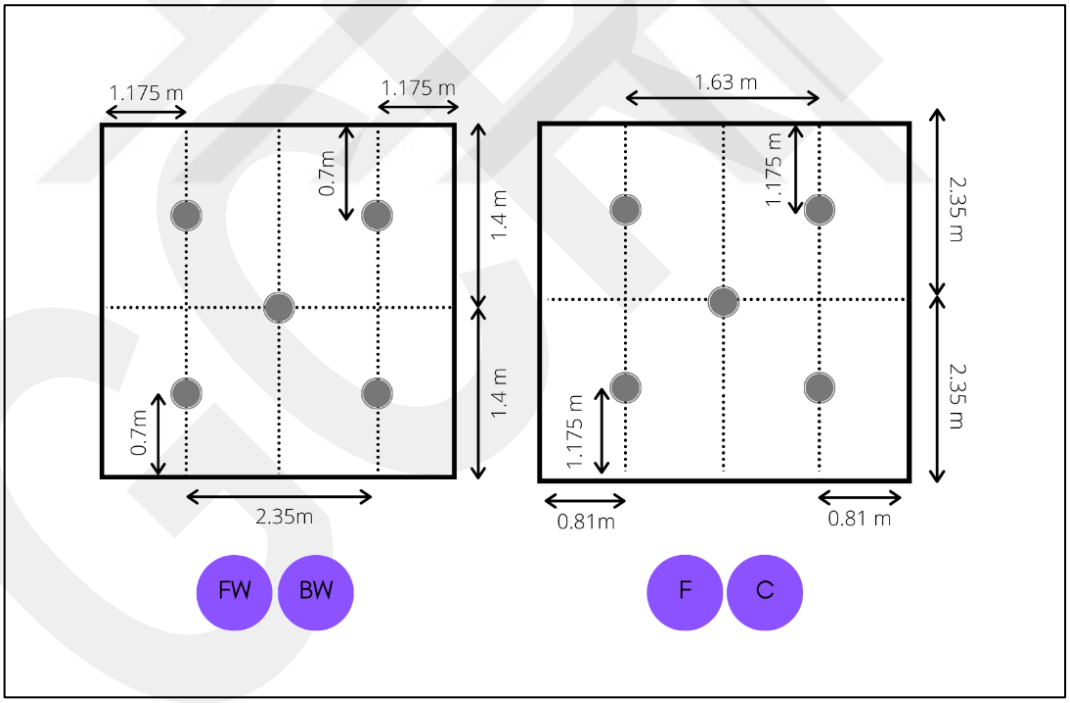

Figure 5.19. The Locations of Taken Temperatures for Front Wall, Back Wall, Ceiling, and Floor

5.5. Methods to Obtain the MRT

The MRT values can be obtained using different methods, which are indicated in chapter 3; calculation methods, measurement methods, and assumptions. Table 5.4 depicts the methods used to obtain the MRT values with the specified case subscripts in the thesis. Above all, since the measurement methods were indicated as the most accurate method [51, 52], the globe thermometer measurement method was used as a reference method.

Table 5.4. Used Methods to Obtain MRT Values in the Thesis

Methods	**Named As**	**Case Subscripts**
Measurement Method (Reference)	Globe Thermometer $MRT = \left[(T_g + 273.15)^4 + \frac{1.1\times10^8\times v_a^{0,6}}{\varepsilon D^{0.4}} \times (T_g - T_a)\right]^{0.25} - 273.15\ (°C)$	R
Calculation Methods	Calculation Method Based on Angle Factors Method $MRT = \left[\sum_i^n F_{p-i}T_i\right] = T_1F_{p-1} + T_2F_{p-2} + \cdots + T_nF_{p-n}$	C1
	Calculation Method Based on The Surface Areas Method $MRT = \frac{T_1A_1 + T_2A_2 + \cdots + T_nA_n}{A_1 + A_2 + \cdots + A_n}$	C2
Assumptions	Resultant Temperature Method $MRT = 2T_o - T_a$	A1
	AUST (MRT) Method $MRT = T_{air} - \frac{7c}{T_{out} - 45}$	A2
	Equality of MRT to T_a $MRT = T_a$	A3
	Nagano's Assumption $MRT = 0.99T_a - 0.01$	A4
	Inference of MRT From Globe Temperature $MRT = 1.75T_g - 0.75T_a$	A5
	Beshir and Ramsey's Method $MRT = T_g + 1.8v^{0.5}(T_g - T_a)$	A6
	McIntyre's Method $MRT = T_g + 2.44v^{0.5}(T_g - T_a)$	A7
	Equality of MRT to T_g $MRT = T_g$	A8

5.6. Comparison of the Results

After obtaining the MRT values using different methods, which were indicated in Table 5.5, the values stemmed from calculation methods, and assumptions were compared with the reference method. During the comparison, an X-Y chart was plotted between each method and the reference method. The Mean Absolute Percentage Error (MAPE), Root Mean Squared Error (RMSE), Mean Squared Error (MSE), and Determination of Multiple Coefficient (R^2) were used to find out the accuracies of each method. The MAPE is shown in equation 5.4, RMSE is depicted in equation 5.5, the MSE and R^2 are shown in section 5.2.2, equations 5.2 and 5.3, respectively [138, 141-144].

$$MAPE = \frac{100}{N}\sum_{i=1}^{N}\left|\frac{A_i - Z_i}{A_i}\right| \tag{5.4}$$

$$RMSE = \sqrt{\frac{\sum_{i=1}^{N}(A_i - Z_i)^2}{N}} \tag{5.5}$$

Here, where Z_i defines the forecast values, A_i depicts the actual values, and N represents the number of data samples [144].

CHAPTER 6

RESULTS AND DISCUSSION

The results and discussion section of the thesis include three different sections: calibration results of developed globe thermometer, results of calculated angle factors of the case building, comparison of the methods to obtain MRT. Figure 6.1 illustrates the flow chart of the results and discussion of the thesis.

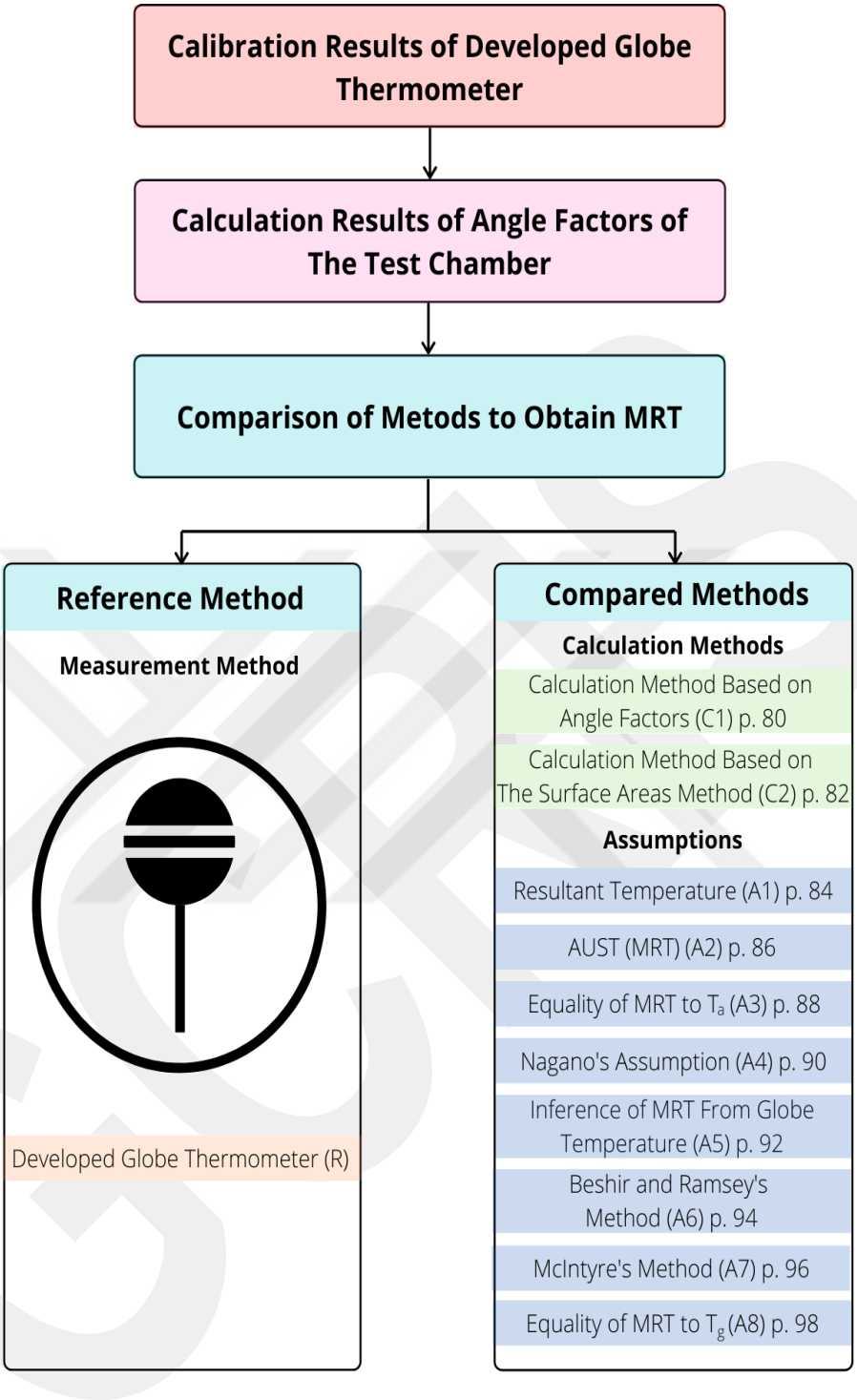

Figure 6.1. Results and Discussion Sections in the Thesis with Page Numbers

6.1. Calibration Results of The Developed Globe Thermometer

Total of 872 MRT data from the commercial globe thermometer – TESTO Globe Thermometer 0602 0743 [59] – and the developed globe thermometer was collected in eight days to calibrate the developed globe thermometer. The comparison of the MRT data between the developed globe thermometer and commercial one was depicted in Figure 6.2. Furthermore, the calibration results were given in table 6.1.

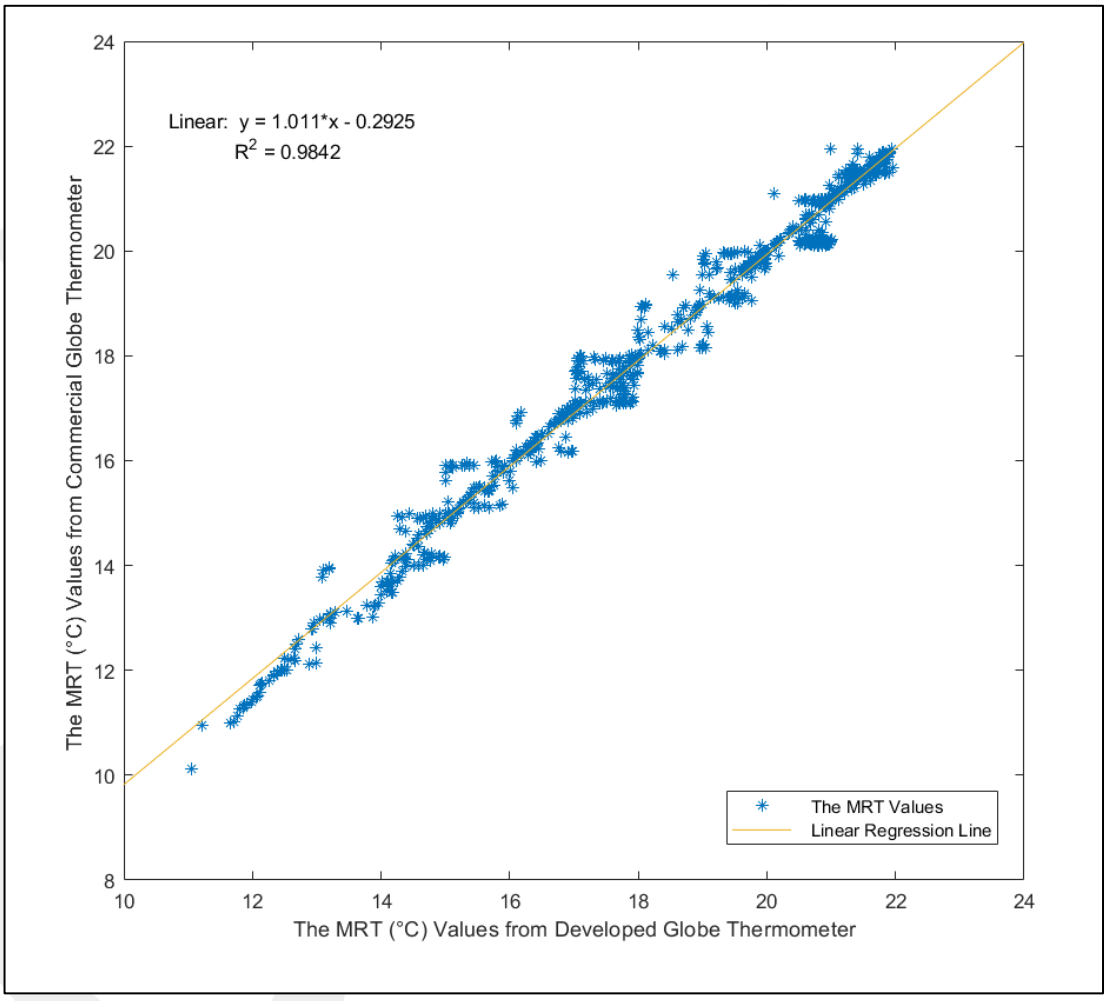

Figure 6.2. Comparison of The MRT Data Stemmed from Commercial Globe Thermometer and Developed Globe Thermometer via Linear Comparative Comparison Method

Table 6.1. The Calibration Results of the Developed Globe Thermometer

Variables	**Values**
Intercept	-0.2925
Slope	1.0124
R^2	0.9842
MSE	0.1256

Figure 6.2 indicates that the developed globe thermometer matched close values with the commercial globe thermometer. It is worth to note that, under 16°C of the MRT, the developed globe thermometer measured slightly higher values than the commercial globe thermometer data. One of the reasons of the difference between commercial and developed globe thermometer data could be the diameter difference. Since the developed globe thermometer has 0.15 mm less diameter comparing the commercial globe thermometer, the air volume is lower inside the sphere, which causes a decrease in response time. In other words, the developed globe thermometer reached thermal equilibrium faster than the commercial globe thermometer due to the smaller diameter. [145, 146]. In conclusion, the calibration results showed that the MRT values demonstrate an excellent coherence with an R^2 of 0.98 while the MSE value is 0.12.

The normality distribution of the residuals for the calibration process is shown in a histogram graph as the Figure 6.3. The normality assumption is acceptable if the values spread is equally classified around zero [138]. As shown in the figure 6.3, the residuals distributed normally, which indicated that the developed GT successfully measured the MRT values.

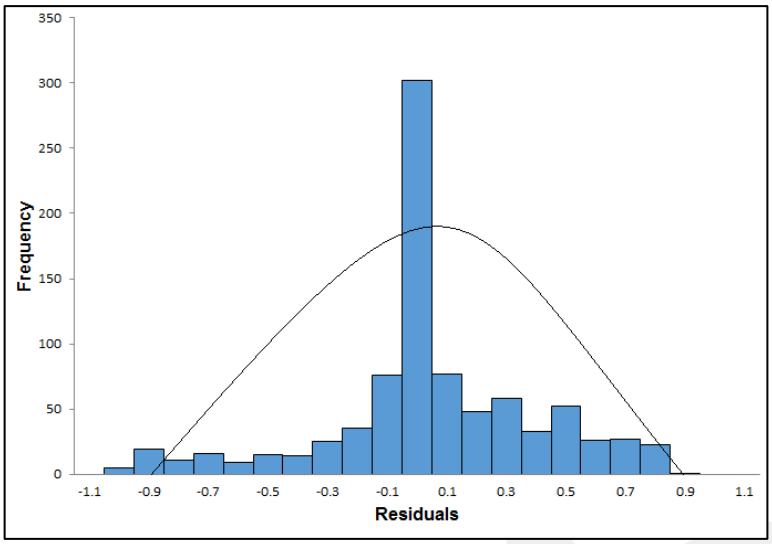

Figure 6.3. Distribution of Residuals

On the other hand, the initial price of the developed globe thermometer was only US$60, which is nearly ten times lower than the commercial globe thermometer. The most expensive part of the developed globe thermometer was the copper sphere due to the manufacturing process and neat work. The detailed prices of the components were depicted in table 6.2. It is worth bearing in mind that the prices could be different for different models or types of sensors and materials.

Table 6.2. The Price of Utilized Materials in Developed Globe Thermometer

Materials	**Price**
Copper Sphere	US$ 35
Silicone (Adhesive)	US$ 3
K-Type Temperature Sensor	US$ 4
Microcontroller and Connection Cables	US$ 10
Matt-Black Colour Spray	US$ 4
Wood Handle	US$ 4
Total Price	**US$ 60**

6.2. Calculation Results of the Angle Factors of the Case Building

The angle factors of the case building were calculated by using equations 3.6, 3.7, and 3.8, and the coefficient table (Table 3.2) as described in the section 3.2. It is vital to remind that the calculation method of the angle factors was described in section 3.2. The coefficients of *a*, *b* and *c*, in equations 3.6, 3.7, and 3.8, were depicted in table 6.3 with the aid of Figure 5.15.

Table 6.3. The Coefficients Table to Calculate the Angle Factors

Walls	Sections	a	b	c	a/c	b/c
Back Wall (BW)	1	2.350	1.700	1.625	1.446	1.046
	2	2.350	1.700	1.625	1.446	1.046
	3	2.350	1.100	1.625	1.446	0.677
	4	2.350	1.100	1.625	1.446	0.677
Front Wall (FW)	1	2.350	1.700	1.625	1.446	1.046
	2	2.350	1.700	1.625	1.446	1.046
	3	2.350	1.100	1.625	1.446	0.677
	4	2.350	1.100	1.625	1.446	0.677
Left Wall (LW)	1	1.625	1.700	2.350	0.691	0.723
	2	1.625	1.700	2.350	0.691	0.723
	3	1.625	1.100	2.350	0.691	0.468
	4	1.625	1.100	2.350	0.691	0.468
Right Wall (RW)	1	1.625	1.700	2.350	0.691	0.723
	2	1.625	1.700	2.350	0.691	0.723
	3	1.625	1.100	2.350	0.691	0.468
	4	1.625	1.100	2.350	0.691	0.468
Celling (C)	1	2.350	1.625	1.700	1.382	0.956
	2	2.350	1.625	1.700	1.382	0.956
	3	2.350	1.625	1.700	1.382	0.956
	4	2.350	1.625	1.700	1.382	0.956
Floor (F)	1	2.350	1.625	1.100	1.477	2.136
	2	2.350	1.625	1.100	1.477	2.136
	3	2.350	1.625	1.100	1.477	2.136
	4	2.350	1.625	1.100	1.477	2.136

It is worth to remind that the angle factors were calculated for a seated occupant according to the head level of the occupant, which was described in ASHRAE-55 [9] as 1.1 m. The calculation results of angle factors were depicted in Table 6.4.

Table 6.4. Results of Calculation of Angle Factors

Surface	Angle Factor
Back Wall (BW)	0.184
Front Wall (FW)	0.184
Left Wall (LW)	0.099
Right Wall (RW)	0.099
Ceiling	0.157
Floor	0.238
Total	**0.961**

In the case building, the angle factor of the floor was calculated as 0.233. It means that 10°C changes in the floor surface cause a 2.33°C change in the MRT and 1.165°C in the operative temperature while the other surface temperatures were constant. Moreover, the effects on the MRT of the surfaces can be compared by using angle factors. For instance, the angle factors of the LW and the FW were calculated as 0.099 and 0.184, respectively. These angle factors were indicated that a 1°C change in the FW is affected 1.86 times more than LW to the MRT.

6.3. Measurement Results

The total of 699 data, to compare the calculation methods and assumptions with the reference method, were collected between 6th July 2020 to 19th April 2021 in the case building. The distribution of the MRT Data with the Reference Method in the Study is illustrated in Figure 6.4. Furthermore, the collected data of T_a, T_{out}, and MRT values were given in Figure 6.5. In addition, the MRT data for the cases are depicted in Figure 6.6. An example day of collected data was also given in Appendix A.

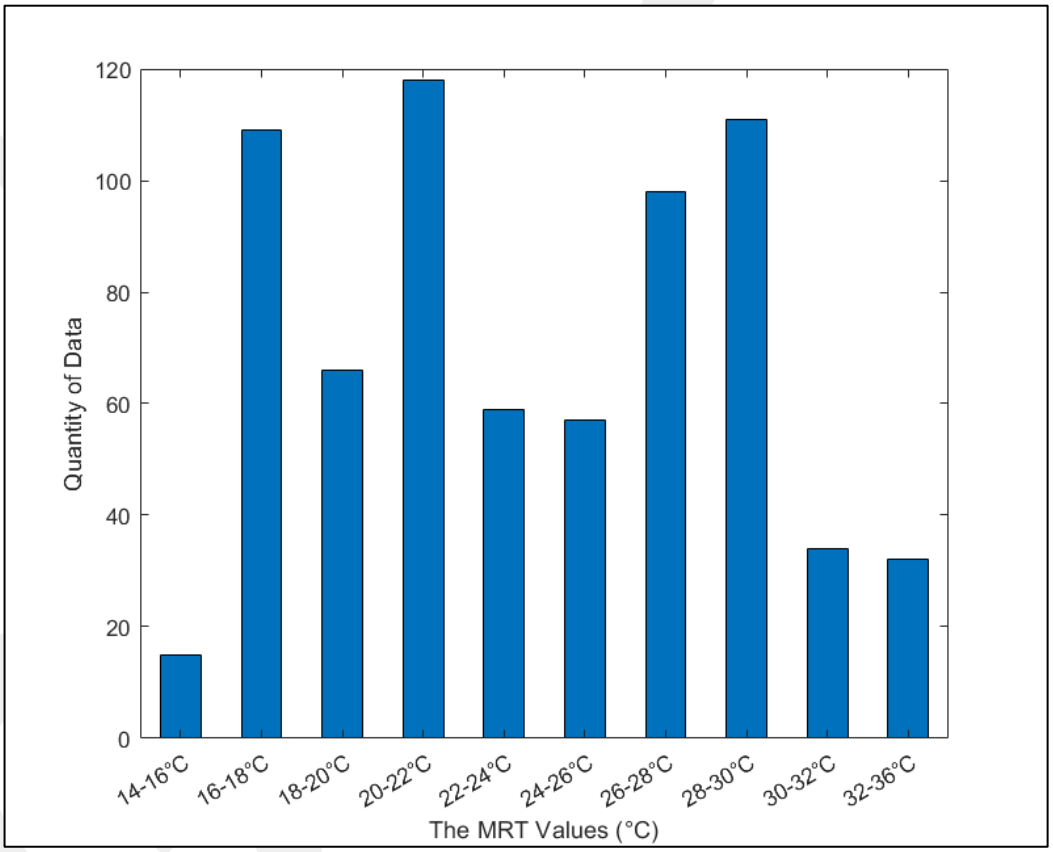

Figure 6.4. Distribution of the MRT Data with the Reference Method in the Study

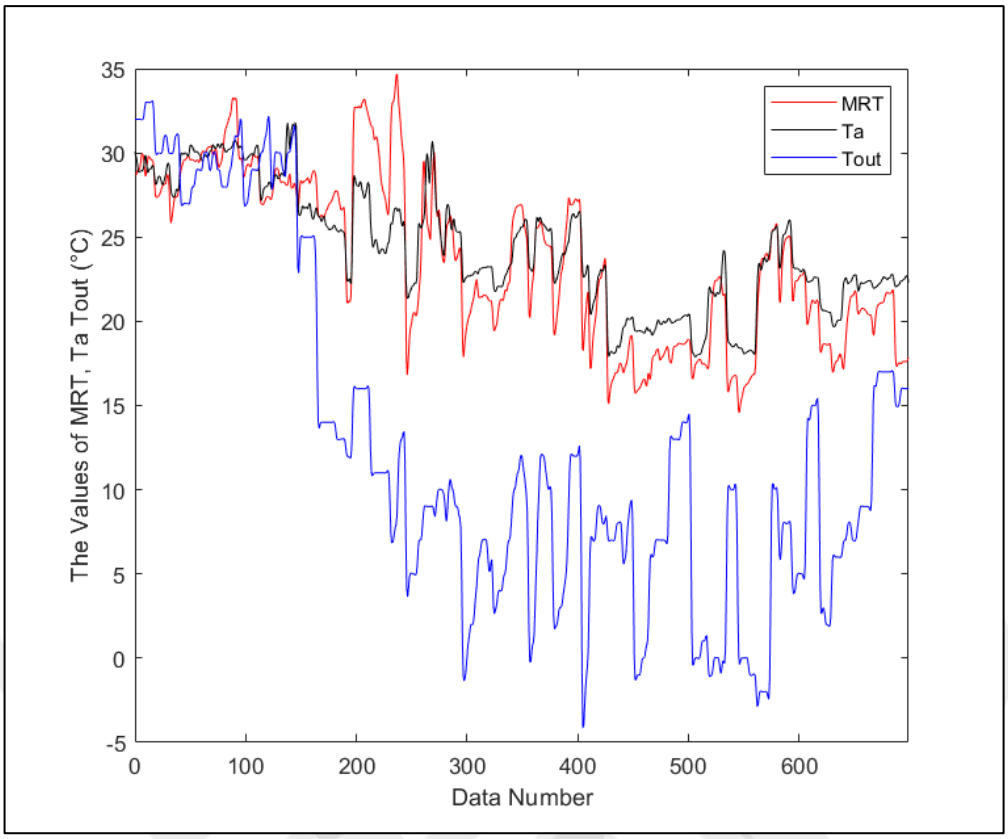

Figure 6.5. T_a, $T_{out,}$ and MRT values of the data. (Note: The Data Number was arrayed by dates with starting on 6th July 2020 and ending with 19th April 2021 in the Graph)

Figure 6.4 depicts that the temperature values of the MRT, T_a and T_{out} were close to each other in higher T_{out} values. Even though it is certain that the T_{out} was affected the MRT and T_a since it affects the left wall temperature directly, while the T_{out} values were decreased, the temperature difference between the T_{out} and both the T_a and MRT increased since the internal wall temperatures were not changed as dramatically as T_{out}. Moreover, since the measurement campaign was performed in-office hours (09:00-17:00), the left wall temperature was affected by the sunlight, and the left wall temperature was more than the T_{out} in conditions when T_{out} is low. Besides, the MRT and T_a seem generally close to each other since the temperature range is high in this graph. However, this graph is misleading while the detailed comparison between each other is analysed. The detailed comparison between the T_a and MRT is explained in section 6.4.5.

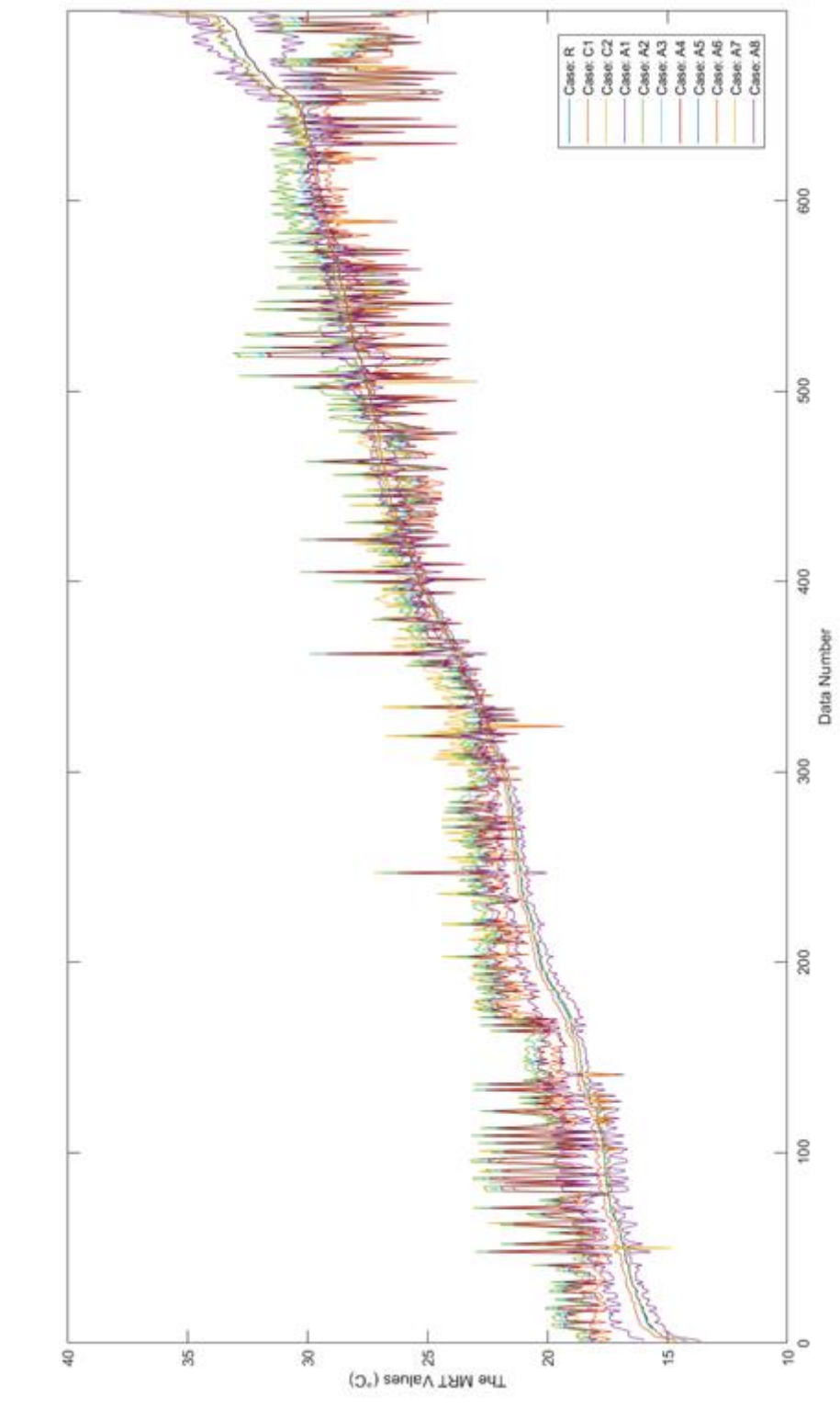

Figure 6.6. Distribution of the MRT Data with the Reference Method in the Study. (Note: The Data Number was arrayed by temperature values from lower to higher.)

Figure 6.6 shows that the error between the compared methods was high in low (14-18°C) and high temperature (30-36°C) values. The sharp changes in the MRT values were happened with the sharp temperature changes in the window temperature on cloudy days. The detailed comparison between the methods to obtain the MRT is discussed in section 6.4.

6.4. Comparison of Methods to Obtain the MRT

Assumptions and calculation methods to obtain the MRT were compared by the reference method of measurement method by using the developed globe thermometer. The compared methods were depicted in Table 5.5. It is worth to remind that the MAPE, MSE, RMSE, and R^2 were used to determine their accuracies with respect to the reference method. The utilized statistical methods were already discussed in section 5.6 in Methodology Section. Finally, the comparison of the results was discussed separately for each method in different sections.

6.4.1 Comparison of the Cases: C1 and R

The comparison of the MRT values stemmed from the C1 and R was illustrated in Figure 6.7.

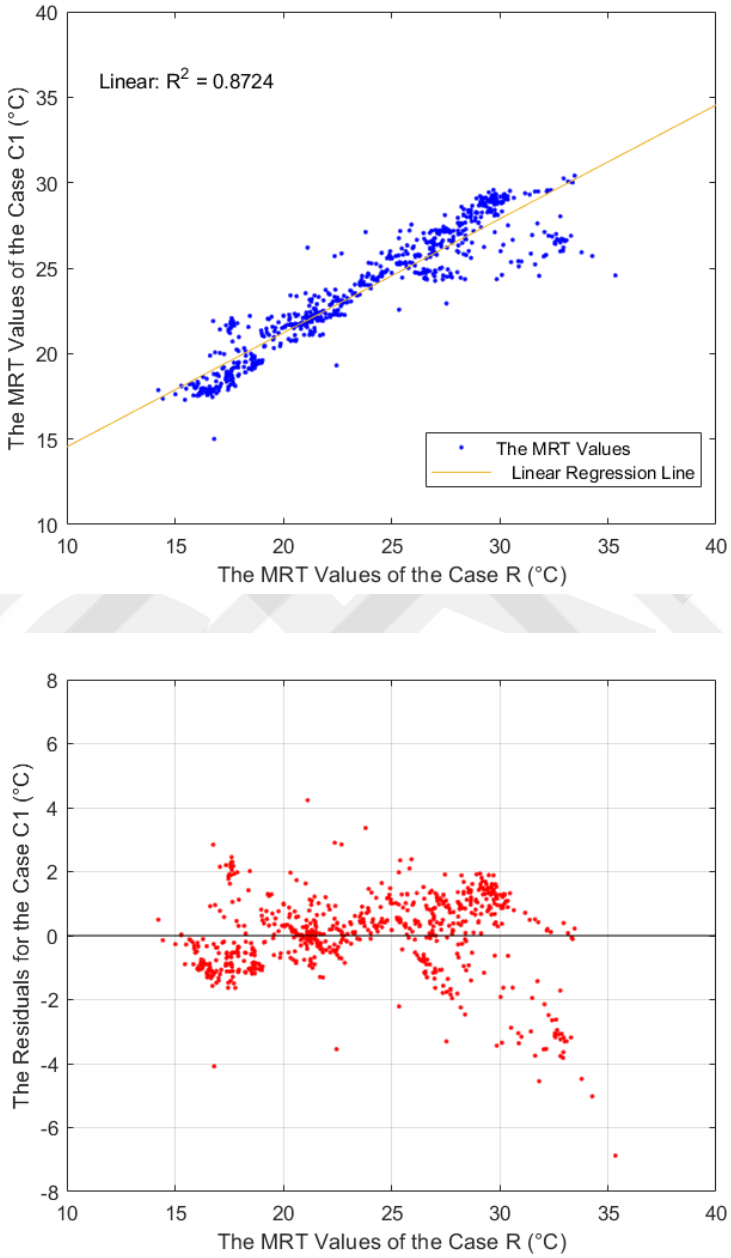

Figure 6.7. The Graph for Comparison of the MRT Values of Cases with Residuals: C1 and R

The C1 wrongly estimated the MRT values compared to reference model. It is clear to see that the magnitude of error increases by increasing the air temperature values. The fluctuations above the MRT values between 24°C to 28°C were due to the sharp temperature changes in the window temperature, which varies quickly on cloudy days, compared to the temperatures of other walls. The sharp temperature changes in the window surface affected the results of the calculation method directly since it calculated the MRT value instantaneously, whereas the measurement method cannot measure instantaneously. The statistical criteria of the MSE, MAPE, RMSE, and R^2 values are depicted in Table 6.5.

Table 6.5. Statistical Criteria Results for Comparison of Cases of the C1 and R

Statistical Criteria	**Result**
MSE	4.270
RMSE	2.066
MAPE	6.282
R^2	0.872

6.4.2 Comparison of the Cases: C2 and R

The comparison of the MRT values stemmed from the C2 and R was illustrated in Figure 6.8.

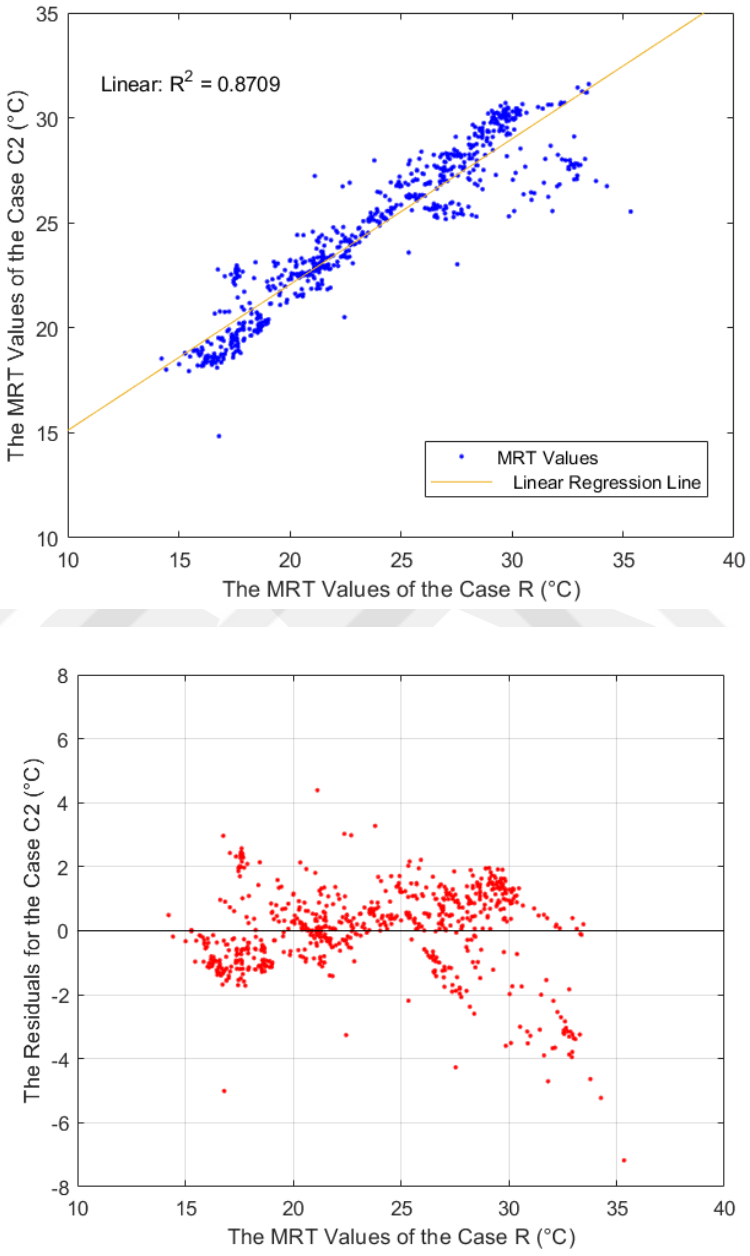

Figure 6.8. The Graph for Comparison of the MRT Values of Cases with Residuals: C2 and R

The C2, which was based on surface areas, were generally underestimated the MRT values. Moreover, the fluctuations above 24°C occurred on cloudy days since the window, where is in the left wall, the temperature changed consistently. The statistical criteria of MSE, MAPE, RMSE, and R^2 values for the comparison are depicted in Table 6.6.

Table 6.6. Statistical Criteria Results for Comparison of Cases of the C2 and R

Statistical Criteria	**Result**
MSE	4.840
RMSE	2.200
MAPE	8.095
R^2	0.870

6.4.3 Comparison of the Cases: A1 and R

The comparison of the MRT values stemmed from the A1 and R was illustrated in Figure 6.9.

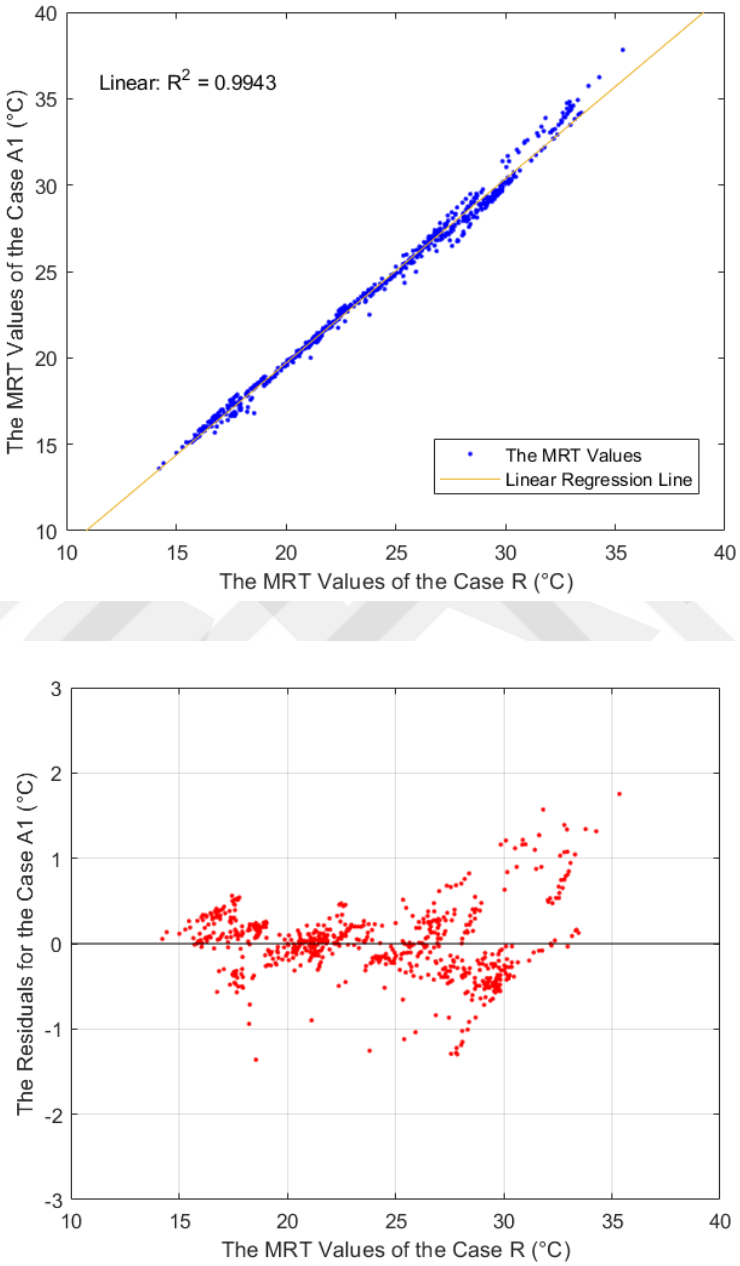

Figure 6.9. The Graph for Comparison of the MRT Values of Cases with Residuals: A1 and R

It is worth to remind that the formula of the A1 was given in Equation 14 and the operative temperature was taken equal to the developed globe temperature. Overall, the MRT values were underestimated below 25°C, and both under and overestimated above 25°C. Since the globe temperature was used, both in the A1 and the reference method, the measured MRT values and estimations were associated between each other. It is vital to identify that while the developed globe thermometer has a 135mm copper sphere, the standard globe thermometer has 150mm. The change in the diameter is affected the equilibrium time since the air volume different inside the copper. Hence, it is possible that the errors may be different when the standard globe diameter is used. The statistical criteria of MSE, MAPE, RMSE, and R^2 values for the comparison are depicted in Table 6.7.

Table 6.7. Statistical Criteria Results for Comparison of Cases of the A1 and R

Statistical Criteria	**Result**
MSE	0.266
RMSE	0.516
MAPE	1.567
R^2	0.994

6.4.4 Comparison of the Cases: A2 and R

The comparison of the MRT values stemmed from the A2 and R was illustrated in Figure 6.10.

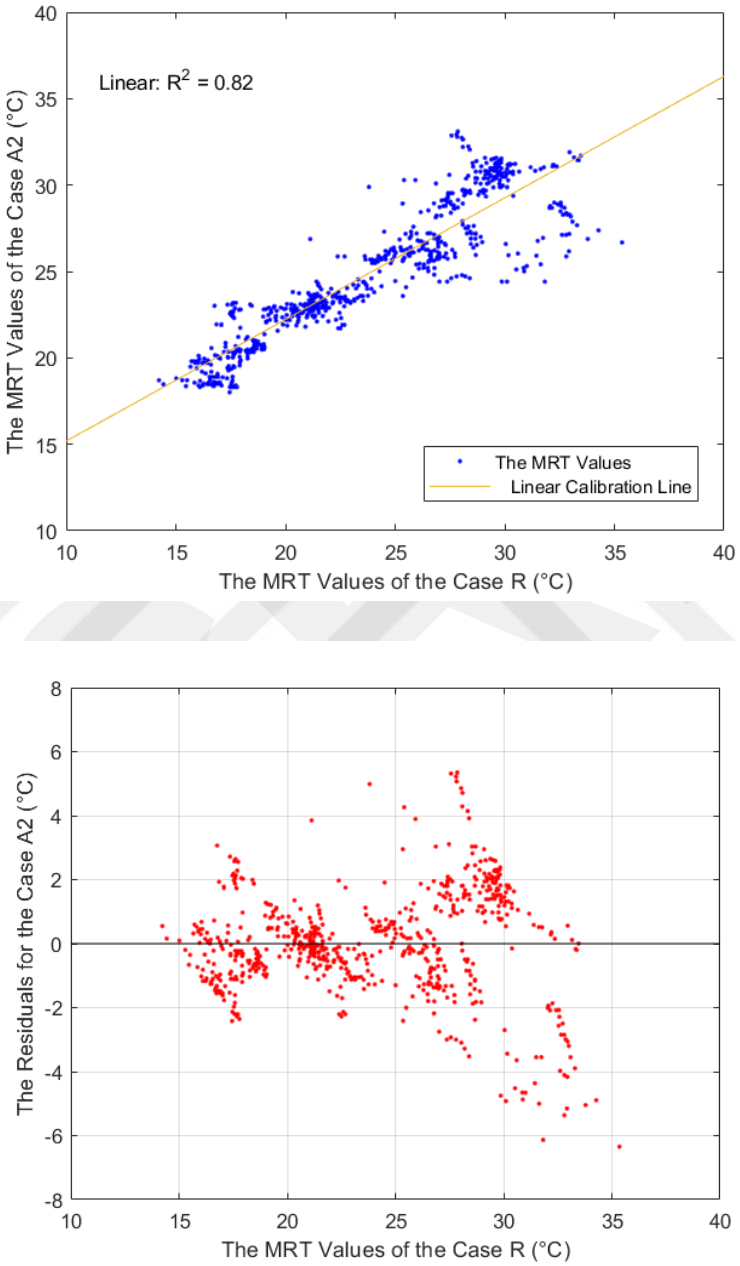

Figure 6.10. The Graph for Comparison of the MRT Values of Cases with Residuals: A2 and R

It is worth the remind that the fenestration is important to estimate the MRT value for A2. The value of *c* was selected as a 2 since the fenestration is higher than 5% in the case building. The results indicated that the A2 expected the MRT values with a high error. The wrong estimation occurred since the assumption was not considering the wall temperatures directly and calculated the MRT value via T_a and effect of outdoor temperature. It should be underlined that, the "c" value is selected as a 2 in any case if the fenestration is higher than 5%. While considering the fenestration is more than 70% in the case building (window to wall ratio is 3.6), the assumption was estimated the MRT results incorrectly. The statistical criteria of MSE, MAPE, RMSE, and R^2 values for the comparison are depicted in Table 6.8.

Table 6.8. Statistical Criteria Results for Comparison of Cases of the A2 and R

Statistical Criteria	**Result**
MSE	6.019
RMSE	2.453
MAPE	9.185
R^2	0.820

6.4.5 Comparison of the Cases: A3 and R

The comparison of the MRT values stemmed from the A3 and R was illustrated in Figure 6.11.

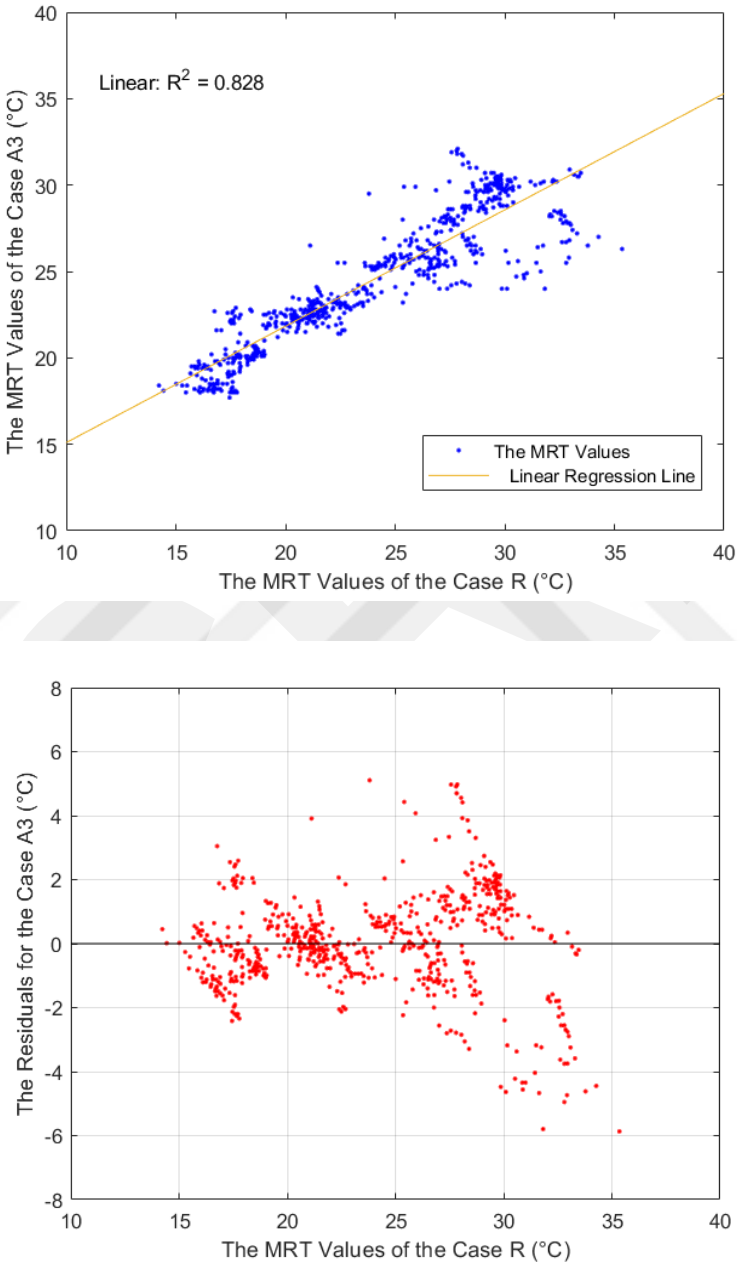

Figure 6.11. The Graph for Comparison of the MRT Values of Cases with Residuals: A3 and R

The MRT values are generally underestimated in the application of the case A3. The MRT values are generally higher than T_a when the window temperature is greater than T_a. In addition, the opposite can be seen in the lower MRT values. The reason to see high values of the errors in the residuals between 24°C and 28°C is the difference between the glazing surface and the T_a. As Figures 6.4 and 6.5 depicts, among the collected data, the temperature difference between T_a and the glazing surface was up to 10°C in fair weather. The statistical criteria of MSE, MAPE, RMSE, and R^2 values for the comparison are depicted in Table 6.9.

Table 6.9. Statistical Criteria Results for Comparison of Cases of the A3 and R

Statistical Criteria	**Result**
MSE	5.251
RMSE	2.291
MAPE	7.793
R^2	0.828

6.4.6 Comparison of the Cases: A4 and R

The comparison of the MRT values stemmed from the A4 and R was illustrated in Figure 6.12.

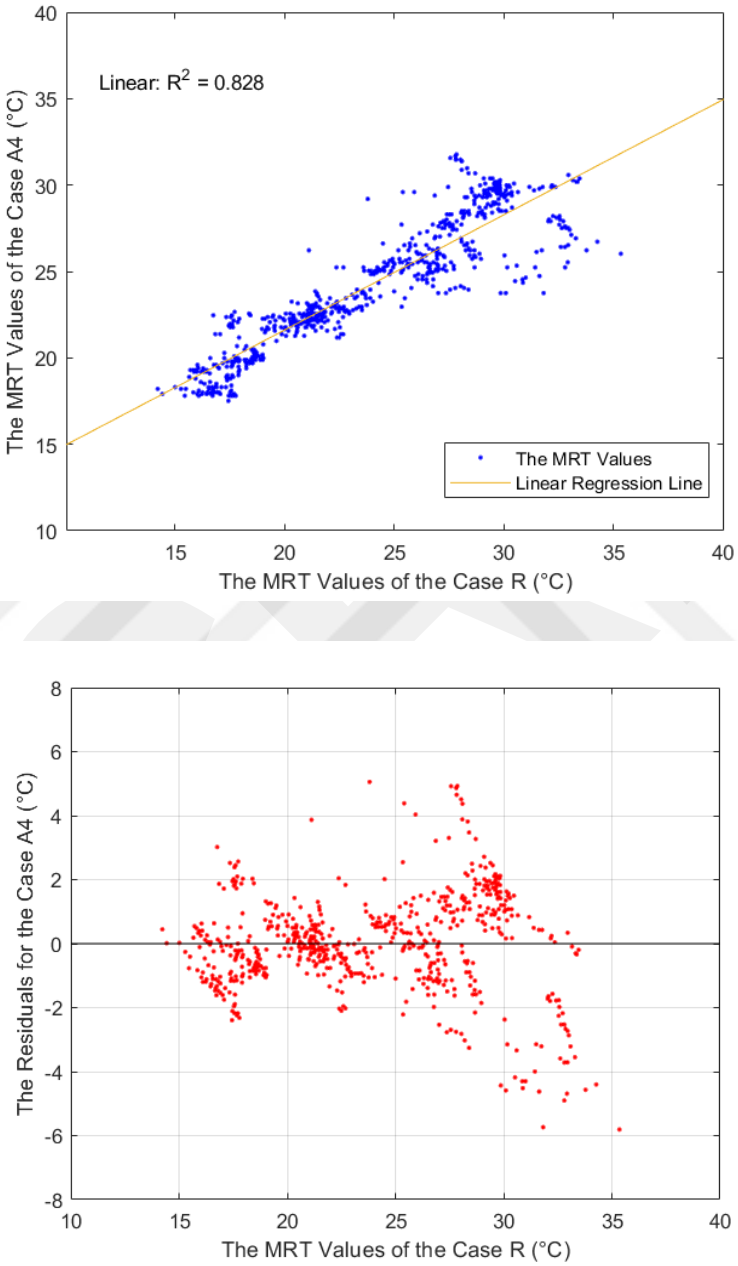

Figure 6.12. The Graph for Comparison of the MRT Values of Cases with Residuals: A4 and R

Because the A4 is only dependent on $T_{a,}$ the data distribution is similar to the assumption of the equality of the MRT to T_a. The discussions performed in section 6.3.5 are valid for this assumption also. The statistical criteria of MSE, MAPE, RMSE, and R^2 values for the comparison are depicted in Table 6.10.

Table 6.10. Statistical Criteria Results for Comparison of Cases of the A4 and R

Statistical Criteria	**Result**
MSE	5.064
RMSE	2.250
MAPE	7.495
R^2	0.828

6.4.7 Comparison of the Cases: A5 and R

The comparison of the MRT values stemmed from the A5 and R was illustrated in Figure 6.13.

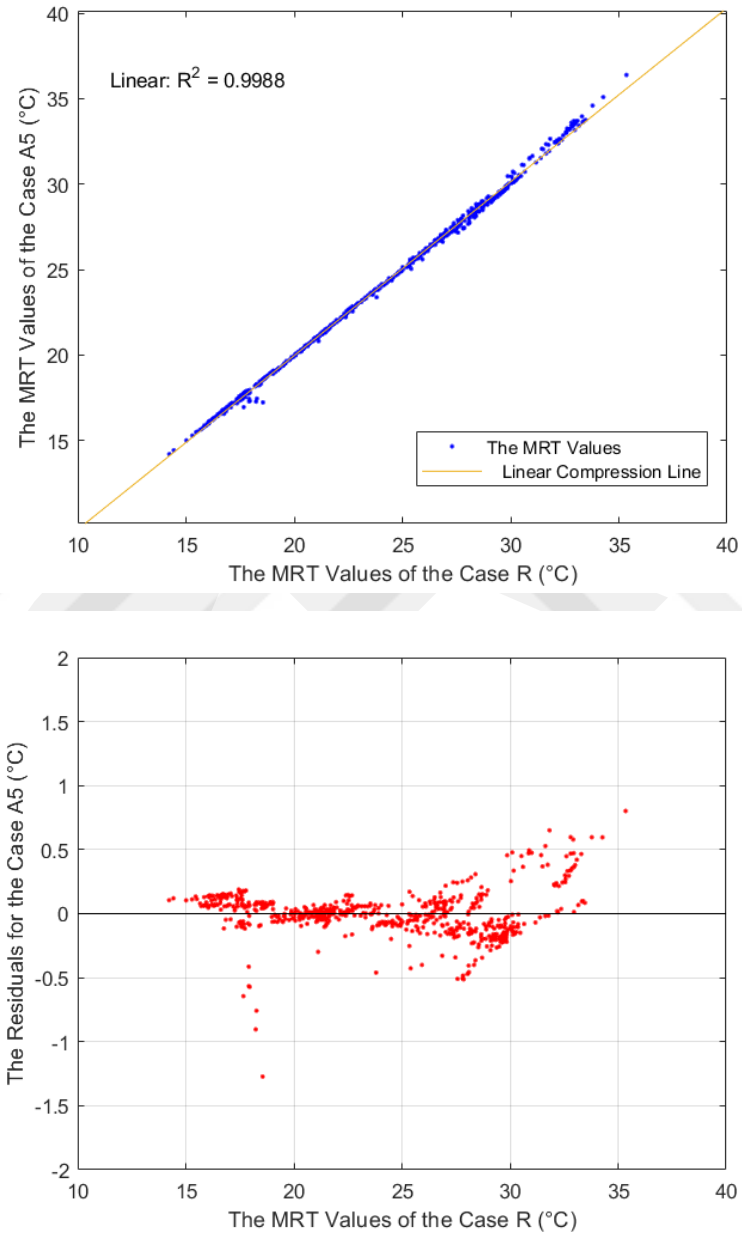

Figure 6.13. The Graph for Comparison of the MRT Values of Cases with Residuals: A5 and R

In comparison, the difference between the MRT values was slightly changed, and they were underestimated in low and high MRT values. It is worth to remind that because the experiments are conducted in the still air, and the window and door were kept closed in the case building, the air velocity was taken as 0.1 m/s in the case building [147, 148]. The results of the statistical criteria of MSE, RMSE, MAPE, and R^2 of the comparison are depicted in Table 6.11.

Table 6.11. Statistical Criteria Results for Comparison of Cases of the A5 and R

Statistical Criteria	**Result**
MSE	0.038
RMSE	0.195
MAPE	0.436
R^2	0.998

6.4.8 Comparison of the Cases: A6 and R

The comparison of the MRT values stemmed from the A6 and R was illustrated in Figure 6.14.

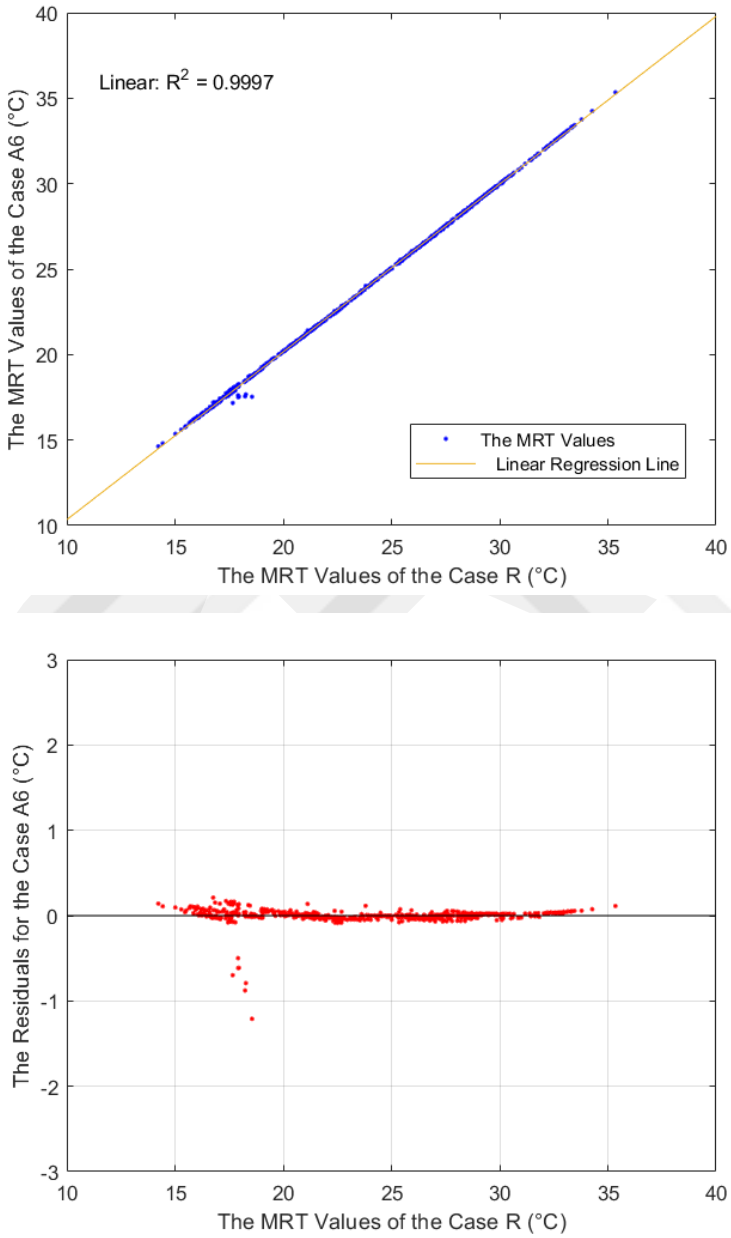

Figure 6.14. The Graph for Comparison of the MRT Values of Cases with Residuals: A6 and R

The MRT results are quite close with the results of the R, and the Mean Absolute Percentage Error (MAPE) was found as 0.51. The results are close since the A6 considers the globe temperature, air velocity, and air temperature at the same time, similarly to the R. The statistical criteria of MSE, MAPE, RMSE, and R^2 values are depicted in Table 6.12.

Table 6.12. Statistical Criteria Results for Comparison of Cases of the A6 and R

Statistical Criteria	**Result**
MSE	0.024
RMSE	0.156
MAPE	0.579
R^2	0.999

6.4.9 Comparison of the Cases: A7 and R

The comparison of the MRT values stemmed from the A7 and R was illustrated in Figure 6.15.

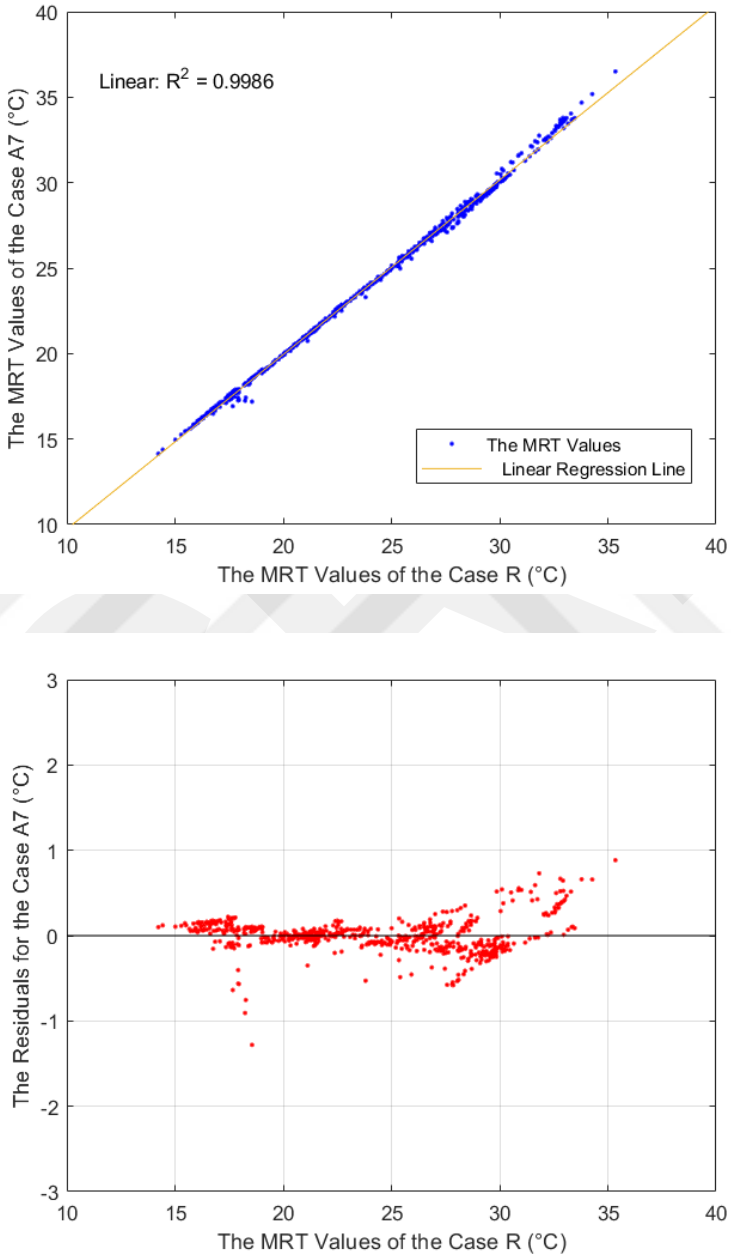

Figure 6.15. The Graph for Comparison of the MRT Values of Cases with Residuals: A7 and R

The A7 was considering the air velocity, globe thermometer and indoor air temperature. The results are closed to A6 since the difference is only in the constant of the second term ($v_a^{0.5}(T_g-T_a)$) in the equation 3.18 (1.8 to 2.44). The increase in the constant revealed the rise in the errors since the effect of (T_g-T_a) increased. The statistical criteria of MSE, MAPE, RMSE, and R^2 values are depicted in Table 6.13.

Table 6.13. Statistical Criteria Results for Comparison of Cases of the A7 and R

Statistical Criteria	**Result**
MSE	0.048
RMSE	0.219
MAPE	0.515
R^2	0.998

6.4.10 Comparison of the Cases: A8 and R

The comparison of the MRT values stemmed from the A8 and R was illustrated in Figure 6.16.

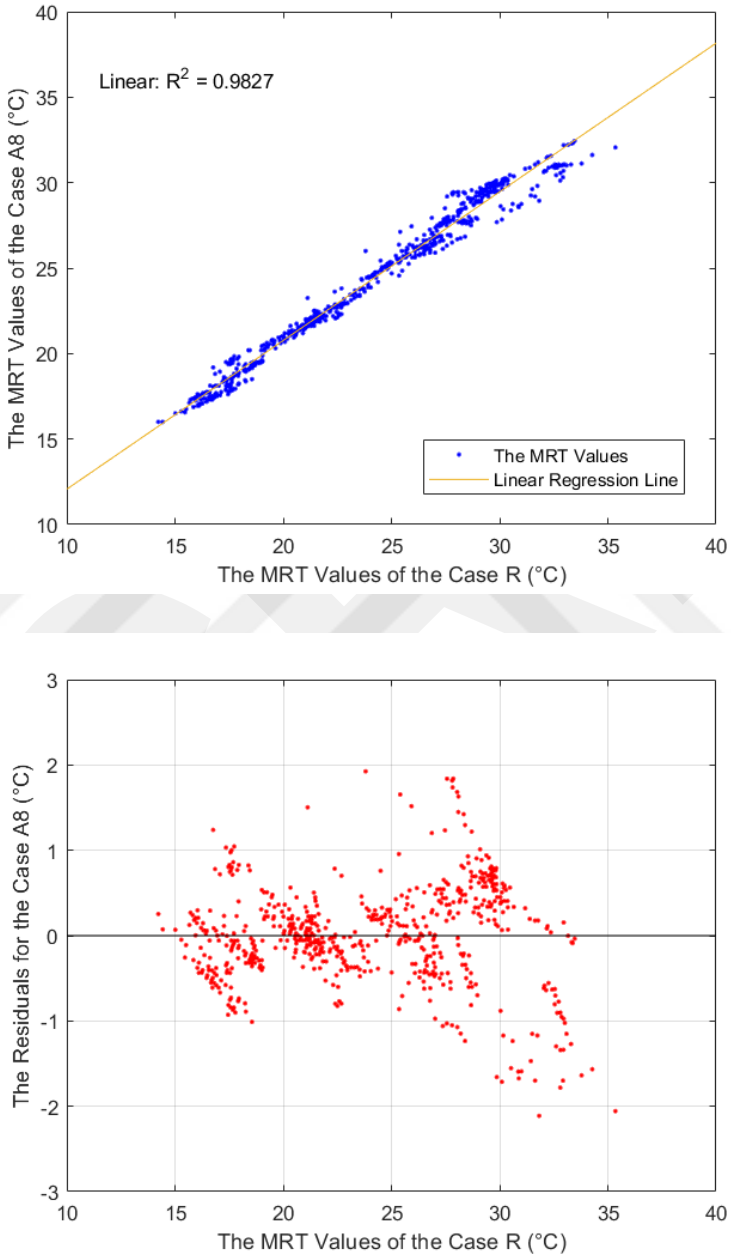

Figure 6.16. The Graph for Comparison of the MRT Values of Cases with Residuals: A8 and R

As Figure 6.16 depicts that the MRT values were under and overestimated in general by A8. Besides, the wrong estimations are increased with increasing the temperature. The reason for the difference was originated due to the difference between equations 3.1 and 3.20. Although, the reference method considers the convective heat transfer, the A8 is not taken into account the convective heat transfer. The statistical criteria of MSE, MAPE, RMSE, and R^2 values for the comparison are depicted in Table 6.14.

Table 6.14. Statistical Criteria Results for Comparison of Cases of the A8 and R

Statistical Criteria	**Result**
MSE	0.812
RMSE	0.901
MAPE	3.211
R^2	0.982

Table 6.15 depicts that the results of statistical criteria for 10 different methods, which are compared with the reference method, to obtain the MRT. Furthermore, the results of MSE values can be seen in Figure 6.17.

Table 6.15. Statistical Criteria Results for Comparison of Calculation Methods and Assumptions with the Reference Method

Compared Methods		**MSE**	**RMSE**	**MAPE**
Calculation Methods	C1	4.270	2.066	6.282
	C2	4.840	2.200	8.095
Assumptions	A1	0.266	0.516	1.567
	A2	6.019	2.453	9.185
	A3	5.251	2.291	7.973
	A4	5.064	2.250	7.495
	A5	0.038	0.195	0.436
	A6	0.024	0.156	0.579
	A7	0.048	0.219	0.515
	A8	0.812	0.901	3.211

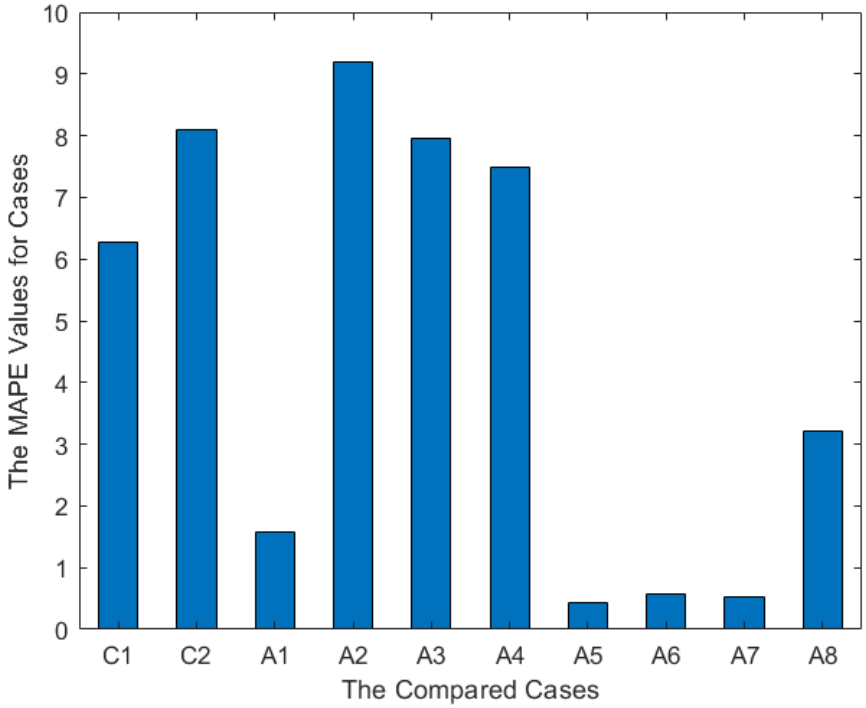

Figure 6.17. Comparison of the Mean Squared Errors (MAPE) of 10 Compared Method

6.5. Limitations

Even though the objective of the study was basically comparison of the methods in order to obtain the MRT in indoor environments, some limitations should be considered for the study. The limitations of this study are listed below.

- In commercial devices, the standard globe thermometer has 0.4mm thick, 150mm diameter of the copper sphere [53]. In contrast, the developed globe thermometer has a 0.6 mm thick, 135 mm diameter copper sphere. Since the response time has changed with the changes in the air volume inside the copper sphere [12, 60, 61], more accurate results in the calibration process could be obtained by using the diameter of the standard globe thermometer.
- In the calibration process of the developed globe thermometer, the operator caused temperature variations during the calibration period by opening the door to check the results. However, this error is negligible in this study.

- The sum of the angle factors is theoretically identified as 1 [11]. However, in the real examples, the angle factor calculation may differ from the theoretical value [149]. The sum of angle factors is found as 0.961 for the case building. It is certain that a small amount of error occurs in the calculation step for this reason.
- Even though the additional heat sources were controlled and eliminated in the case building, an occupant was inside the case building while taking wall temperature measurements in the measurement campaign. Therefore, the occupant slightly affected the globe temperature and indoor air temperature. It is worth to remind that the case building is a real office building instead of a well-insulated test chamber.
- The results of this study were examined with 699 data in the case building. Larger data sets and taking measurements in different places are necessary to verify the correlations.

CHAPTER 7

CONCLUSIONS

The thesis represents the methods to obtain the MRT and the accuracies of widely used two calculation methods and eight assumptions, comparing with the globe thermometer measurement method in a case building which is an office building located in Atılım University Ankara/Turkey. The reason to compare calculation methods and assumptions because the most accurate method to obtain the MRT was indicated as a measurement method [51, 52].

First, a globe thermometer was constructed to use as a reference device for the study, since the industrial globe thermometer has a high cost. After construction, a measurement campaign for the calibration of the developed globe thermometer was held between 23.01.2020 to 01.02.2020 during the heating season. As a result of the collected data, the developed globe thermometer, which was calibrated as one of the widely used calibration methods – The Linear Comparative Calibration Method –, gives close results between the well-known industrial globe thermometer. The difference between the developed and industrial globe thermometers was occurred due to the difference between the diameters of the copper spheres.

Secondly, a total of 10 different methods (2 calculation methods and 8 assumptions) to obtain the MRT was compared with the developed globe thermometer via in-situ measurement. The measurement campaign for comparison study was held between 06th July 2020 to 19th April 2021, which contains both the heating and cooling seasons.

The results indicated that the C1 and C2 methods calculated the MRT values with a large error compare to reference method. The main reason of this large error is since the calculation methods calculate the MRT directly and affect sharp changes of the temperature on the walls with large window. In contrast, the effects of the sharp changes of the temperature on the walls with windows are seen after the equilibrium

time in the reference method. In the case of C2, the effects of walls remained the same, and the position of the occupant was not considering. Since the distance between the walls and occupant is different, the error of C2 was higher than C1.

On the other hand, in comparison between assumptions (cases A1 to A8) and the reference method, the results revealed that assumptions could estimate the MRT values inaccurately. The highest error was found in the case of A2 with a MAPE of 9.185% due to the wrong estimation of fenestration. It should be underlined that one of the most used methods to obtain MRT, which is the equality of the MRT to T_a occurred incorrect results with a MAPE of 7.793%. Moreover, the assumptions which considered fewer parameters to estimate the MRT values were given less accurate results while comparing the reference method. On the other hand, the accuracies of the assumptions consider more parameters to estimate the MRT more accurately. The MAPE values of the cases A5, A6, and A7, which are estimating the MRT values with considering more than one parameter, were found lower than 1%.

The findings of this study revealed that researchers must consider the errors while using the calculation methods and assumptions. The outcome of this study can assist the architects, engineers, and researchers who desire to obtain MRT in indoor environments with a detailed list of obtaining methods and their accuracies.

It is worth to remind that two crucial limitations need to be reminded. First, during the calibration of the globe thermometer, temperature variations which were caused by the operator by opening the door to check the results were negligible in this study. Latter, during the measurement for the comparison of the MRT values, the wall temperatures were taken by the occupant who affects the T_a and T_g, and this effect was also negligible in this study.

Further works need to be carried out to compare the assumptions and calculation methods with different measurement methods. Moreover, the comparison can be performed in different locations of the case building, and the difference between the MRT values can be discussed.

REFERENCES

[1] J.E. Brumbaugh, *Audel HVAC Fundamentals Volume 1: Heating Systems, Furnaces and Boilers*. John Wiley & Sons, 2004, pp. 1-7. ISBN: 0-764-54206-0.

[2] H.W. Stanford III, *HVAC water chillers and cooling towers: fundamentals, application, and operation*. CRC Press, 2011, pp. 31-47. ISBN 978-1-4398-6211-7.

[3] W.L. Angel, *HVAC design sourcebook*. McGraw-Hill Education, 2020, pp. 1-5. ISBN 978-1-26-045725-4.

[4] P. Bertoldi, M. Economidou, V. Palermo, B. Boza-Kiss, and V. Todeschi. "How to finance energy renovation of residential buildings: Review of current and emerging financing instruments in the EU." *Wiley Interdisciplinary Reviews: Energy and Environment* vol.10, no. 1, e384, 2021.

[5] M. Macarulla, and L.C. Casals. "Paradoxes Between Energy Labeling and Efficiency in Buildings," in *Project Management and Engineering Research*, Switzerland: Springer, 2017, pp. 371-380.

[6] A.E. Keleş, E. Önen, and J. Górecki, "Make saving crucial again: building energy efficiency awareness of people living in urban areas." *Advances in Building Energy Research*, pp. 1-14, 2021.

[7] Eurostat, "Final energy consumption in the residential sector by use, EU-28, 2017 (Online Data Code: nrg_bal_c)", Internet: https://ec.europa.eu/eurostat/statistics-explained/index.php?title=File:Final_energy_consumption_in_the_residential_sector_by_use,_EU-28,_2017_.png [May 05, 2021].

[8] L. Yang, Y. Haiyan, and J. C. Lam. "Thermal comfort and building energy consumption implications–a review." *Applied energy* vol.115, pp. 164-173, 2014.

[9] American Society of Heating, Refrigerating and Air-Conditioning Engineers. "ASHRAE Standard-55: Thermal Environmental Conditions for Human Occupancy", 2020.

[10] International Organization for Standardization, "ISO 7726: Ergonomics of the thermal environment instruments for measuring physical quantities", Geneva, Switzerland, 1998.

[11] J. Babiak, B. Olesen, and D. Petráš, *Low temperature heating and high temperature cooling : embedded water based surface heating and cooling systems (REHVA Guidebook No:7)*. Brussels: Federation of European Heating, Ventilation and Air Conditioning Associations, 2013, pp. 1-19. ISBN 978-2-9600468-6-1.

[12] F.R.D.A. Alfano, M. Dell'Isola, B.I. Palella, G. Riccio, and A. Russi, "On the measurement of the mean radiant temperature and its influence on the indoor thermal environment assessment." *Building and Environment*, vol. 63, pp. 79-88, 2013.

[13] R. Carter, *The human brain book: An illustrated guide to its structure, function, and disorders*. New York: Dorling Kindersley Publishing, 2019, pp. 8-10.

[14] H.H. Zhang, Y. Liu, X.Y. Xiong, G. M. Shi, C.Y. Wang, and E. I. Wei, "Investigating Thermal Cooling Mechanisms of Human Body Under Exposure to Electromagnetic Radiation." *IEEE Access*, vol. 7, pp. 9697-9703, 2019.

[15] M. Prek, "Thermodynamic analysis of human heat and mass transfer and their impact on thermal comfort" *Int. J. Heat Mass Transfer*, vol. 48, pp. 731–739, 2005.

[16] A.M. Roberts, and A. Roberts, *The complete human body*. New York: Dorling Kindersley Publishing. 2010, pp. 292-299.

[17] C. Turhan, & G.G. Akkurt, "The relation between thermal comfort and human-body exergy consumption in a temperate climate zone." *Energy and Buildings*, vol. 205, 109548, 2019.

[18] K. Nakamura "Afferent pathways for autonomic and shivering thermoeffectors." *Handbook of clinical neurology* vol. 156, pp. 263-279, 2018.

[19] P.O. Fanger, *Thermal comfort analysis and applications in environmental engineering*, Copenhagen: Danish Technical Press, 1970, pp. 244.

[20] A.P. Gagge, A.P. Fobelets and L. Berglund. "A standard predictive Index of human reponse to thermal enviroment." *Transactions/American Society of Heating, Refrigerating and Air-Conditioning Engineers*, vol. 92(2B), pp.709-731, 1986.

[21] B.W. Jones "Capabilities and limitations of thermal models for use in thermal comfort standards." *Energy and Buildings* vol. 34, no. 6, pp. 653-659, 2002.

[22] G. Rizzo and M. Beccali A. Nucara, "Thermal Comfort", in *Encyclopedia of Energy*, vol. 6 Boston, USA: Elsevier, pp. 55-64, 2004. https://doi.org/10.1016/B0-12-176480-X/00551-9

[23] P. Danca, A. Vartires and A. Dogeanu, "An overview of current methods for thermal comfort assessment in vehicle cabin." *Energy Procedia*, vol. 85, pp.162-169, 2016.

[24] K. Fabbri, "The Indices of Feeling—Predicted Mean Vote PMV and Percentage People Dissatisfied PPD." *Indoor Thermal Comfort Perception*, pp. 75-125, 2015.

[25] A.C. Van der Linden, A.C. Boerstra, A.K. Raue, S.R. Kurvers, R.J. de Dear, "Adaptive temperature limits: A new guideline in The Netherlands: A new approach for the assessment of building performance with respect to thermal indoor climate." *Energy and Buildings*, vol. 38(1), pp. 8-17, 2006.

[26] J.F. Nicol, M.A. Humphreys, “Adaptive thermal comfort and sustainable thermal standards for buildings.” *Energy and Buildings*, vol. 34, pp. 563-572, 2002.

[27] M.H. Hasan, F. Alsaleem, M. Rafaie, “Sensitivity study for the PMV thermal comfort model and the use of wearable devices biometric data for metabolic rate estimation.” *Building and Environment*, vol. 110, pp. 173-183, 2016.

[28] D. C. Hoang, Y. K. Tan, H. B. Chng and S. K. Panda, "Thermal energy harvesting from human warmth for wireless body area network in medical healthcare system," in *2009 International Conference on Power Electronics and Drive Systems (PEDS)*, 2009, pp. 1277-1282.

[29] M. Luo, Z. Wang, K. Ke, B. Cao, Y. Zhai, X. Zhou, “Human metabolic rate and thermal comfort in buildings: The problem and challenge.” *Building and Environment*, vol. 131, pp. 44-52, 2018.

[30] G. Havenith, I. Holmér, K. Parsons, “Personal factors in thermal comfort assessment: clothing properties and metabolic heat production.” *Energy and Buildings*, vol. 34 (6), pp. 581-591, 2002.

[31] J. Yao, F. Yang, Z. Zhuang, Y. Shao, P.F. Yuan, “The effect of personal and microclimatic variables on outdoor thermal comfort: A field study in a cold season in Lujiazui CBD, Shanghai.” *Sustainable Cities and Society*, vol. 39, pp. 181-188, 2018.

[32] R. McMullan, *Environmental science in building*. London: Palgrave Macmillan Education, 2017, pp. 14-70.

[33] Ç, Çakır, "Assessing thermal comfort conditions. A case study on the METU Faculty of Architecture building " Master's thesis, Middle East Technical University, Turkey, 2006.

[34] S. Jing, L. Baizhan, T. Meilan, and L. Hong, "Impact of relative humidity on thermal comfort in a warm environment." *Indoor and Built Environment*, vol. 22, pp. 598-607, 2013.

[35] M. Vellei, M. Herrera, D. Fosas, S. Natarajan, “The influence of relative humidity on adaptive thermal comfort.” *Building and Environment*, vol. 124, pp. 171-185, 2017.

[36] Digital Temperature and Relative Humidity Sensor with M12 Connector, HygroVUE10, Campbell Scientific. Internet: https://www.campbellsci.com/hygrovue10 [May 19, 2021].

[37] M. Taleghani, M. Tenpierik, S. Kurvers, A. van den Dobbelsteen, “A review into thermal comfort in buildings.” *Renewable and Sustainable Energy Reviews*, vol. 26, pp. 201-215, 2013.

[38] C. Cândido, R.J. de Dear, R. Lamberts, L. Bittencourt, “Air movement acceptability limits and thermal comfort in Brazil's hot humid climate zone.” *Building and Environment*, vol. 45(1), pp. 222-229, 2010.

[39] K. Hsieh “The Effect of Air Velocity on Thermal Comfort At Moderate Activity Levels.” Master’s Thesis, B.S. Taiwan Chung-Hsin University, Taiwan, 1985.

[40] Anenometer, TESTO 425, TESTO, UK. Internet: https://www.testo.com/en-UK/testo-425/p/0560-4251 [May 19, 2021].

[41] R. Niemelä, M. Hannula, S. Rautio, K. Reijula, J. Railio, “The effect of air temperature on labour productivity in call centres—a case study.” *Energy and Buildings*, vol. 34(8), pp. 759-764, 2002.

[42] L. Lan, P. Wargocki, Z. Lian, “Quantitative measurement of productivity loss due to thermal discomfort”, *Energy and Buildings*, vol. 43(5), pp. 1057-1062, 2011.

[43] W. Cui, G. Cao, J.H. Park, Q. Ouyang, Y. Zhu, “Influence of indoor air temperature on human thermal comfort, motivation and performance.” *Building and Environment*, vol. 68, pp. 114-122, 2013.

[44] J. Van Hoof, “Forty years of Fanger's model of thermal comfort: comfort for all?.” *Indoor Air*, vol. 18(3), pp.182-201, 2008.

[45] R.J. de Dear, T. Akimoto, E.A. Arens, G. Brager, C. Candido, K.W.D. Cheong, B. Li, N. Nishihara, S.C. Sekhar, S. Tanabe, and J. Toftum, “Progress in thermal comfort research over the last twenty years.” *Indoor Air*, vol. 23(6), pp.442-461, 2013.

[46] J. Van Hoof, M. Mazej and J.L. Hensen, “Thermal comfort: research and practice.” *Frontiers in Bioscience*, vol. 15(2), pp.765-788, 2010.

[47] I. Atmaca, O. Kaynakli, A. Yigit, “Effects of radiant temperature on thermal comfort.” *Building and Environment*, vol. 42(9), pp. 3210-3220, 2007.

[48] E. Halawa, J. van Hoof, V. Soebarto, “The impacts of the thermal radiation field on thermal comfort, energy consumption and control—A critical overview.” *Renewable and Sustainable Energy Reviews*, vol. 37, pp. 907-918, 2014.

[49] D. Wang, G. Chen, C. Song, Y. Liu, W. He, T. Zeng, J. Liu, “Experimental study on coupling effect of indoor air temperature and radiant temperature on human thermal comfort in non-uniform thermal environment.” *Building and Environment*, vol. 165, 106387, 2019.

[50] G. Gan, “Analysis of mean radiant temperature and thermal comfort.” *Building Services Engineering Research and Technology*, vol. 22(2), pp. 95-101, 2001.

[51] N. Kántor and J. Unger, “The most problematic variable in the course of human-biometeorological comfort assessment—the mean radiant temperature.” *Central European Journal of Geosciences*, vol. 3(1), pp.90-100, 2011.

[52] P.Höppe, “Ein neues Verfahren zur Bestimmung der mittleren Strahlungstemperatur in Freien. [A new measurement procedure to obtain the mean radiant temperature outdoors].” *Wetter und Leben*, vol 44, 147–151, 1992 (in German).

[53] H.M. Vernon, “The measurement of radiant heat in relation to human comfort.” *Journal of Commercial Hygiene*, vol.14, pp. 95-111, 1932.

[54] P. Aparicio, J.M. Salmerón, Á. Ruiz, F.J. Sánchez, and L. Brotas. “The globe thermometer in comfort and environmental studies in buildings.” *Journal of Construction*, vol. 15(3), pp. 57-66, 2016.

[55] C.L. Tan, N.H. Wong, and S. K. Jusuf, “Outdoor mean radiant temperature estimation in the tropical urban environment”. *Building and Environment*, vol. 64, pp. 118-129, 2013.

[56] S. Manavvi, E. Rajasekar, “Estimating outdoor mean radiant temperature in a humid subtropical climate.” *Building and Environment*, vol. 171, 106658, 2020.

[57] L.A. Kuehn, R.A. Stubbs, and R.S. Weaver, “Theory of the globe thermometer.” *Journal of Applied Physiology*, vol. 29(5), pp. 750-757, 1970.

[58] J.F. Clarke and W. Bach “Comparison of the comfort conditions in different urban and suburban microenvironments.” *International Journal of Biometeorology*, vol. 15, pp.41-54, 1971.

[59] TESTO Globe Thermometer 0602 0743, TESTO, UK. Internet: https://www.testo.com/en-UK/globe-probe-o-150mm-tc-type-k-for-measuring-radiant-heat/p/0602-0743 [May 19, 2021]

[60] B.W. Olesen, J. Rosendahl, L.N. Kalisperis, L.H. Summers, and M. Steinman, “Methods for measuring and evaluating the thermal radiation in a room.” *ASHRAE transactions*, vol. 95, pp. 1028-1044, 1989.

[61] S. Godbole, “Investigating the Relationship Between Mean Radiant Temperature (MRT) and Predicted Mean Vote (PMV): A Case Study in a University building.” Master's thesis, KTH Royal Institute of Technology, Stockholm, 2018.

[62] Two Sphere Radiometer, United Scientific, USA Internet: https://www.unitedsci.com/radiometer.html [May 19, 2021].

[63] C. Kwong C. Lam, Y. Gao, H. Yang, T. Chen, Y. Zhang, C. Ou, J. Hang, “Interactive effect between long-term and short-term thermal history on outdoor thermal comfort: Comparison between Guangzhou, Zhuhai and Melbourne.” *Science of The Total Environment*, vol. 760, 144141, 2021.

[64] International Organization for Standardization, “ISO 7730: Ergonomics of the thermal environment — Analytical determination and interpretation of thermal comfort using calculation of the PMV and PPD indices and local thermal comfort criteria”, Geneva, Switzerland, 2015.

[65] C. Marino, A. Nucara, M. Pietrafesa, “Thermal comfort in indoor environment: Effect of the solar radiation on the radiant temperature asymmetry.” *Solar Energy*, vol. 144, pp. 295-309, 2017.

[66] A. Simone, B.W. Olesen, J.L. Stoops and A.W. Watkins, “Thermal comfort in commercial kitchens (RP-1469): Procedure and physical measurements (Part 1).” *HVAC&R Research*, vol. 19:8, pp. 1001-1015, 2013

[67] K. Parsons, *Human thermal environments: the effects of hot, moderate, and cold environments on human health, comfort, and performance*. New York: CRC press, 2014, ISBN 978-1-4665-9599-6.

[68] H. Guo, M. Ferrara, J. Coleman, M. Loyola, F. Meggers, “Simulation and measurement of air temperatures and mean radiant temperatures in a radiantly heated indoor space.” *Energy*, vol. 193, 116369, 2020.

[69] Y. Ozeki, M. Konishi, C. Narita, and S.I. Tanabe, “Angle factors between human body and rectangular planes calculated by a numerical model”. *Transactions-American Society of Heating Refrigerating and Air Conditioning Engineers*, vol. 106(2), pp. 511-520, 2000.

[70] Y. Wang, X. Meng, L. Zhang, Y. Liu, E. Long, “Angle Factor Calculation for the Thermal Radiation Environment of the Human Body,” in *Proceedings of the 8th International Symposium on Heating, Ventilation and Air Conditioning*, 2013, vol. 261 pp. 447-455.

[71] Y.C Chen, T.P.Lin and A. Matzarakis, “Comparison of mean radiant temperature from field experiment and modelling: a case study in Freiburg, Germany.” *Theoretical and Applied Climatology*, vol. 118 pp. 535-551, 2014.

[72] Verein Deutscher Ingenieure (Association of German Engineers), “Methods for the human-biometerological assessment of climate and air hygiene for urban and regional planning”. Part I: Climate, VDI guideline 3787. Part 2. Beuth, Berlin, 1998.

[73] G. Gan, “Numerical Method for a Full Assessment of Indoor Thermal Comfort.” *Indoor Air*, vol. 4(3), 154–168, 1994.

[74] A. Matzarakis, F. Rutz & H. Mayer, “Modelling radiation fluxes in simple and complex environments—application of the RayMan model.” *International Journal of Biometeorology*, vol. 51 pp.323-334, 2007.

[75] P.J. Crank, A. Middel, M. Wagner, D. Hoots, M. Smith, A. Brazel, “Validation of seasonal mean radiant temperature simulations in hot arid urban climates.” *Science of The Total Environment*, vol. 749, 141392, 2020.

[76] S. Thorsson, F. Lindberg, I. Eliasson, B. Holmer, “Different methods for estimating the mean radiant temperature in an outdoor urban setting.” International *Journal of Climatology: A Journal of the Royal Meteorological Society*, vol. 27(14), pp.1983-1993, 2007.

[77] J.A. Acero and J. Arrizabalaga, “Evaluating the performance of ENVI-met model in diurnal cycles for different meteorological conditions” T*heoretical and Applied Climatology*, vol. 131 pp. 455-469, 2018.

[78] F. Binarti, M.D. Koerniawan, S. Triyadi and S.S. Utami, “Maximizing the ENVI-met Capability of Modelling the Mean Radiant Temperature of a Tropical Archaeological Site,” in *IOP Conference Series: Earth and Environmental Science*, 2020, vol. 541(1), p. 012005.

[79] F. Lindberg, B. Holmer & S. Thorsson, “SOLWEIG 1.0 – Modelling spatial variations of 3D radiant fluxes and mean radiant temperature in complex urban settings.” *International Journal of Biometeorology*, vol. 52, pp. 697-713, 2018.

[80] F. Lindberg and C.S.B. Grimmond, “The influence of vegetation and building morphology on shadow patterns and mean radiant temperatures in urban areas: model development and evaluation.” *Theoretical and Applied Climatology*, vol. 105 pp.311-323, 2011.

[81] T. Chaudhuri, Y. C. Soh, S. Bose, L. Xie and H. Li, "On assuming Mean Radiant Temperature equal to air temperature during PMV-based thermal comfort study in air-conditioned buildings," in *IECON 2016 - 42nd Annual Conference of the IEEE Industrial Electronics Society*, 2016, pp. 7065-7070.

[82] M. Dawe, P. Raftery, J. Woolley, S. Schiavon, F. Bauman, “Comparison of mean radiant and air temperatures in mechanically-conditioned commercial buildings from over 200,000 field and laboratory measurements.” *Energy and Buildings*, vol. 206, 109582, 2020.

[83] B.L. Kilkis, “COOLP: A computer program for the design and analysis of ceiling cooling panels.” *ASHRAE Transactions* vol. 101(2), pp. 703-710, 1995.

[84] K. Nagano, T. Mochida, “Experiments on thermal environmental design of ceiling radiant cooling for supine human subjects.” *Building and Environment*, vol. 39(3), pp. 267-275, 2004.

[85] M. Kazkaz, M. Pavelek, “Operative temperature and globe temperature.” *Eng. Mech*, vol. 20, pp. 319-325, 2013.

[86] X. Gong, “Investigation of a radiantly heated and cooled office with an integrated desiccant ventilation unit.” Doctor of Philosophy Thesis, Texas A&M University, USA, 2007.

[87] M.V. JOKL, “4 New Thermal Comfort Standards of the Czech Republic,” in *Standards for Thermal Comfort: Indoor air temperature standards for the 21st century*, 2006, pp.40-49.

[88] D. ROWE, “24 Warm and Sweaty: Thermal Comfort in Two Naturally Ventilated Offices in Sydney, NSW,” in *Standards for Thermal Comfort: Indoor air temperature standards for the 21st century*, 2006, pp.234,241.

[89] S. Carlucci, *Thermal comfort assessment of buildings*, Milan: Springer, 2013, pp. 21-56. ISBN 978-88-470-5238-3.

[90] M. Itani, N. Ghaddar, K. Ghali, A. Laouadi, “Development of heat stress charts for older people under indoor environmental conditions.” *Energy and Buildings*, vol. 224, 10274, 2020.

[91] G. Çalış , M. Kuru , B. Alt, “Bir Eğitim Binasinda Isıl Konfor Koşullarının Analizi: İzmir’de Bir Alan Çalişması [Analysis of Thermal Comfort Conditions in an Educational Building: A Case Study in Izmir].” *Uludağ University Journal of The Faculty of Engineering*, vol. 22(2), pp. 93-106 (in Turkish).

[92] O. Al-Hafith, B.K. Satish and P. De Wilde, “The impact of courtyard geometry on its mean radiant temperature,” in J*ournal of Physics: Conference Series, IOP Publishing*, 2019 vol. 1343, p. 012022.

[93] K.J. Moss, *Heat and mass transfer in buildings*, New York: Taylor and Francis, 2007, pp.1-26. ISBN 978–0–415–40907–0.

[94] M. Beshir, J.D. Ramsey, “Heat stress indices: A review paper.” *International Journal of Industrial Ergonomics*, vol. 3(2), pp. 89-102, 1988.

[95] J.D. Ramsey and C.P. Chai, “Inherent variability in heat-stress decision rules.” *Ergonomics*, vol. 26(5) pp. 495-504, 1983.

[96] T. Bedford and C.G. Warner, “The Globe Thermometer in Studies of Heating and Ventilation.” *Journal of Hygiene*, vol. 34 pp.458-473, 1934.

[97] D.A. McIntyre, *Indoor Climate*, London: Applied Science, 1980.

[98] Y. Xia, W. Lin, W. Gao, T. Liu, Q. Li, A. Li, “Experimental and numerical studies on indoor thermal comfort in fluid flow: A case study on primary school classrooms.” *Case Studies in Thermal Engineering*, vol. 19, 100619, 2020.

[99] J. Gao, Y. Wang, P. Wargocki, “Comparative analysis of modified PMV models and SET models to predict human thermal sensation in naturally ventilated buildings.” *Building and Environment*, vol. 92, pp. 200-208, 2015.

[100] F. Nicol, M. Humphreys, and S. Roaf, *Adaptive thermal comfort: principles and practice*. Melbourne:Routledge, 2012 pp. 44-52. ISBN 978-0-415-69159-8.

[101] M. Vellei. “Thermal Comfort, Control and Energy Use.” Doctoral dissertation, University of Bath, UK, 2017.

[102] J. Herrmann & A. Matzarakis “Mean radiant temperature in idealised urban canyons—examples from Freiburg, Germany.” *International Journal of Biometeorology*, vol. 56, pp. 199–203, 2012.

[103] C. Marino, A. Nucara, M. Pietrafesa, E. Polimeni and S. Costanzo, "Outdoor Mean Radiant Temperature Estimation: Is the Black-Globe Thermometer Method a Feasible Course of Action?," in 2*018 IEEE International Conference on Environment and Electrical Engineering and 2018 IEEE Industrial and Commercial Power Systems Europe (EEEIC / I&CPS Europe)*, 2018, pp. 1-7.

[104] J. Fischereit, “The simple urban radiation model for estimating mean radiant temperature in idealised street canyons.” *Urban Climate*, vol. 35, 100694, 2021.

[105] D.T. Reindl, W.A. Beckman, J.A. Duffie, “Diffuse fraction correlations.” *Solar Energy*, vol. 45(1), pp. 1-7, 1990.

[106] H. Staiger, “Die Strahlungskomponente im thermischen Wirkungskomplex für operationelle Anwendungen in der Human-Biometeorologie. [The radiation component in the thermal complex for operational applications in human biometeorology]”, Doctoral dissertation, Albert-Ludwigs-Universität, German, 2015.

[107] C.L. Tan, N.H. Wong, S.K. Jusuf, “Effects of vertical greenery on mean radiant temperature in the tropical urban environment.” *Landscape and Urban Planning*, vol. 127, pp. 52-64, 2014.

[108] N. Walikewitz, B. Jänicke, M. Langner, F. Meier, W. Endlicher, “The difference between the mean radiant temperature and the air temperature within indoor environments: A case study during summer conditions.” *Building and Environment*, vol. 84, pp. 151-161, 2015.

[109] S.H. Yoo, "Mathematical solutions for mean radiant temperature calculation in a rectangular or non-rectangular geometry." *Int. J. Adv. Mech. Civ. Eng*, vol. 5(4), pp. 42-46, 2018.

[110] F. Kalmár, T. Kalmár, “Interrelation between mean radiant temperature and room geometry”, *Energy and Buildings*, vol. 55, pp. 414-421, 2012.

[111] D. Aviv, E. Teitelbaum, T. Kvochick, K. Bradford, and F. Meggers, “Generation and Simulation of Indoor Thermal Gradients: MRT for Asymmetric Radiant Heat Fluxes,” in *Proceedings of Building Simulation*, 2019, pp. 381-388.

[112] D. Xing, N. Li, “Three-dimensional heat transfer of globe thermometers in indoor environments controlled by radiant systems.” *Building and Environment*, vol. 188, 107505, 2021.

[113] C. Turhan, “Comparison of Indoor Air Temperature and Operative Temperature -Driven HVAC Systems by Means of Thermal Comfort and Energy Consumption.” *Mugla Journal of Science and Technology*, vol.6 (1), pp. 156-163, 2020.

[114] A. Simone, and B.W. Olesen, “An experimental study of thermal comfort at different combinations of air and mean radiant temperature,” in Pr*oceedings of the 9th International Conference on Healthy Buildings*, 2009, Syracuse NY, USA.

[115] S.V. Patankar, *Numerical Heat Transfer and Fluid Flow*. New York: CRC Press, 1980, pp. 126-130. ISBN:9781315275130

[116] B.P. Leonard, “A stable and accurate convective modelling procedure based on quadratic upstream interpolation”, *Computer Methods in Applied Mechanics and Engineering*, vol. 19, pp. 59-98, 1979

[117] J. Han, J. Bae, J. Jang, J. Baek and S.B.Leigh, “The Derivation of Cooling Set-Point Temperature in an HVAC System, Considering Mean Radiant Temperature.” *Sustainability*, vol . 11(19), 5417, 2019.

[118] J.S. Haberl, C. Culp, D.E. Claridge, “ASHRAE’s Guideline 14-2002 for Measurement of Energy and Demand Savings: How to Determine What was Really Saved by the Retrofit,” in *Proceedings of the Fifth International Conference for Enhanced Building Operations*, 2005, Pittsburgh, Pennsylvania, USA pp. 1-13.

[119] D.S. Lee, E.J. Kim, Y.H. Cho, J.W. Kang, J.H Jo, “A field study on application of infrared thermography for estimating mean radiant temperatures in large stadiums”, *Energy and Buildings*, vol. 202, 109360, 2019.

[120] D.P DeWitt and G.D Nutter, *Theory and practice of radiation thermometry*, New York: John Wiley and Sons, USA, 1988. ISBN: 0-471-61018-6.

[121] Köppen-Geiger Climate Classification Internet: http://koeppen-geiger.vu-wien.ac.at/ [May 19, 2021].

[122] Turkish State Meterological Service, Weather Data: Extreme Maximum, Minimum and Average Temperatures Measured in Long Period. Internet: https://www.mgm.gov.tr/eng/forecast-cities.aspx?m=ANKARA [May 20, 2021].

[123] S Wang, and Y Li, “Suitability of acrylic and copper globe thermometers for diurnal outdoor settings.” *Building and Environment*, vol. 89, pp. 279-294, 2015.

[124] J. Black, and R.A. Kohser, *DeGarmo's Materials and Processes in Manufacturing*, 11th Edition, Kendallville: Wiley & Sons, 2011. ISBN: 978-1-119-49282-5.

[125] O. Music, J.M. Allwood, K. Kawai, “A review of the mechanics of metal spinning.” *Journal of Materials Processing Technology*, vol. 210(1), pp. 3-23, 2010.

[126] C.C Wong, T.A Dean, J Lin, “A review of spinning, shear forming and flow forming processes.” *International Journal of Machine Tools and Manufacture*, vol. 43(14), pp.1419-1435, 2003.

[126] J. Carvill, “Thermodynamics and heat transfer.” *Mechanical Engineer's Data Handbook*, Manchester, United Kingdom: Butterworth-Heinemann, 1993, pp.102-145.

[127] International Organization for Standardization, “ISO7243 Ergonomics of the thermal environment — Assessment of heat stress using the WBGT (wet bulb globe temperature) index”, Geneva, Switzerland, 2017.

[128] Datasheet of K-Type Temperature Sensor, DS18B20 Maxim Integrated, USA Internet: https://datasheets.maximintegrated.com/en/ds/DS18B20.pdf [May 20, 2021].

[129] Arduino UNO, Ardiuno, Italy. Internet: https://store.arduino.cc/usa/arduino-uno-rev3 [May 20, 2021].

[130] Datasheet of Temperature and Relative Humidity Sensor, DHT22, Guangzhou Aosong Electronics Co., Ltd, China. Internet: https://www.sparkfun.com/datasheets/Sensors/Temperature/DHT22.pdf [May 20, 2021].

[131] F.R.D.A Alfano, M. Dell'isola, G. Ficco, B.I. Palella, G. Riccio, "On the measurement of the mean radiant temperature by means of globes: An experimental investigation under black enclosure conditions." *Building and Environment*, vol. 193, 107655, 2021.

[132] British Standards Institution, "Thermocouples – Part 1: E.M.F. Specifications and Tolerances, BS EN 60584- 1: 2013", BSI, London, UK, 2013.

[133] Thermocouple Tolerances with classes, Thermal Detection Limited, Stockton, UK. Internet: https://thermal-detection.com/storage/app/media/Tech%20Data/Thermocouple%20tolerance%20chart.pdf [May 20, 2021].

[134] Datasheet of SD Card Module, CATALEX, China. Internet: http://curtocircuito.com.br/datasheet/modulo/cartao_micro_SD.pdf [May 20, 2021].

[135] G.A. Seber, and A.J. Lee, *Linear regression analysis*. Ney Jersey, USA: John Wiley & Sons, 2003, pp.139-163. ISBN: 9780471415404.

[136] D.C. Montgomery, E.A. Peck, and G.G. Vining, Introduction to linear regression analysis New Jersey, USA: John Wiley & Sons, 2012 pp.17-113 ISBN: 9780470542811

[137] MATLAB ver. R2018b.

[138] C. Turhan, T. Kazanasmaz, I.E. Uygun, K.E. Ekmen, and G.G. Akkurt, "Comparative study of a building energy performance software (KEP-IYTE-ESS) and ANN-based building heat load estimation." *Energy and Buildings*, vol. 85, pp. 115-125, 2014.

[139] G. Gan, "Evaluation of room air distribution systems using computational fluid dynamics."*Energy and Buildings*, vol. 23(2), pp. 83-93, 1995.

[140] Infrared Thermometer, Extech Instruments 42530 (EXTECH 42530) Internet: http://www.extech.com/products/42530 [May 20, 2021].

[141] K. Moustris, K.A. Kavadias, D. Zafirakis, J.K. Kaldellis, "Medium, short and very short-term prognosis of load demand for the Greek Island of Tilos using artificial neural networks and human thermal comfort-discomfort biometeorological data." *Renewable Energy*, vol. 147, pp. 100-109, 2020

[142] T. Chai, and R.R. Draxler, "Root mean square error (RMSE) or mean absolute error (MAE)?–Arguments against avoiding RMSE in the literature." *Geoscientific Model Development*, vol. 7(3), pp. 1247-1250, 2014.

[143] M. Ćalasan, S.H.A. Aleem, A.F. Zobaa, "On the root mean square error (RMSE) calculation for parameter estimation of photovoltaic models: A novel exact analytical solution based on Lambert W function." *Energy Conversion and Management*, vol. 210, 112716, 2020.

[144] R.Dash, and P.K. Dash, "MDHS–LPNN: a hybrid FOREX predictor model using a Legendre polynomial neural network with a modified differential harmony search technique," in *Handbook of neural computation* pp. 459-486. Academic Press. 2017.

[145] M.A. Humphreys, "The optimum diameter for a globe thermometer for use indoors." *Annals of Occupational Hygiene*, vol. 20(2), pp. 135–140, 1977.

[146] E.N. Hey, "Small globe thermometers." Jo*urnal of Physics E: Scientific Instruments*, vol. 1(9), 955, 1968.

[147] M.Prek, "Exergy analysis of thermal comfort." *International Journal of Exergy*, vol. 1(3), pp. 303-315, 2004.

[148] C. Song, G. Duan, D. Wang, Y. Liu, H. Du, G. Chen, "Study on the influence of air velocity on human thermal comfort under non-uniform thermal environment." *Building and Environment*, vol. 196, 107808, 2021.

[149] Robert Bean, P., 2021. Mean Radiant Temperature, Indoor Environmental Quality with Energy Efficiency Internet: www.healthyheating.com/Definitions/Mean%20Radiant_pg5.htm [May 20, 2021].

APPENDIX A

AN EXAMPLE DAY FROM THE COLLECTED DATA

DATE (DD/MM/YYY)										
13.01.2021										
9	8	7	6	5	4	3	2	1	DATA NUMBER	
13:58	13:48	13:38	13:28	13:18	13:08	12:58	12:48	12:38	TIME (HH:MM)	
17.80	17.70	17.70	17.30	17.10	17.40	17.30	17.20	16.90	LW (Brick)	WALL TEMPERATURES (°C)
18.00	18.00	17.90	17.50	17.50	17.70	17.30	17.30	16.70	LW (Window)	
19.80	19.60	19.60	19.30	19.30	19.40	19.30	19.30	18.80	RW	
19.90	19.60	19.50	19.10	19.20	19.40	19.20	19.10	18.70	FW	
19.80	19.20	19.50	19.10	19.30	19.50	19.20	19.20	18.60	BW	
19.90	19.60	19.40	19.20	19.20	19.60	19.40	19.20	18.70	C	
19.10	19.00	18.80	18.40	18.60	18.60	18.50	18.20	18.00	B	
18.60	18.50	18.20	18.00	18.10	18.00	18.00	18.00	18.20	T_a (°C)	
2.00	1.00	1.00	1.00	1.00	0.00	0.00	0.00	0.00	T_{out} (°C)	
18.06	17.87	17.87	17.94	17.94	17.87	17.81	17.75	17.25	T_g (°C)	
17.59	17.34	17.54	17.79	17.72	17.67	17.57	17.47	16.49	R	MRT VALUES FOR CASES (°C)
18.71	18.45	18.40	18.06	18.16	18.33	18.14	18.01	17.60	C1	
19.47	19.21	19.15	18.80	18.89	19.08	18.88	18.76	18.31	C2	
17.52	17.24	17.54	17.88	17.78	17.74	17.62	17.50	16.30	A1	
18.93	18.82	18.52	18.32	18.42	18.31	18.31	18.31	18.51	A2	
18.60	18.50	18.20	18.00	18.10	18.00	18.00	18.00	18.20	A3	
18.40	18.31	18.01	17.81	17.91	17.81	17.81	17.81	18.01	A4	
17.66	17.40	17.62	17.90	17.82	17.77	17.67	17.56	16.54	A5	
17.75	17.51	17.68	17.91	17.85	17.80	17.70	17.61	16.71	A6	
17.64	17.38	17.62	17.89	17.82	17.77	17.66	17.56	16.52	A7	
18.06	17.87	17.87	17.94	17.94	17.87	17.81	17.75	17.25	A8	